POWER ELECTRONICS DESIGN IMPLICATIONS OF NOVEL PHOTOVOLTAIC COLLECTOR GEOMETRIES AND THEIR APPLICATION FOR INCREASED ENERGY HARVEST

A Thesis

by

AMULYA KARAVADI

Submitted to the Office of Graduate Studies of
Texas A&M University
in partial fulfillment of the requirements for the degree of

MASTER OF SCIENCE

August 2011

Major Subject: Electrical Engineering

Power Electronics Design Implications of Novel Photovoltaic Collector Geometries and Their Application for Increased Energy Harvest

POWER ELECTRONICS DESIGN IMPLICATIONS OF NOVEL PHOTOVOLTAIC COLLECTOR GEOMETRIES AND THEIR APPLICATION FOR INCREASED ENERGY HARVEST

A Thesis

by

AMULYA KARAVADI

Submitted to the Office of Graduate Studies of
Texas A&M University
in partial fulfillment of the requirements for the degree of

MASTER OF SCIENCE

Approved by:

Chair of Committee,	Robert S. Balog
Committee Members,	Prasad Enjeti
	Haiyan Wang
	Sreeram Vaddiraju
Head of Department,	Costas Georghiades

August 2011

Major Subject: Electrical Engineering

ABSTRACT

Power Electronics Design Implications of Novel Photovoltaic Collector Geometries and Their Application for Increased Energy Harvest. (August 2011)

Amulya Karavadi, B.E, Osmania University

Chair of Advisory Committee: Dr. Robert S. Balog

The declining cost of photovoltaic (PV) modules has enabled the vision of ubiquitous photovoltaic (PV) power to become feasible. Emerging PV technologies are facilitating the creation of intentionally non-flat PV modules, which create new applications for this sustainable energy generation currently not possible with the traditional rigid, flat silicon-glass modules. However, since the photovoltaic cells are no longer coplanar, there are significant new requirements for the power electronics necessary to convert the native form of electricity into a usable form and ensure maximum energy harvest. Non-uniform insolation from cell-to-cell gives rise to non-uniform current density in the PV material, which limits the ability to create series-connected cells without bypass diode or other ways to shunt current, which is well known in the maximum power tracking literature. This thesis presents a modeling approach to determine and quantify the variations in generation of energy due to intentionally non-flat PV geometries. This will enable the power electronics circuitry to be optimized to harvest maximum energy from PV pixel elements – clusters of PV cells with similar operating characteristics.

This thesis systematically compares different geometries with identical two-dimensional projection “footprints” for energy harvest throughout the day. The results show that for the same footprint, a semi-cylindrical surface harvests more energy over a typical day than a flat plate. The modeling approach is then extended to demonstrate that by using non flat geometries for PV panel, the availability of a remotely located stand-alone power system can be increased when compared to a flat panel of same footprint. These results have broad application to a variety of energy scavenging scenarios in which either total energy harvested needs to be maximized or unusual geometries for the PV active surfaces are required, including building-integrated PV. This thesis develops the analysis of the potential energy harvest gain for advanced non-planar PV collectors as a necessary first step towards the design of the power electronics circuits and control algorithms to take advantage of the new opportunities of conformal and non-flat PV collectors.

To my guruji and my family…

ACKNOWLEDGEMENTS

I would like to express my thanks and regards to my advisor, Dr. Robert Balog, for his constant guidance and support which made this work possible. He supported all my ideas, acknowledged all my decisions and guided me constantly to move forward with my research. I am happy to have had an opportunity to pursue my research under his guidance and I am thankful to him for the many things I have learned, during the course of my work.

I would like to thank Dr. Prasad Enjeti, Dr. Haiyan Wang and Dr. Sreeram Vaddiraju for sparing their valuable time in serving on my defense committee. I am also grateful to the entire staff of the Electrical Engineering Department for supporting me during my academic program at Texas A&M University. I am thankful to my research group of Mehran, Samantha, Harish, Poornima and Soma, for their assistance with not only my research but also my academics.

I am deeply indebted to my parents, sister and brother-in-law, whose love, support and encouragement have greatly contributed to the completion of this work. I would like to thank Tejasvi Krishna for his valuable assistance with my research. I am also very thankful to all my friends, Vinuthna, Sirisha and Balakrishna for supporting me throughout my work and for making my stay in College Station a wonderful experience. Last but not least, I would like to thank Aditya for helping me realize my potential and achieve my dreams.

NOMENCLATURE

Az, az	Azimuth (azimuth angle)
BAPV	Building Applied Photovoltaics
BIPV	Building Integrated Photovoltaics
CdTe	Cadmium Telluride
CIGS	Copper Indium Gallium Selenide
DoE	Department of Energy
DSSC	Dye-Sensitized Solar Cells
El, el	Elevation (elevation angle)
ESI	Energy Storage Interface
MPPT	Maximum power point tracking
NREL	National Renewable Energy Laboratories
NSRDB	National Solar Radiation Data Base
PV	Photovoltaics
SUAS	Small Unmanned Aerial System

TABLE OF CONTENTS

CHAPTER Page

Page

LIST OF FIGURES

Page

Page

Page

Page

LIST OF TABLES

Page

CHAPTER I

INTRODUCTION

Motivation for the research

The sun is the single most abundant form of energy on earth and provides over 150,000 terawatts of power per year which is over 6,000 times the projected total energy consumed worldwide in 2035 [1]. Yet less than 1% of the global electrical energy consumption (a fraction of the total energy consumption) comes from a direct photon-to-electron conversion [2]. Fundamental research in material science and energy conversion has led to three generations of photovoltaic (PV) technologies. However, PV, currently in use commercially is still limited to the first generation form-factor, which is a rigid flat-module. The three generations differ from each other, with respect to the main material used to convert the solar energy to electrical energy and also with respect to current state of efficiencies and costs associated with the manufacturing processes. The following sections give the description of each generation of photovoltaic technology.

First generation photovoltaic

The first generations of PV cells were created using crystalline silicon, in either single- or multi-crystalline. While the first generation PV cells have the highest recorded efficiency of the three generations, , the manufacturing cost for these PV cells is also the highest as these PV cells require extremely pure silicon [3, 4].

This thesis follows the style of *IEEE Transactions on Power Electronics*.

Second generation photovoltaic

This generation uses less silicon, or none at all in the PV module. The result is lower cost compared to first generation cells but also lower energy conversion efficiency. Conversion efficiency is defined as the percentage of solar energy falling on the cell that is converted to electric energy. Technologies that belong to this generation are most frequently associated with thin film PV cells, designs that use minimal materials and less costly manufacturing processes. The most popular second generation PV cells are copper indium gallium selenide (CIGS) PV cells, cadmium telluride PV cells, amorphous silicon PV cells, and micromorphous silicon PV cells [3, 4].

Third generation photovoltaic

Third generation PV cells, which remain in the research stage, are sought after to achieve the best of both prior generations. The primary reason was to make PV cells cheaper without having to compromise on its efficiency [3]. This generation aims to use non-toxic and abundant material for energy conversion. Some of the third generation PV cells include polymer PV cells, dye-sensitized PV cells, and hybrid PV cells among others [3]. The first generation technology efficiencies are limited by Shockley–Queisser criteria, which states that "cell that consists of a single p–n junction, generates just one electron–hole pair for each incoming photon, is exposed to un-concentrated sunlight, and wastes as heat any incoming photon energies in excess of the semiconductor band gap, can achieve a maximum efficiency of 31%" [5]. This third generation photovoltaics are trying to overcome this limit by violating one or more of the Shockley–Queisser criteria and attain efficiencies greater than first generation photovoltaics [5, 6].

A review of the PV cell fabrication literature shows that the state-of-the-art silicon (first-generation) and thin film (second-generation) PV can attain efficiencies of ~25% [7-9] and 19.4%, [10-14] respectively, but are cost-prohibitive for terrestrial use. The drive to lower the cost of fabricating PV such as roll-to-roll processing [15] and printing led to the development of third-generation PV (e.g. polymer inorganic nano-particle PV [16-18] and dye-sensitized solar cells or DSSCs [19]). The current and predicted efficiencies vs. costs for various generation technologies are summarized in the Figure 1.

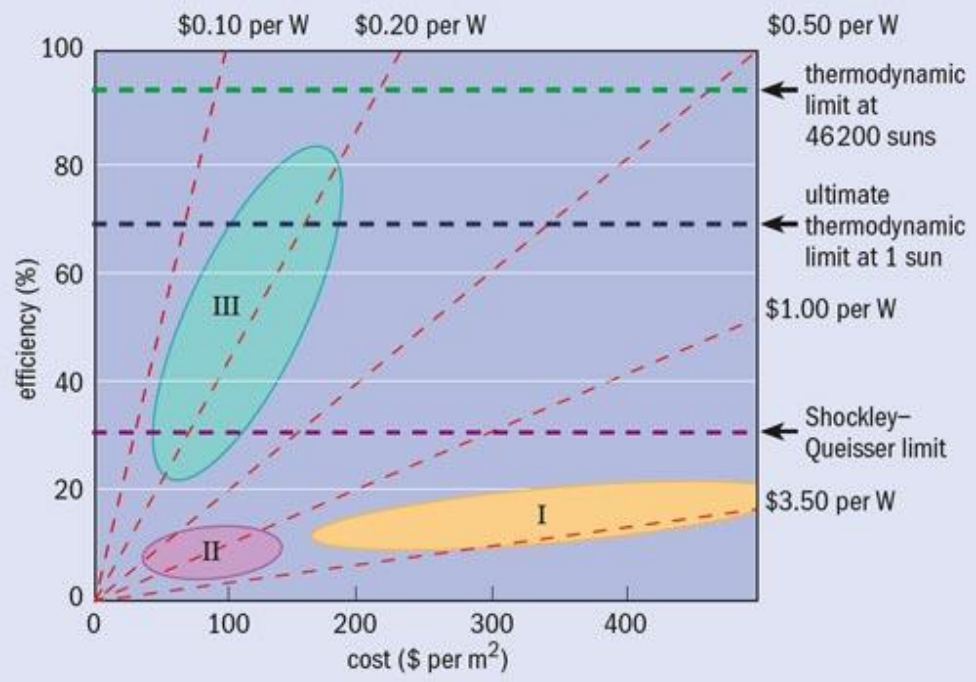

Figure 1: Comparison of predicted efficiencies of various generations of PV modules [5]

It can be seen from the Figure 1, that, to obtain higher efficiencies and lower costs, PV technology is moving towards third generation technologies, which means PV module need no longer be a flat panel because of the limitations imposed by traditional silicon-based technologies which are unable to be flexed or molded but there is more flexibility in the module. An inorganic-organic hybrid PV cell can now be fabricated on flexible substrates will give rise to arbitrary geometries for applications previously not possible, as shown in Figure 2. Conformal coating the PV cells to the body material of small aircraft can create supplemental energy and reduce the fuel payload and extend the mission run time, an important advantage for military (small unmanned aerial system, SUAS) and non-military uses (autonomous aircraft for disaster recovery). Similarly, personal energy generation requires conforming “solar fabric” that can be woven into clothing or embedded into shelters.

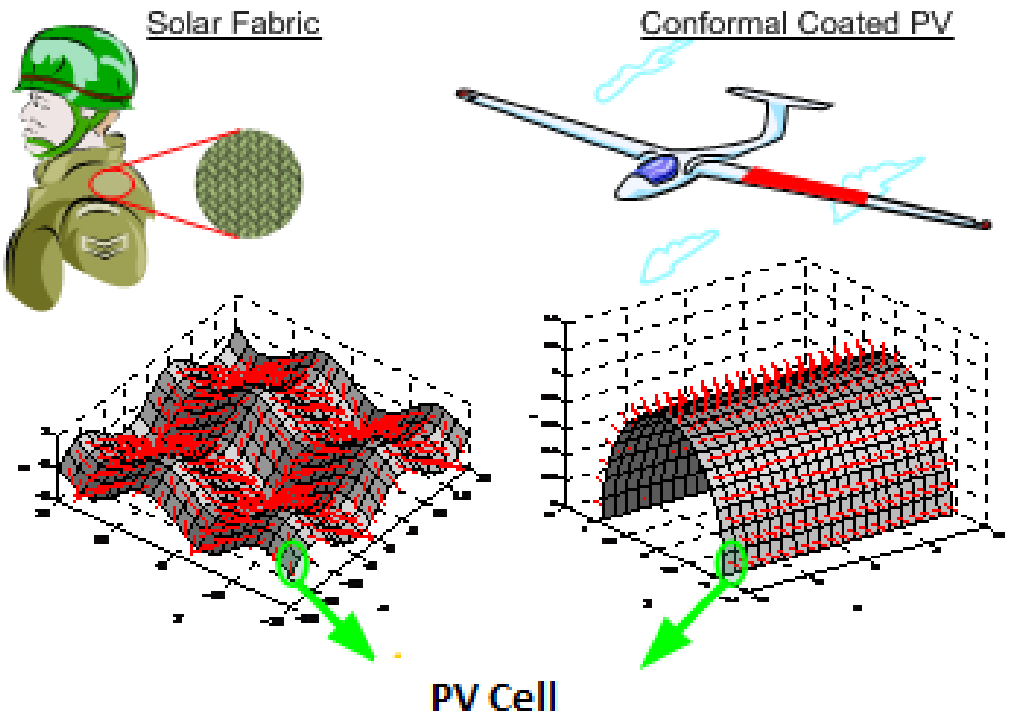

Figure 2: Conceptual vision: flexible / conformal next-generation photovoltaic energy systems examples

If we consider the current state of research in the field of PV systems, all the research that is being done is geared towards reducing the costs associated with it. Department of Energy (DoE) of United States has identified area of technological improvements [20] in a PV system, the specific changes that can be made to improve performance, increase reliability, or reduce cost of components and other elements of installed system cost and came up with the following table shown in Figure 3. It can be seen that for PV modules the research is geared to increasing the module efficiencies and reducing the costs.

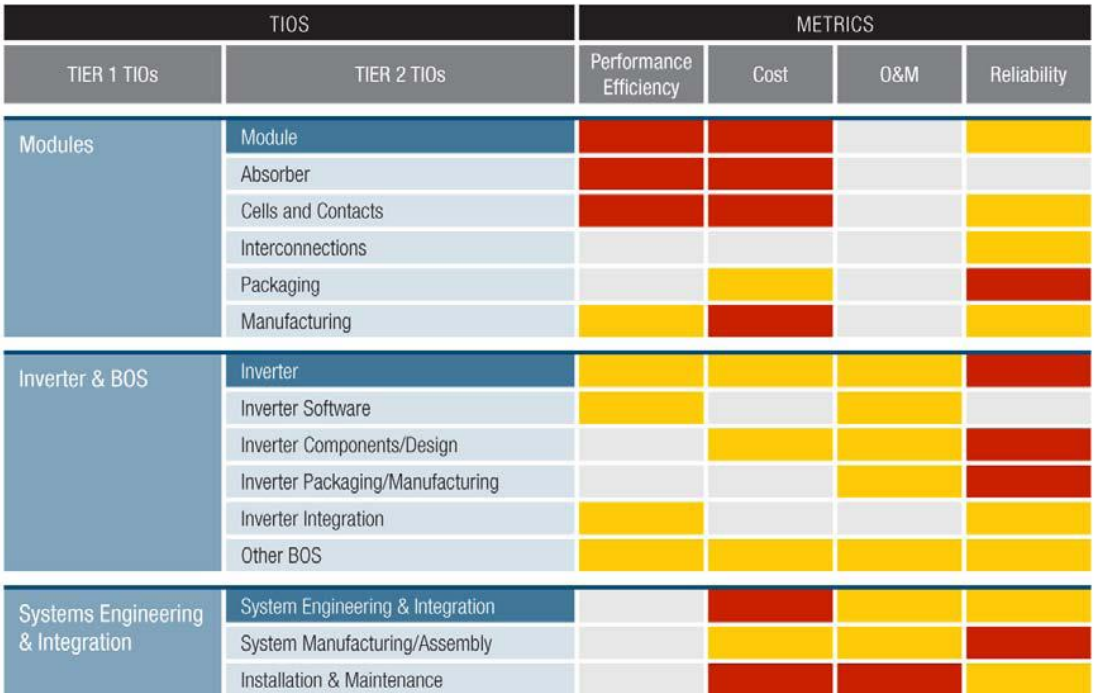

Figure 3: Areas of research identified and funded by DoE [20]

Also, if the general trend of PV module prices are considered, the Figure 4 from Solarbuzz Market research indicates that, the prices are consistently falling since 2001 and they have tendency reduce in future making PV more affordable [21]. The reasons for the reduction can be associated with various factors like, research progressing towards increasing efficiencies, increasing trend towards using second and third generation PV modules and also economies of scale owing to ubiquitous use of PV for various applications like solar fabric, building integrated photovoltaics (BIPV), building applied photovoltaics (BAPV) etc., The distinction is building applied PV is a retrofit

added to the building long after construction is done, while building integrated PV means the architects, building designers, building owners designed the photovoltaics into the skin and roof of the building from day one.

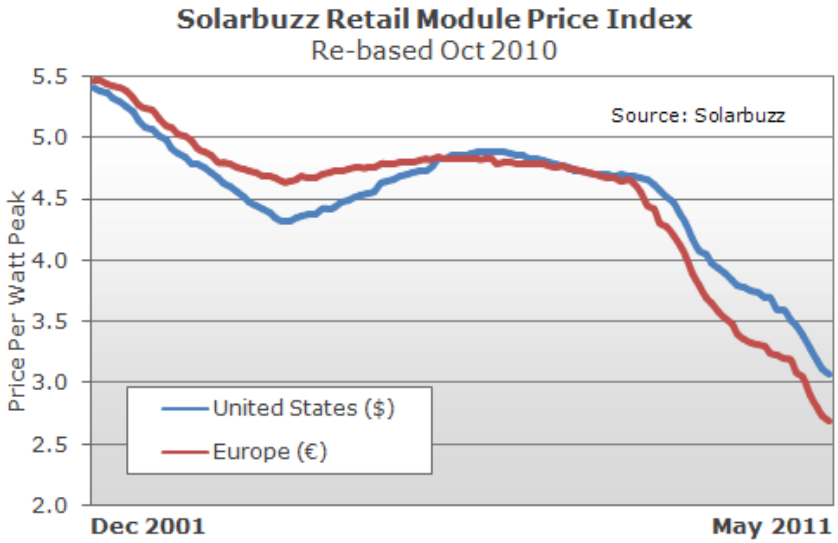

Figure 4: Trend of PV module price [21]

It can be concluded from the above discussion that PV modules will likely be flexible as new generations of technology are commercialized. One important factor that needs to be considered as technology progresses towards flexible PV is the efficient power conversion and usage of it for various applications i.e. the power electronics aspect of it.

Significance of the research

The commercially available PV cells are flat and the entire panel is either completely exposed to light or not, except when there is shading on certain portions of

the panel due to clouds or buildings. Emerging PV technologies like thin film technologies [22], organic PV [23] and building integrated photovoltaics BIPV [24] etc., the capability to use geometries different from flat plate exists, but in doing so, we must consider the effects of shading and other mis-match due to inherent geometry itself. As understood from past research, shading on a PV panel can drastically reduce the performance of the whole system [25].

The low electrical power density in photovoltaic cells requires a large surface area to collect and convert incident solar radiation (insolation) into electricity. To ensure maximum efficiency, the direct-beam radiation (the dominant energy) must be normal to the incident surface [26] such that view factor [27] is maximized, which is why mechanical tracking systems are often used in high-performance systems. Non-planar geometries offer new opportunities for conformal and flexible PV modules as illustrated in the solar fabric and conformal examples in Figure 2 but have significant implications for the cell interconnection and power electronics needed to collect and convert the electricity generated to a useful form. This is because, in non-flat PV modules the surface normal vectors need not be aligned with the direct-beam insolation which creates varying view factor i.e. the average area of the surface that is effectively exposed to sun, creating gradients in total incident solar radiation (insolation) across the surface of the module. This causes non-uniform current density, leading to locally circulating currents which reduces efficiency if not managed properly. Figure 5 shows the electrical characteristics of a typical PV cell. Although the short-circuit current is proportional to the insolation, the actual operating voltage and current, it depends on how the cell is

interconnected to other cells. Series-connecting the PV cells, which is the customary configuration used to built higher voltage, forces the current in each cell to be identical, thus the bypass diode in the simplified circuit model (the simplified model neglects resistance terms that contribute to the slope at the *x* and *y* intercept) must conduct the difference in current between the cells with the highest illumination and the lesser-illuminated cells. Since this necessarily means that the diode is forward biases, the results is losses and "hot spot" internal heating of those cells. Thus, the power generated by *n* series-connected cells is limited by cell with the least illumination as in the case of the cell pointed farthest from the sun. The most comprehensive method to ensure maximum energy harvest is to provide an individual power converter for each cell[28] but this is not cost effective in general and not feasible when considering nanostructured cells. Thus a solution to maximize the energy harvested while minimizing the number of the power electronic devices required.

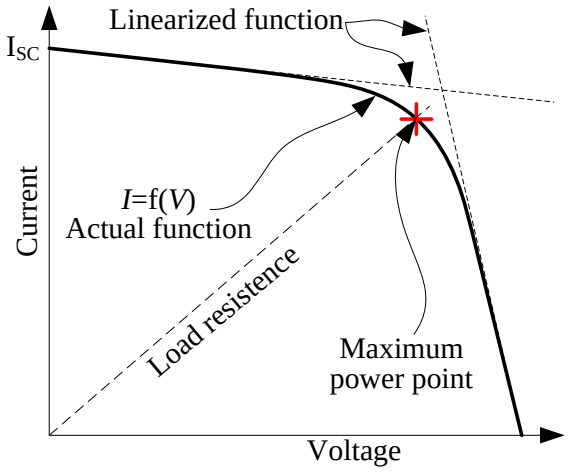

Figure 5: Electrical operation of a PV cell.

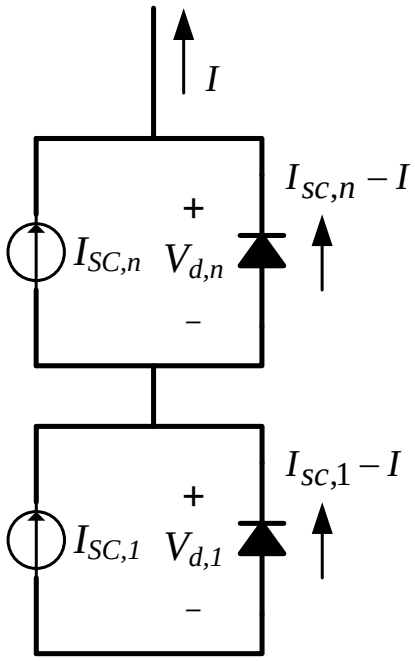

Figure 6: Simplified electrical model of a PV cell

Concept of pixelization

To minimize the number of power electronic devices required and to maximize the energy harvest, it is required to group together PV cells with homogenous thermal and electrical operation characteristics. This group of cells need not be physically adjacent to each other. Such a group can be called a *pixel*. When the module is partitioned into pixels with minimized variation in current density of the cells comprising the pixel, each pixel can generate different currents which limit the ability to arbitrarily interconnect these pixels (such as the common series-connection) without adding bypass diode or extra circuitry. Thus the concept of pixelization is to identify homogeneous or nearly homogenous cell to be grouped into a cluster and treated as one

generation unit. Once the pixels are identified, the specifications for the power electronics interface can be developed and the converter topology, and control algorithms can be designed.

To be able to optimize the required power electronic circuitry to efficiently convert the energy, the variations in the generation of currents in each pixel need to be understood which depends on the amount of insolation falling on the pixel. But this varies from pixel to pixel because not all parts of the surface are exposed to sun light at one point of the day. The average area that is exposed to sunlight is given by the term called view factor of the surface. This when multiplied by the area of the cell and the direct insolation at that point of day results in the insolation on that cell. Thus, to understand the variations in the capture of insolation by a PV geometry, and from there, to understand the variations in the generation of currents across the entire surface, it is required that the variations in the view factors across the surface be understood. These variations in the insolation capture across the surface can be then used to get the *v-i* characteristics of the cell. Once this variation is obtained, this information will form the basis for a power electronics design engineer to design the appropriate circuitry to maximize the energy generation. The following flow chart in Figure 7 depicts the process that formed the basis for this research.

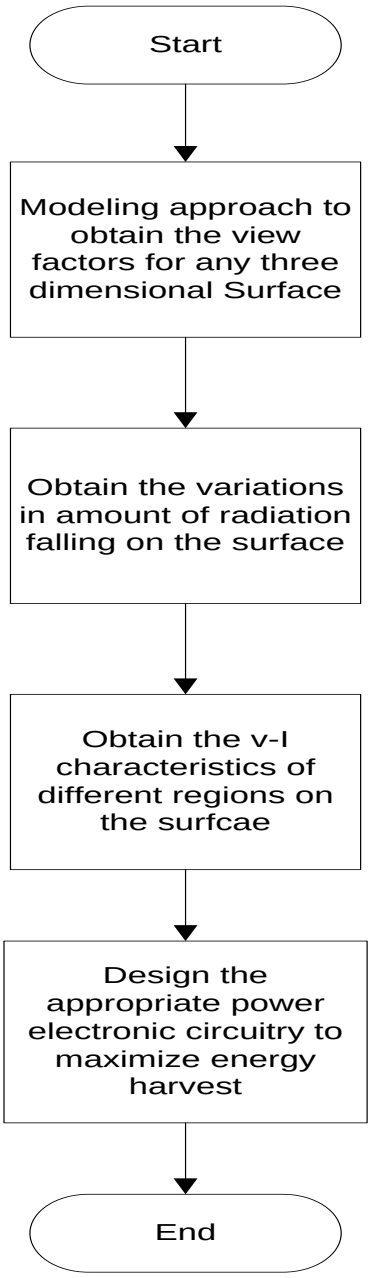

Figure 7: Flow chart to illustrate the significance of research

This thesis presents a modeling approach to understand the variations in the energy capture owing to complex geometries of PV panel that can be used in various applications and be in a position to design better power electronics circuitry to maximize

this energy harvest. Implicit in this thesis is the assumption that one day PV technology will be at such a low cost that the cells no longer dominate system cost. If PV is abundantly and economically available, with the emerging PV technologies, we have the opportunity to harvest more energy by using geometry different from flat panel, depending on the application.

The thesis presents modeling approach to calculate the view factors for various geometries like semi-cylinder, cylinder, and hemisphere, sinusoidal and wavy geometries to calculate the effective amount of insolation falling on the surface. The thesis presents a comparison of the effective energy capture to draw conclusions about which geometry captures more energy and to what applications can it be effectively used. The thesis also uses a electrical model [29] to calculate the availability of a autonomous, stand-alone, power system to supply electricity to a remote unattended load and proves that using a non flat geometry for a PV module instead of a flat PV panel, for a given footprint , there is increase in the availability of the system and thereby reducing amount of storage required.

Previous work

Previous power electronics work in this area has focused on designing efficient power electronic converters for minimizing the shading effect and maximizing the energy harvest by coming up with novel Maximum Power Point Tracking (MPPT) algorithms only for flat panels. The idea of MPPT is not new, but still every year numerous research papers are being published advancing towards better and faster techniques. To date the count of research papers on MPPT in photovoltaics (PV),

appearing in IEEEXplore database, is around an impressive total of 300 [30]. The Ref. [31-34] have made a comprehensive study of various MPPT algorithms for grid connected and isolated photovoltaic systems which include Constant Voltage (CV) and Constant Current (CV) techniques. The review of existing MPPT techniques can be broadly categorized into two areas, improved topology based and improved algorithm based. Improved topology based MPPT techniques [35-39] use a basic MPPT algorithm like perturb & observe (P&O) or incremental conductance (InC) but the converter topologies are evolved into superior architectures to make the conversion system independent of shading effects. Improved algorithm based techniques use variable step size strategy [40-43] which is not practical for rapidly fluctuating environmental conditions. Various other MPPT techniques were proposed in literature [30, 44-47] to include rapid variations in conditions. Also researchers have discussed multiple input DC-DC converters for renewable energy systems [48-50]. These topologies are useful in taking input from a set of panels and using a single converter to maximize the power.

Another interesting research topic that is going on is in the field of AC- PV modules [51-56]. An AC-PV module is a photovoltaic module with an integral DC to AC inverter which have advantages over central inverter systems-the main ones being a low minimum system size (and hence a low barrier to market entry) and the ability to site individual modules without concern for shading and orientation. Reliability studies of a PV system have shown that PV inverter is the least reliable component and needs to be replaced at least twice during the 25 years life time of PV modules [57-61]. To improve the reliability of the PV system microinverters are being used in PV systems.

Microinverters have become the trend for future PV system development due to many reasons including (1) improved energy harvest; (2) ease of expandability; (3) lower installation costs; (4) “Plug-and-Power” operation; and (5) modular design with high economies of scale potential [62-64]. Also various high efficient PV-Power converters have been proposed to improve the efficiency and reduce the costs associated with the PV systems [65-68]. This entire research is based on the assumption that panel is flat and there is shading only due to clouds and buildings. However as the technology is progressing towards flexible PV it is up to power electronic engineers to start designing more efficient power electronic circuitry to mitigate the shading effects due to inherent geometry itself.

Thesis organization and chapter summaries

The thesis is divided to seven chapters and the subsequent sections provide chapter summaries for each chapter.

Chapter I Introduction

This chapter outlines the motivation for the research and also the significance of the research presented in this thesis.

Chapter II Problem definition

This chapter defines the problem statement which led to the development of this thesis. It also describes the various concepts involved in formulating the problem statement.

Portions of Chapter III, IV and V have been published in [69].

Chapter III Modeling approach

This chapter outlines the modelling approach adopted to get the view factor of various surfaces at every hour of the day as the sun moves across the horizon. It outlines the step by step apprach used to calculate the view fcators of various geometries.

Chapter IV Validation of the approach

This chapter validates the view factors obtained for various surfaces using mathematical analysis. It validates the view factors obtained for flat panel with the theoretical equation already present in the literature. To validate the view factors for other complex geometries the chapter outlines the mathematical approach and proves that view factors obtained are accurate.

Chapter V Application: Increased energy harvest

This chapter systematically compared various geometries and states few applications where various geometries can perform better than a conventional flat plate. It concludes that for applications where energy capture must be high during early morning and evening hours a cylindrical or semi-cylindrical geometry can be used. And in the applications where consistent energy capture is required a solar panel of hemispherical geometry would be ideal.

Chapter VI Application: optimizing energy availability to autonomous stand-alone power system

This chapter presents, how this modeling approach can be used to prove that, for an autonomous power system supplying power to a remotely unattended load like a sensor, the availability of the system can be increased by using a non flat geometry. This

chapter outlines the usage of stand-alone power system and their applications, presents a stand-alone system model described in the literature [29] , applies the modeling approach to calculate the availability of the same system if a non flat PV module is used and proves that indeed the availability can be improved and storage can be reduced.

Chapter VII Conclusion

This chapter presents the conclusion for thesis and also the future work that can be taken up, once the view factors for the surface that is in study are obtained how they can be used to design the efficient power electronic circuitry.

CHAPTER II

PROBLEM DEFINITON

The conventional solar panel is flat and rigid because of the limitations imposed by traditional silicon-based technologies which due to the brittle nature of silicon wafer are unable to be flexed or molded. Until now, the research in the field of photovoltaic energy conversion has been broadly divided into two areas. The first is area where material scientists are continuously striving to increase the efficiency of the cell, and also discovering new techniques to reduce the usage of silicon to reduce the costs. The other area is the electrical engineering field to model power electronic circuitry to maximize the energy generation using novel MPPT control algorithms, to use novel topologies for converter circuits etc., all the research in the field of electrical engineering is based on the assumption that the solar panel is flat and the generation of current is constant across the panel unless there is a shading on the panel. But with the emerging PV technologies from second and third generation, the PV module is no longer flat and rigid, it can molded to any desired shape and geometry based on the application. For building integrated photovoltaics (BIPV) applications it can become a semi-cylinder for windows and walls, or a roof top shingle. In other applications it can be woven into fabric for uniform, tents, sunshades and other applications. This necessitates the need to explore various opportunities for usage of PV as well as issues and problems that may become hindrance to its ubiquitous usage. One of those problems would be the appropriate design of power electronic circuitry for these PV modules.

View factor of a surface

For a given flat PV module, the total surface area that is exposed to any source of light is a factor of a cosine angle, the so called view factor of the surface. View factor can also be defined as the average area of the surface that is effectively exposed to light; the projection of the surface onto a plane that is perpendicular to the direct-beam light source. The concept of view factor is significant and has been in use for a very long time in of the study of heat transfer. Heat transfer is classified into various mechanisms, such as heat conduction, convection, thermal radiation, and phase-change transfer. For solar energy, the transfer of heat through thermal radiation from sun to the PV module placed on earth is considered.

Heat transfer by radiation occurs in any transparent medium, even occurs across vacuum (that is how sun heats the earth). Heat transfer by thermal radiation is the transfer of energy by transmission of electromagnetic radiation described by black body theory [70]. The amount of radiation falling on the surface is dependent upon its view factor which is also known as configuration factor, form factor or shape factor. In radiative heat transfer, a view factor $F_{1\to 2}$ is the proportion of all that radiation which leaves surface A_2 and strikes surface A_1.

To get an idea of what constitutes the view factor of a surface consider the Figure 8. For a simplistic case, the heat transfer theory calculates the view factor between two differential areas at a finite distance is shown:

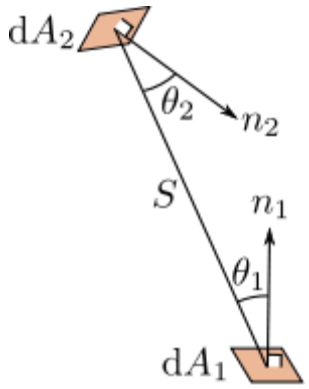

Figure 8: Two differential areas in arbitrary configuration

Taking the limit of a small flat surface gives differential areas. The view factor of two differential areas of areas dA_1 and dA_2 at a distance S is given by:

$$F_{1\to 2} = \frac{\cos\theta_1 \cos\theta_2}{\pi S^2} dA_2 \qquad \text{Eq.1}$$

where θ_1 and θ_2 are the angles between the surface normals and a ray between the two differential areas [71]. View factors for arbitrary surfaces may be calculated by integrating differential view factors over the desired surfaces. But for surfaces at almost infinite distance like surface on earth and sun, the view factor may be obtained by taking the ratio of the projected area of the surface and the actual area of the surface as observed by sun from its position [72]. Thus it can be understood that to get the view factor of a surface with respect to the sun, it is required to obtain the position of the sun in the sky at that particular time, the angle of the surface with its normal and also the angle with respect to the sun. This is obtained by taking the cross product of the normal vector of the surface and the position of the sun in the sky.

Position of the sun

The position of the Sun in the sky, relative to an observer on Earth, at any point of the day, is defined by its altitude angle α (solar elevation angle) and its azimuth angle Ψ as shown in Figure 9.

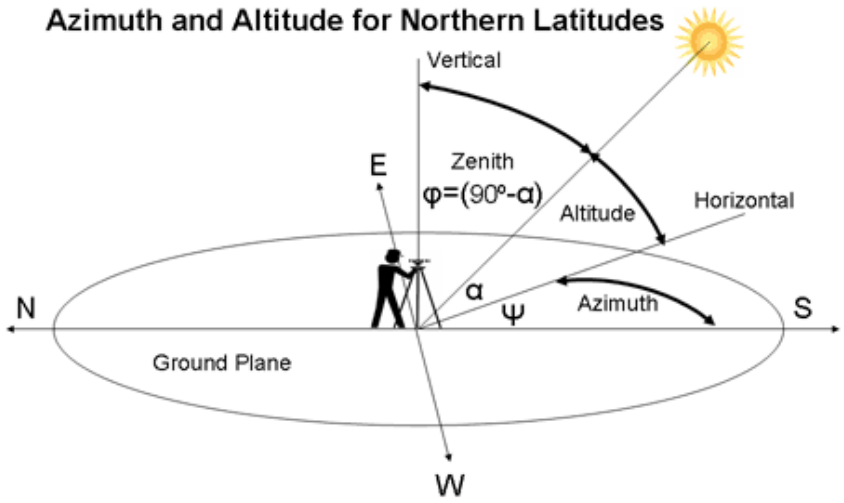

Figure 9: Angles describing the sun's position [73]

Altitude: The solar altitude is the vertical angle between the horizontal and the line connecting to the sun. At sunset/sunrise altitude is 0 and is 90 degrees when the sun is at the zenith i.e., when the sun is directly overhead. The altitude relates to the latitude of the site, the declination angle, which is the angle between the earth-sun line and the equatorial plane and the hour angle which is the angular distance that the earth has rotated.

Azimuth: The azimuth angle is the angle within the horizontal plane measured from true South or North.

Problem definition

For a flat horizontal surface, at any given time of the day and day of the year the entire surface is at a certain angle to the sun. The view factor at any point on the surface is constant for a flat plate and can be computed with well-known methods and equations which are defined in Chapter III, hence we can determine the effective area that is exposed to sun and what would be the amount of insolation falling on it. This would in-turn let us know how much energy would be generated and will allow us to design the specific power electronic components for it.

New flexible PV technologies enable BIPV and other PV applications which are intentionally non-flat. When the surface is no longer flat, the view factor is not constant and it differs at various points on the surface depending on the geometry. When the view factors are different across a surface, the amount of direct-beam solar radiation incident on a particular section will vary, thus the amount of electrical energy generated will be different at various portions of the surface. If the surface does not generate uniform currents, the result is a gradient of current density which could lead to locally circulating currents that can cause hot-spotting and other deleterious effects. Electrically isolating regions can create individual PV cells, but simply connecting these cells in series / parallel combinations presents a maximum power point tracking problem. Thus there is a need to understand these variations in generation of electricity in order to be able to develop the power electronics circuitry and controls to maximize the energy harvest.

To calculate the view factors for a flat panel the literature provides the required equations but same is not the case for non flat geometries. The calculation becomes

complex because the sun moves in two direction both vertical and horizontal and each time the view factor of the each part of the surface ahs to be calculated. This necessitates a modeling approach which can easily and quickly calculate the view factors across the entire surface, for any given geometry, with respect to sun. This thesis presents results from a study which applied view factor and ray-tracing techniques to quantify the insolation on a non-flat PV surface. The technique is first applied to a flat panel to verify the accuracy of the approach and then to a variety of surfaces including semi-cylinder, cylinder, and hemisphere which represent a regular pattern with variation in two dimensions and then to a wavy geometry with variations in 3 dimensions which is representative of a fabric-like surface.

CHAPTER III

MODELING APPROACH

This chapter outlines the step by step modeling approach adopted to get the view factors of various non flat geometries of PV panel.

MATLAB based modeling approach

The view factors obtained from this modeling approach are used to calculate the amount of insolation that is falling on each cell on the surface and thus the amount of electricity that is generated. This generation of electricity would not be uniform since it will be shown that the view factor of the surfaces will not be uniform across the entire surface. This research represents a first step in understanding the implications of non-flat PV surfaces for power electronics and energy harvest. The continuation of this research would be to get this matrix of insolation falling on each cell and generate the *v-i* characteristics of the cell and then design the power electronic circuitry. To facilitate this further research for which MATLAB would be an ideal environment, MATLAB was chosen for the modeling approach. The following block diagram in Figure 10 summarizes how this work will be taken forward and shows why MATLAB became the choice of environment.

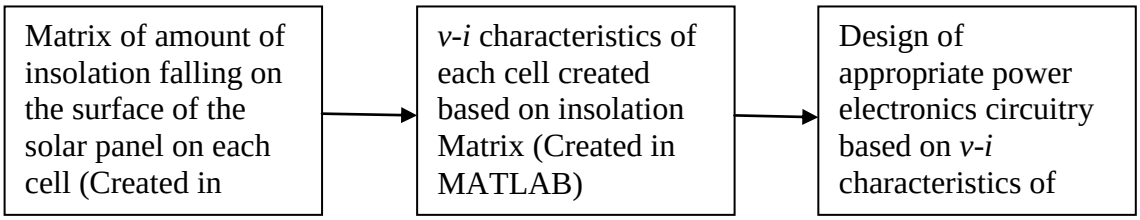

Figure 10: Block diagram explaining the choice for MATLAB as environment

Creation of various non flat PV geometries with normals on each cell on the surface

To demonstrate the non flat PV panels and their geometries various surfaces representing a solar panel were needed to be created. MATLAB Environment has range of functions available to create three dimensional surfaces using its graphics objects. To demonstrate the increasing complexity of the geometries first a flat panel is created and various other geometries like semi-cylinder, cylinder, hemisphere, sinusoidal geometry and a wavy surface representing a solar fabric are created. To create these surfaces `surf(X, Y, Z)` function of MATLAB is used. `Surf(X, Y, Z)` creates a shaded surface using z as surface height. **X** and **Y** are vectors or matrices defining the *x* and *y* components of a surface. **X** and **Y** are vectors, if length(X) = n and length(Y) = m, then [m,n] is the size(Z). These **X**, **Y** and **Z** become different for different geometries and as the complexity of the surface increases these **X**, **Y** and **Z** components become complicated to calculate. The thorough understanding of this function and its algorithm was required to create such complex geometries in MATLAB. The MATLAB programs to create these surfaces are presented in APPENDIX A under the Chapter III section. These surfaces are meshed to represent a single solar cell in all the surfaces. Figure 11-16 are examples of three dimensional surfaces created to

represent possible geometries of non-flat PV modules and are presented in the increasing complexity of their surface geometries. These geometries are created to give an idea of how these can be constructed in MATALB. The dimensions of these surfaces can be scaled according to the requirement. For the calculation of view factor the normalized surfaces with unity dimensions are constructed. View factors take into the effect the shape of the geometry and not the dimensions. The area required is given by the user and is a variable. View factors obtained are universal for that particular geometry. Also the gray color for surfaces is chosen arbitrarily, but in coming sections the color is varied according to the view factor variation.

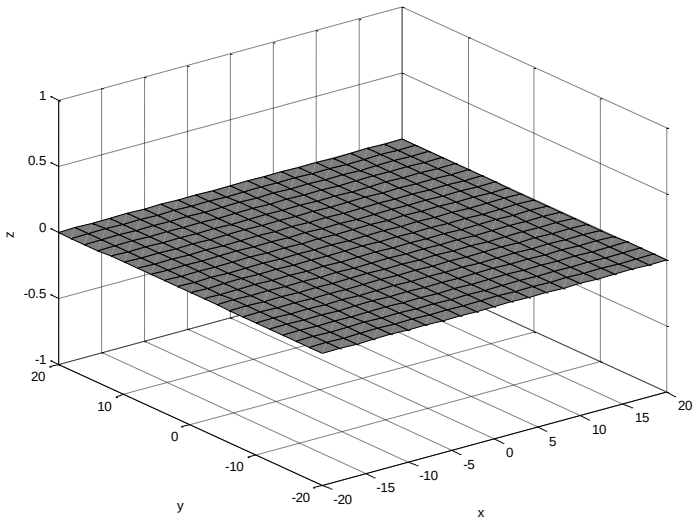

Figure 11: Flat surface modeling a conventional flat solar panel

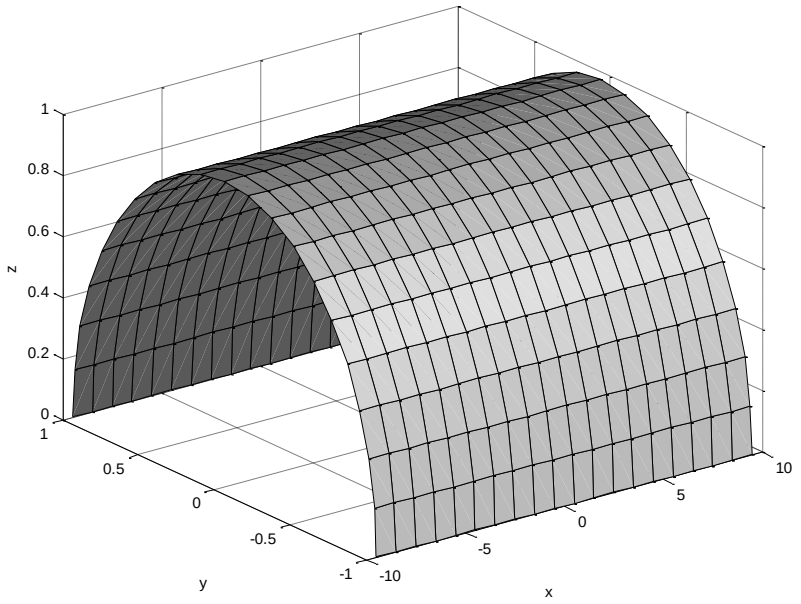

Figure 12: Semi-cylindrical surface

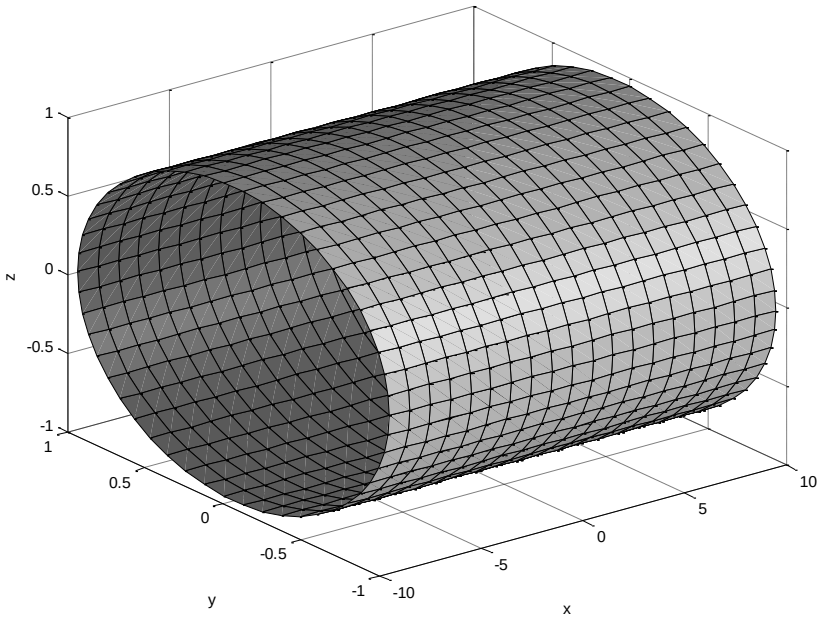

Figure 13: Cylindrical surface

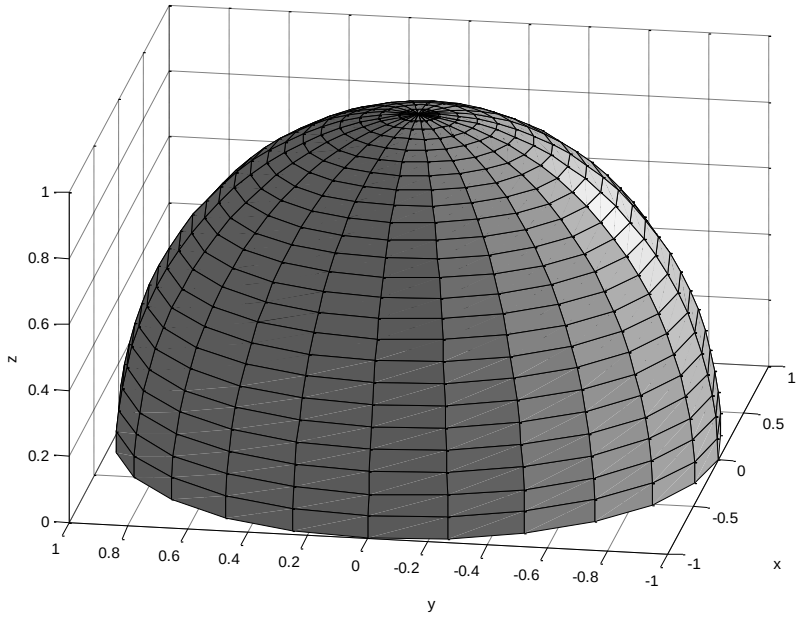

Figure 14: Hemispherical surface

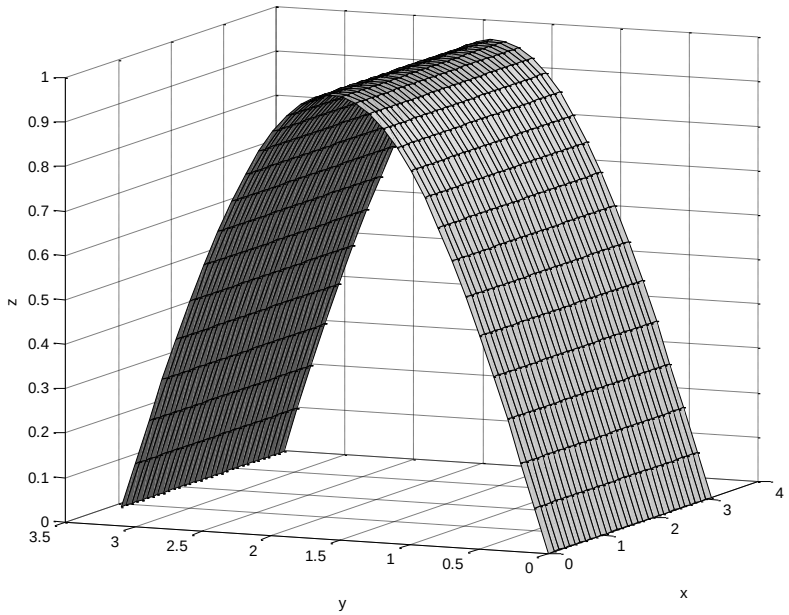

Figure 15: Sinusoidal surface

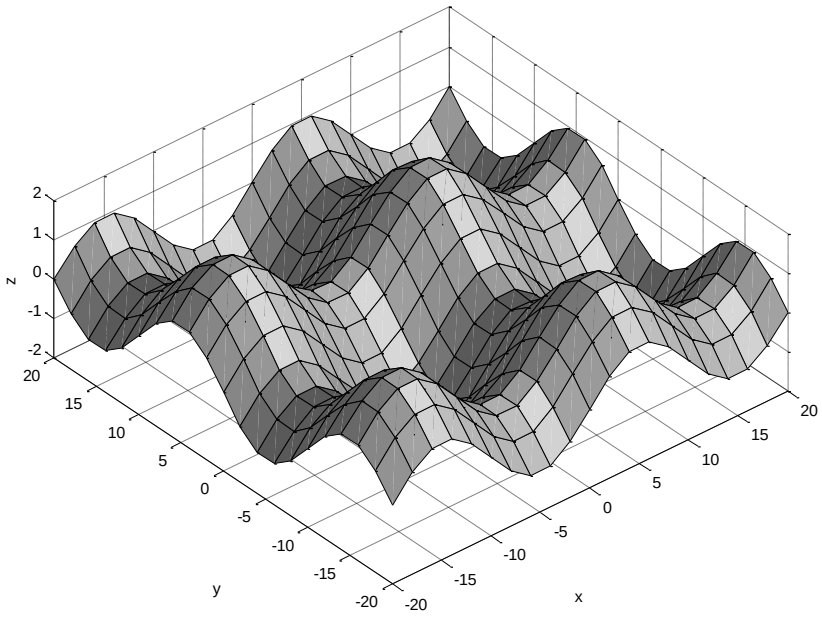

Figure 16: Wavy surface representing a solar fabric

Creation of normal vectors on each cell of the surfaces

Conventional solar panels being perfectly flat all the normal vectors to the individual cells were at same angle to the sun at any point of the day. But since solar fabric has a wavy geometry the cells on it have normal vectors pointing at different angles to sun at a particular time of the day. To demonstrate this, the surfaces that were created were meshed to represent the cells and normal vectors to each of these cells at the centre of the cell were to be created. MATLAB has as a function `surfnorm`() to draw normals at the vertices defined by a surface, but since normal vectors were needed to be drawn at the middle of the surface another invisible surface with the vertices shifted to the middle of the original surface was created and normals to that surface

were drawn to satisfy the requirement. The figures below show the normals on various surfaces:

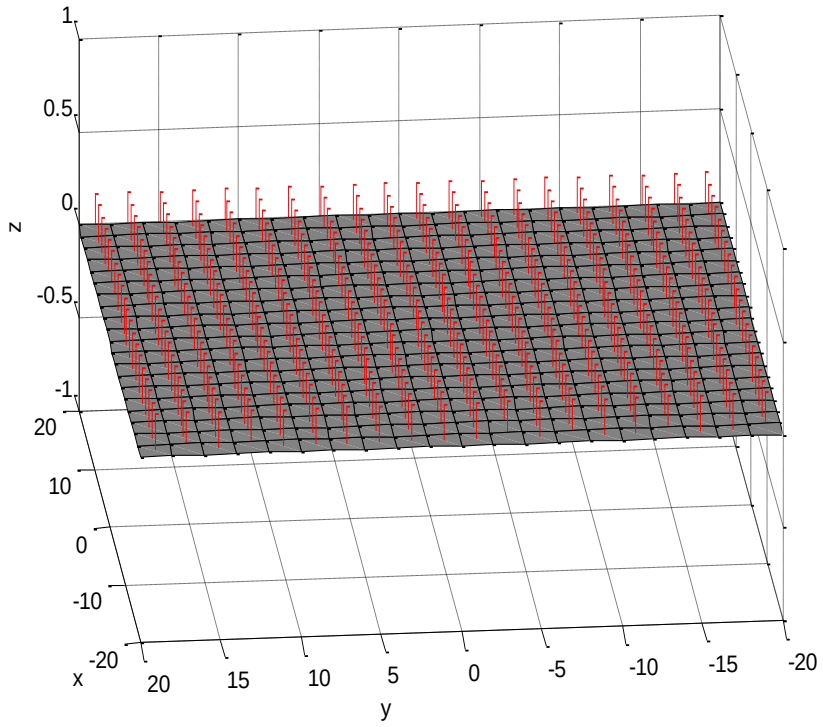

(a)

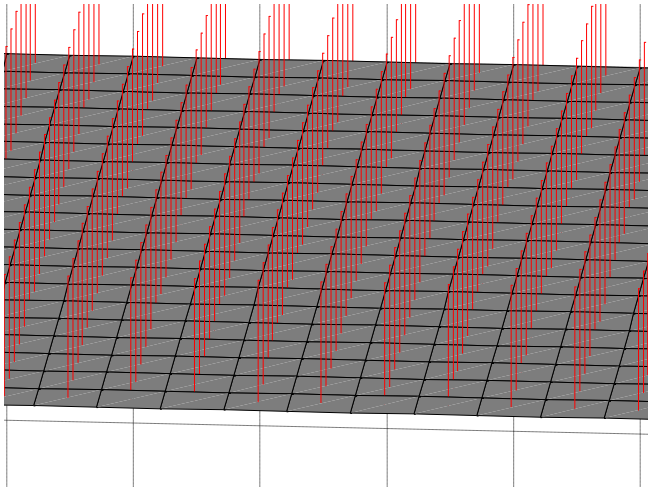

(b)

Figure 17: a) Flat surface representing a conventional solar panel with normals on each cell b) Zoomed in version.

For flat plate shown in Figure 17, comprised of individual cell elements the normal vectors for each cell are pointed in the same direction. So the view factors of each cell would be equal and thus the amount of insolation falling on any part of the surface would be equal. For a semi-cylinder shown in Figure 18, each row of cells has the same surface-normal vectors, but variation exists from row-to-row. Thus the view factors for each row would be same and also the amount of insolation, but from row to row insolation would vary and thus the amount of electricity generated. Similar is the case for cylindrical surface shown in Figure 19. Here it should be noted that the area of each cell is same.

But for the hemispherical surface shown in Figure 20, it should be observed that area of each cell for a hemisphere is reducing as the surface is traced towards the top, and also view factors of each cell are now different depending upon the area of the cell and the direction of sun, thus the view factors are more haphazard and are becoming unpredictable. For the wavy surface in Figure 21, there could be little-to-no regularity of adjacent or proximal cells with essentially random variations of adjacent cells. Clearly a single view factor does not exist for the entire PV surface. And thus this necessitates an approach to get these view factors and understand the variations in generation of electricity across the surface. The next step is to develop a program which will calculate the view factor of each cell that is meshed with respect to the position of the sun at given point of the day which is presented in the next section.

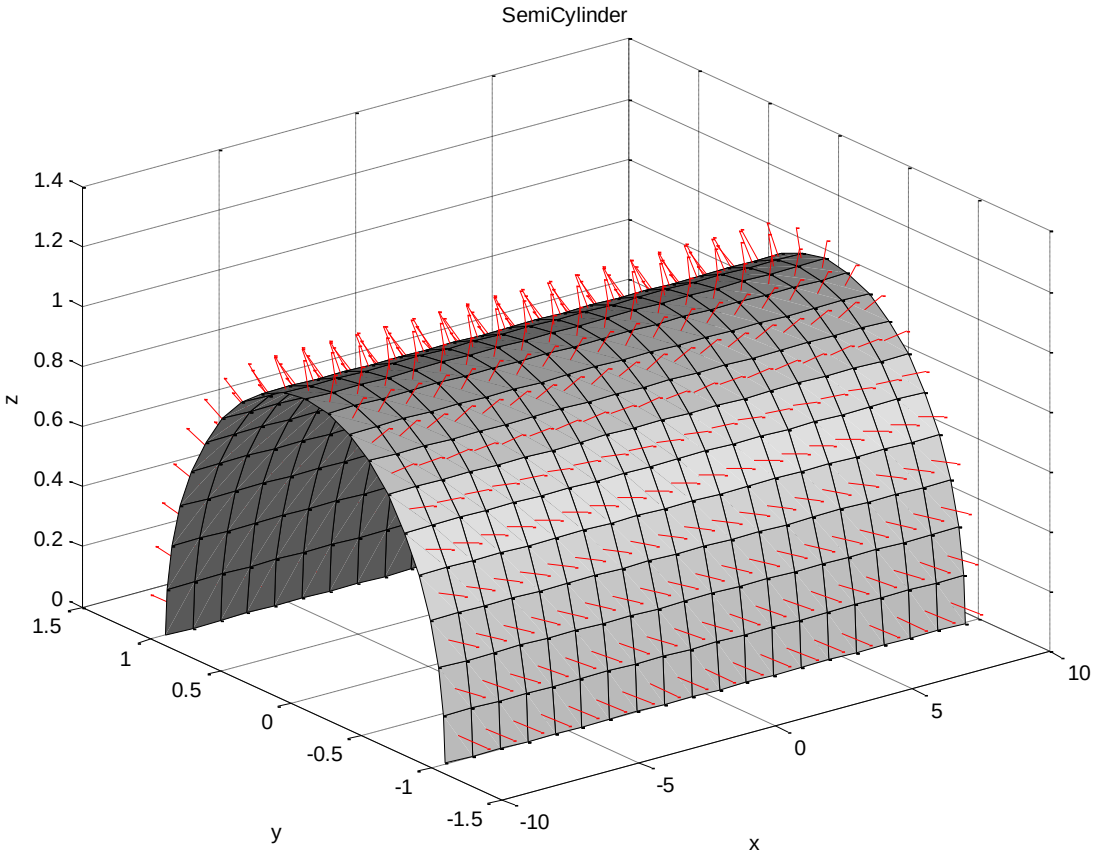

(a)

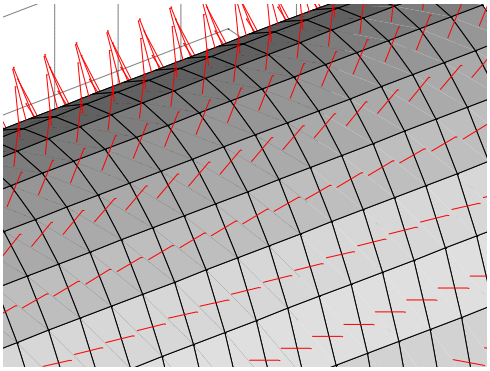

(b)

Figure 18: a) Semi cylindrical surface with normal vectors on each cell b) Zoomed in version

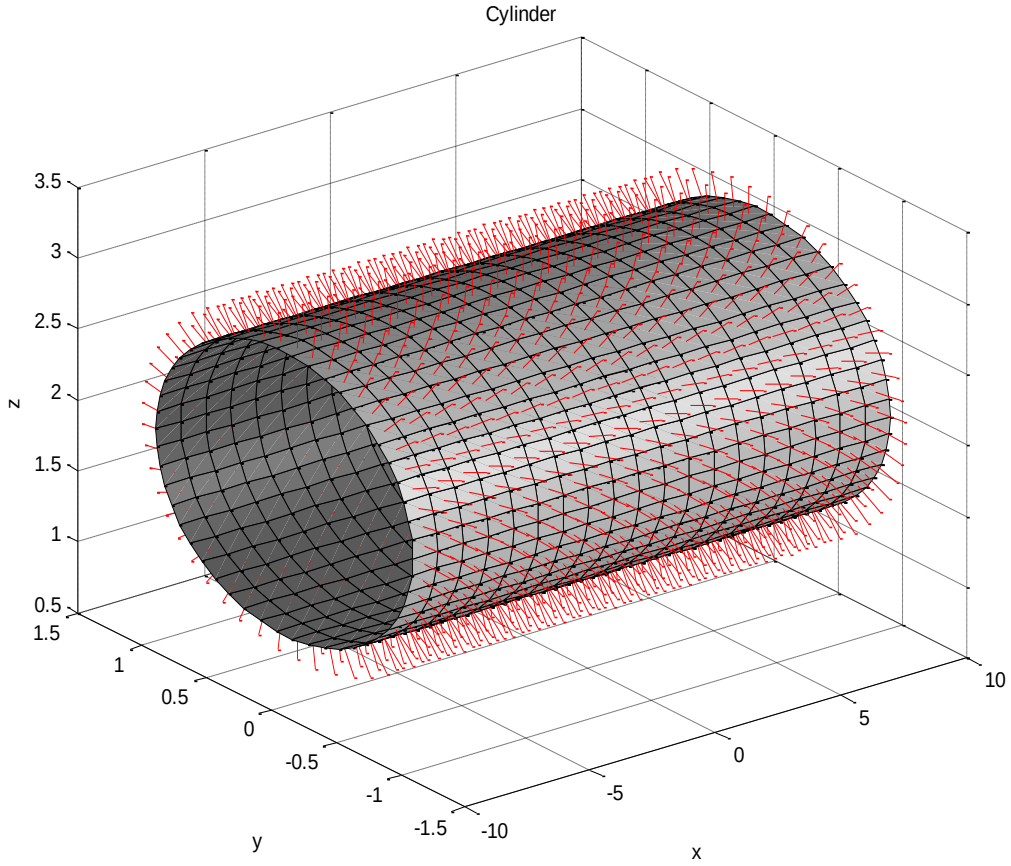

(a)

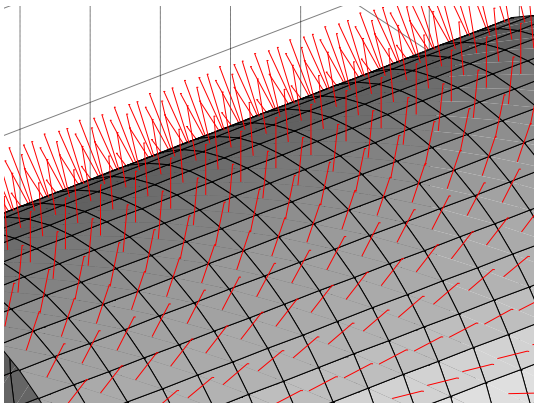

(b)

Figure 19: a) Cylindrical surface with normal vectors on each cell b) Zoomed in version

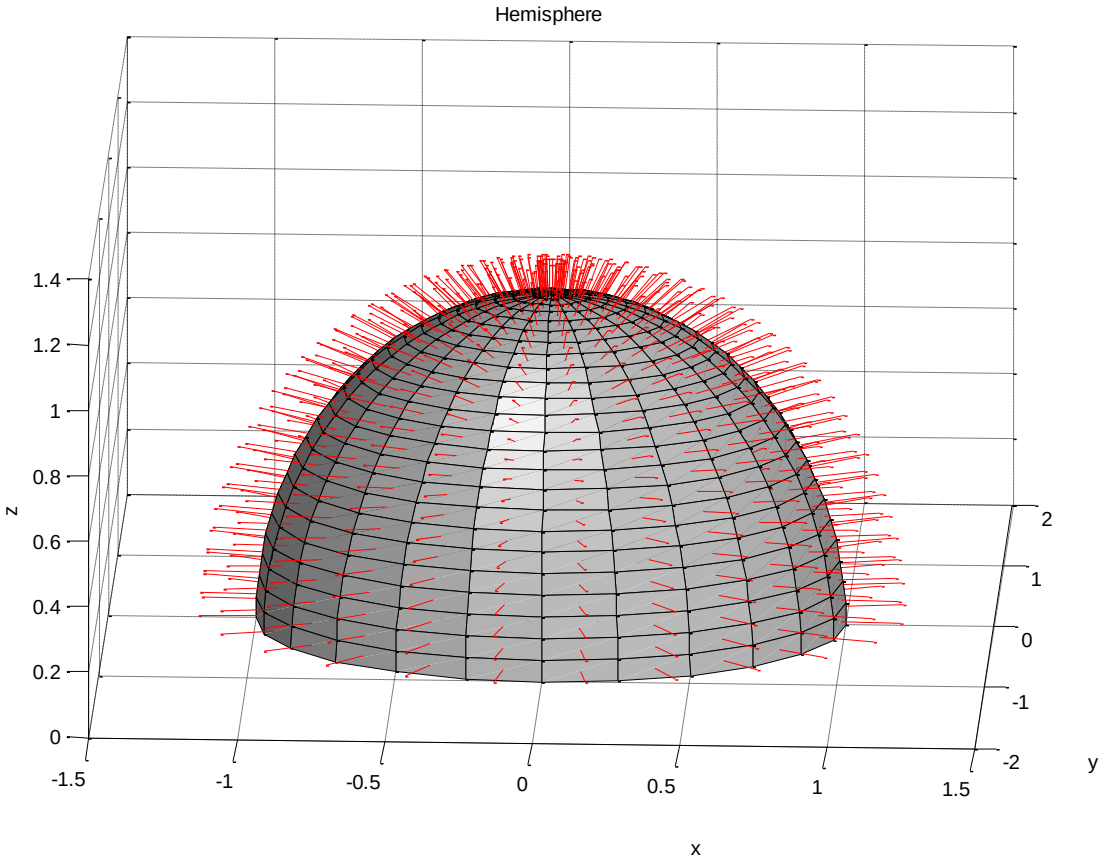

(a)

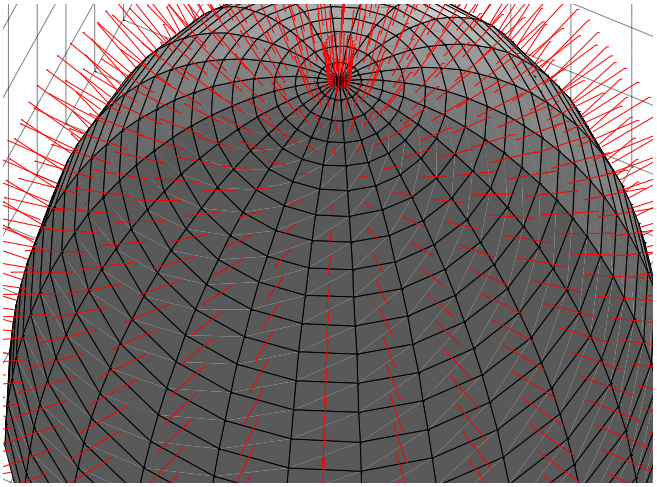

(b)

Figure 20: a) Hemispherical surface with normal vectors on each cell b) Zoomed in version from top

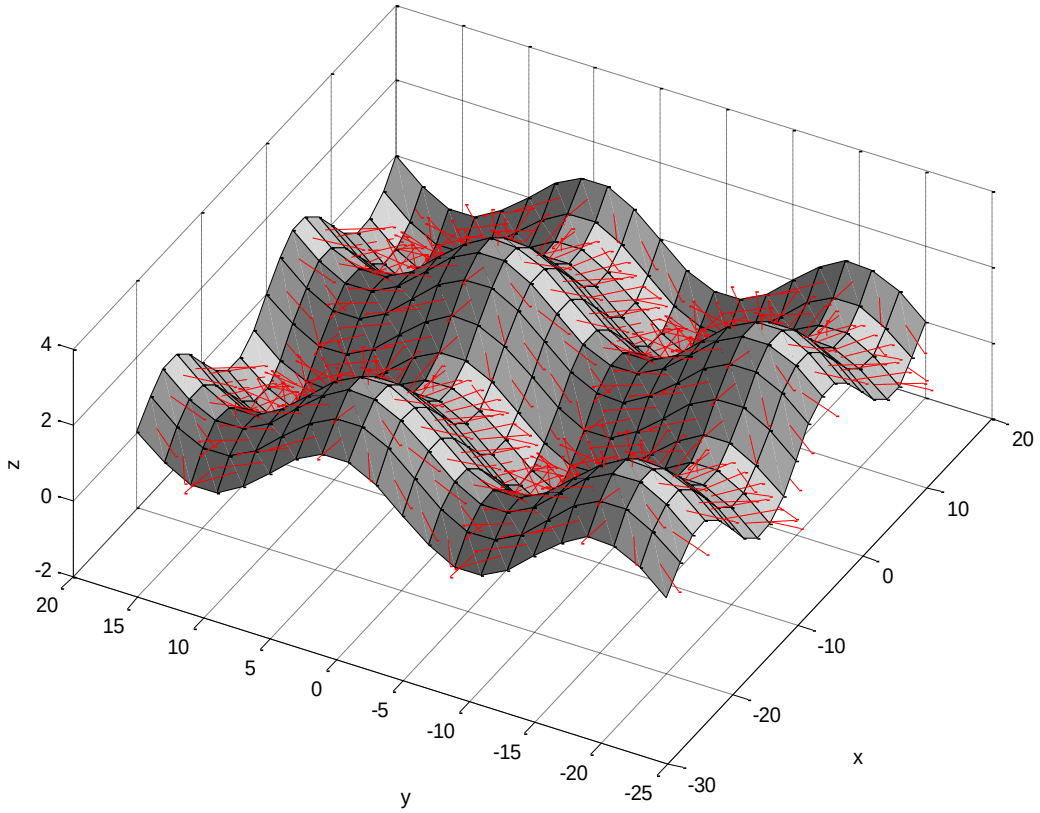

(a)

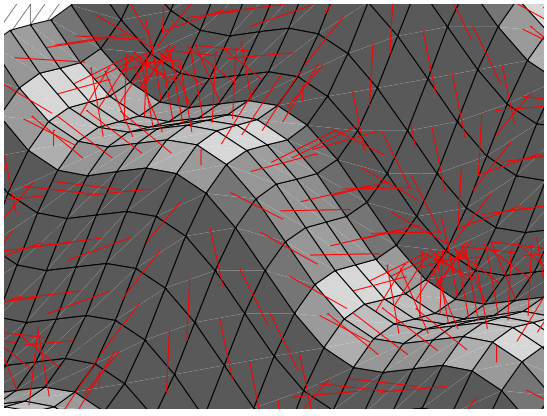

(b)

Figure 21: a) Wavy surface with normal vectors on each cell b) Zoomed in version

Creation of movement of light across the surface as the day progresses

The location of the sun at any time of the day can be described in terms of its altitude or elevation angle (El) β, and its azimuth angle (Az) Φ_s . The azimuth and altitude angles of sun depend on the latitude, day number and most importantly time of the day. Figure 22 illustrates the diagrammatic representation of sun's azimuth and elevation angles. The following are the theoretical equations to determine the value of these angles [74] :

$$\sin\beta = \cos(L)\cos(\delta)\cos(H) + \sin(L)\sin(\delta) \qquad \text{Eq. 2}$$

$$\sin(\phi_s) = \frac{\cos(\delta)\sin(H)}{\cos(\beta)} \qquad \text{Eq. 3}$$

$$\delta = 23.45\sin\left[\frac{360}{365}(n-81)\right] \qquad \text{Eq. 4}$$

$$H = \frac{15}{hour}.(hoursbeforesolarnoon) \qquad \text{Eq. 5}$$

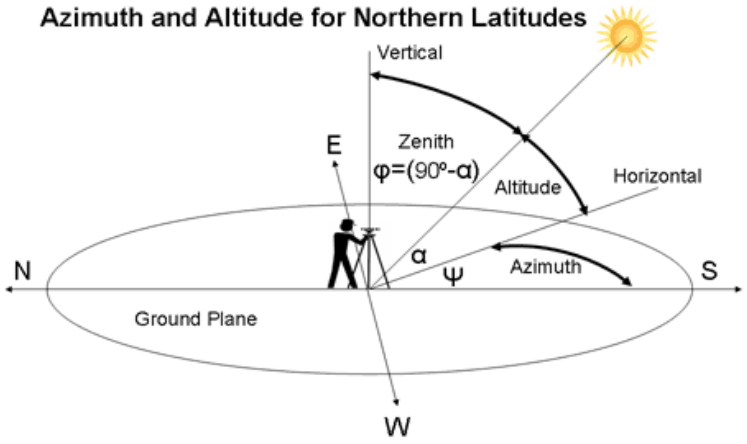

Figure 22: Azimuth and elevation angles of sun [73]

where β is altitude, Φ_s is azimuth, L is Latitude, δ is the declination angle, n is the number of day, and H is the hour angle.

To demonstrate this effect of light (sun) on the surface geometry, a light object was needed to be placed on the surface and the surface had to show the effect of the light by varying the intensity of the color (grayscale) wherever the light shone. Then this light object was needed to be moved across the surface to show the effect of sun as it moves in the horizon as the day progresses. MATLAB has a function `light` (*az*, *el*), where *az* is azimuth and *el* is elevation of light object. The light object placement according to the default *az* and *el* and the MATLAB axes corresponding to these definitions of azimuth and elevation were first understood and later the actual equations to compute the *az* and *el* of sun in a day, given above, were used to get these values. The light object was made to move in the axes as the sun moves as the day progresses. The following figures show the effect of light when the sun is directly above the surface i.e. at noon in summer and in the evening at 4:00 PM, when the sun is at a lower altitude and at an angle to the surfaces.

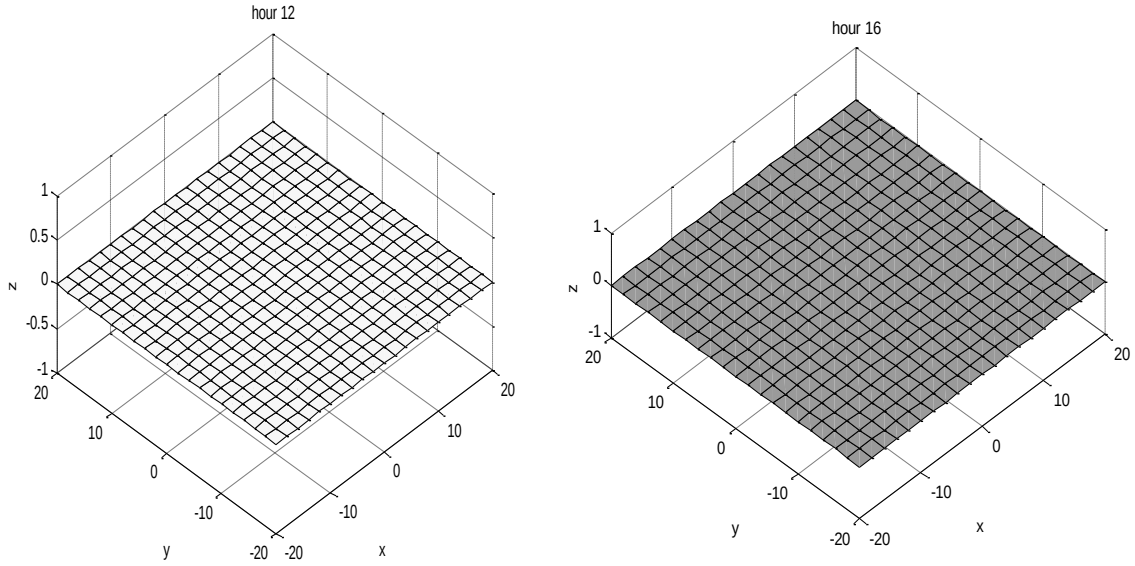

(a) (b)

Figure 23: a) Flat surface at 12:00 PM b) Flat surface at 4:00 PM

It can be seen from Figure 23 that at 12:00 pm the sun is right above the surface in typical summer day and hence the entire surface is seen to be lighted with maximum intensity. But at 4:00 PM the sun is at an angle and the color of the surface shows that there less intensity of sun at that hour.

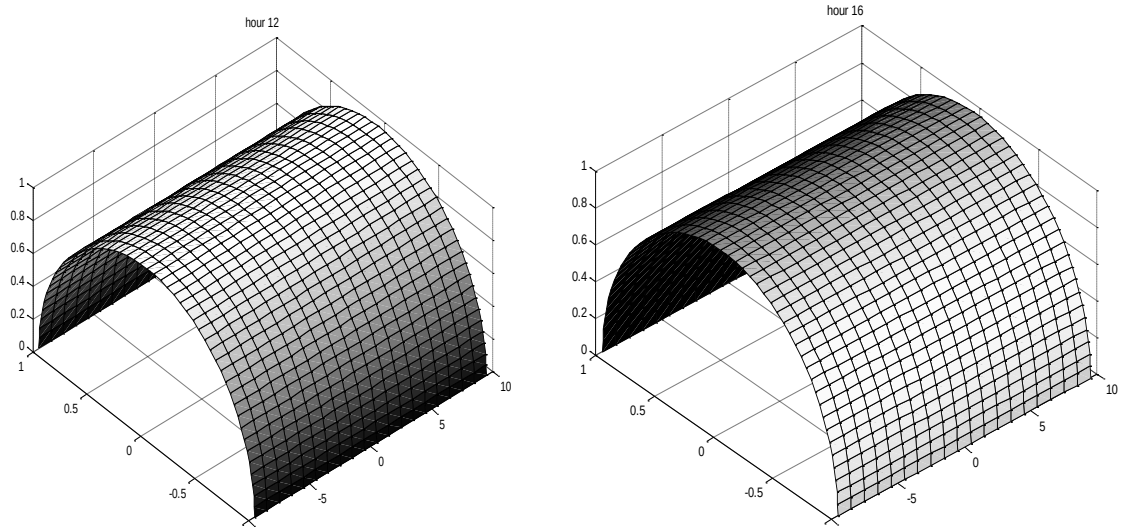

(a) (b)

Figure 24: a) Semi-cylindrical surface showing the effect of sun at 12:00 PM b) At 4:00 PM

The effect of sun on a semi-cylindrical surface is shown in Figure 24. At 12:00 PM the cells on the top of the surface receive the highest illumination and as we trace the surface towards bottom, the illumination of the cells gradually reduces and at 4:00 PM the cells on the right side of the surface will receive highest illumination but the cells on left side of the surface receive very less or no illumination. Thus it can be clearly stated that amount of electricity generated will be different at different parts of the surface due to its inherent geometry.

It is interesting to note that altering the geometry of the PV collection surface can "sculpt" the energy generation profile. This may be useful to help align PV generation supply curves temporally with energy demand curves.

Mapping the color change of the surface with the intensity variation

The grayscale of the surface mesh can be changed based on the viewfactor of each cell with respect to sun. In order for the change in grayscale to be physically meaningful, it bust change in linear proportional to the variation of the intensity of the sun. The solar insolation that strikes a collector depends on the distance between the earth and the sun which varies with the time of the year. A common expression used to calculate the solar flux on a given day is [74]

$$I = Ae^{-km} \qquad \text{Eq. 6}$$

$$m = \frac{1}{\sin\beta} \qquad \text{Eq. 7}$$

$$A = 1160 + 75\sin\left[\frac{360}{365}(n-275)\right](W/m^2) \qquad \text{Eq. 8}$$

$$k = 0.174 + 0.035\sin\left[\frac{360}{365}(n-100)\right] \qquad \text{Eq. 9}$$

where n is the number of the day and β is the altitude of the sun on that particular day. The above expression gives the solar insolation, but the actual insolation striking the collector depends on the view factor of the panel, which is given by the following expression [74],

$$I_c = I\cos\theta \qquad \text{Eq.10}$$

$$\cos\theta = \cos\beta\cos(\phi_s - \phi_c)\sin\tau + \sin\beta\cos\tau \qquad \text{Eq.11}$$

where θ is the incidence angle of the solar panel, β is the altitude angle, Φ_s is the azimuth of the sun and the solar collector is tipped up at an angle τ and faces in a

direction described by its azimuth angle Φ_c (measured relative to due south, with positive values in the southeast direction and negative values in the southwest). This $\cos\theta$ is the view factor for a flat plate and is constant throughout the surface since all the normal vectors point in same direction to the sun at any point of the day, but for non flat geometries these kind of equations are not defined, since each part of the surface has a different view factor, hence we need a modeling approach to be able to get the view factor at any point of the surface and thus the variations in the amount of solar insolation that is being captured on the surface.

In MATLAB the color of the surface changes based on view factors as shown in the above figures, when the light moves across the surface. But validation of this variation of view factor on the surface to be proportional to the variation of actual intensity of the sun was required, to be able to use the approach to calculate the total energy on the surface. The above mentioned equations are used to calculate the actual intensity on the solar panel.

The `surfl()` function in MATLAB changes the view factor data of the surface as the light changes but when using an external light object the view factor data remains constant even though light object is changing its position. This view factor data for each cell is calculated using the cross product between the normal components of the cell and the angles of position of the sun in the sky at that point. The `surfl` function has a built-in light object whose position can be varied using *az* and *el* angles, so the previously calculated values for azimuth and elevation angles of the sun were used in `surfl` function to obtain the view factor data as the light object is moving across the horizon.

Using these functions the view factor data for a flat plate is collected and the mean of the view factor data is plotted against the actual insolation of the sun on a flat plate using theoretical equation. The following is the graph in Figure 25 plotted on a summer day.

It is seen from the Figure 25 that view factor change needs to be multiplied by a scaling factor to get the actual insolation falling on the flat panel. The Table 1 gives scaling values that needs to be multiplied to get the actual insolation falling on a flat panel calculated from the theoretical equation. It is observed that the scaling values are equal to the actual intensity of the sun at the given hour of the day. It can concluded from the above table that the MATLAB function `surfl` () changes the view factor of each cell on the surface assuming that the intensity of the light is constant at unity. Thus the value of view factor data needs to be multiplied with the actual insolation of the sun on that day at that hour to get the actual value of insolation falling on the solar panel. Thus mapping of view factor data with the insolation was done.

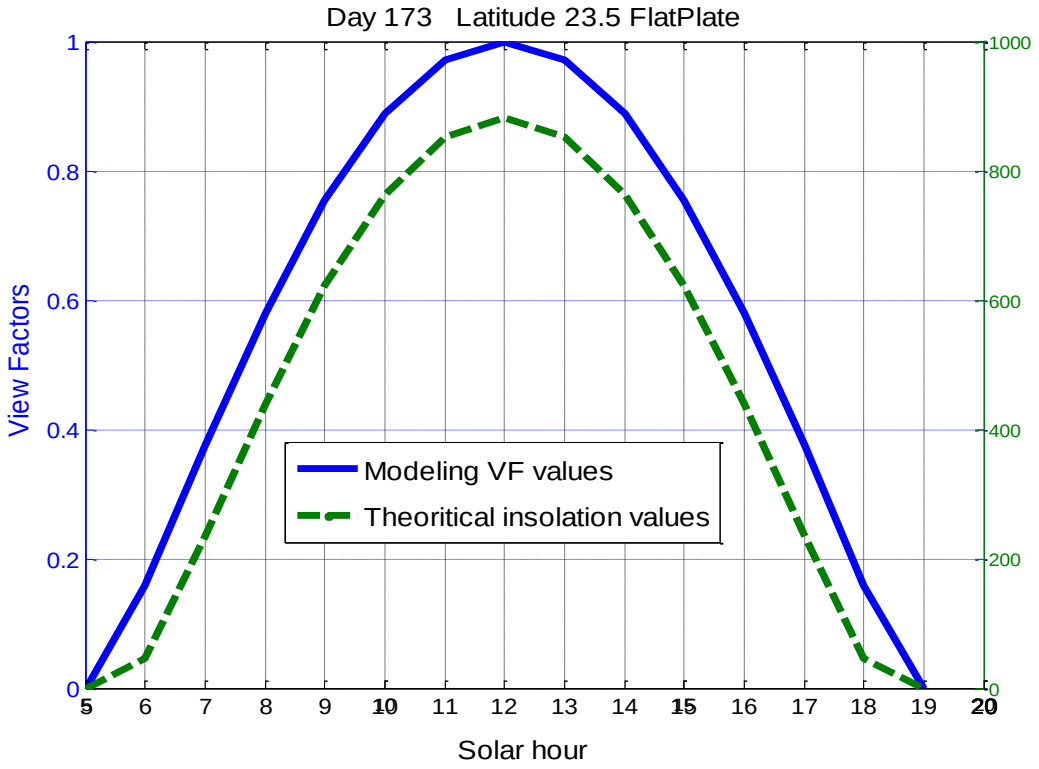

Figure 25: View factor of the flat panel against the theoretical insolation

Table 1: Mapping the view factor data with the intensity of sun

Hour of the day	Scaling Factor	Actual intensity of the sun(W/m^2)
6	294.1544	294.1544
7	626.3047	626.3047
8	759.5399	759.5399
9	825.0508	825.0508
10	859.9676	859.9676
11	877.5289	877.5289
12	882.9139	882.9139
13	877.5289	877.5289
14	859.9676	859.9676
15	825.0508	825.0508
16	759.5399	759.5399
17	626.3047	626.3047
18	294.1544	294.1544

This approach is used to compute the view factors of various surfaces that were created. Validation these view factors is essential and it is done in Chapter IV.

Creation of surfaces with a tilt and azimuth angle

The previously generated non-flat surfaces were in a hoizontal orientation lying flat on ground without any tilt. But for optimum performance and high energy capture, the conventional flat panel is tipped up at a certain angle known as tilt of the panel (τ) depending on the latitude of the deployment site , and also faces in a direction described by its azimuth angle Φ_c (measured relative to due south, with positive values in the southeast direction and negative values in the southwest) to change the time at which peak generation occurs. Similar will be the case for semi-cylindrical and cylindrical geometry. But when we consider a hemispherical surface the geometry by itself is symmetrical in all directions and would not be logical to tilt or change the azimuth of this surface. This modelling approach enables us to incorporate this tilt angle and colloectors azimuth angle for any surface and helps us get the view factors for those angles easily. As it can be seen, to get the view factors mathematically for various geometires lying flat on ground is itself difficult, and if it is needed to tilt the non-flat panel and needed to get the view factors for those surfaces it would be much more difficult unless we have such modelling approaches.

The following is the reference direction axes for all the figures presented. The east is represented by positive Y axis, and West is represented by Negative Y-axis and the South is represented by Positive X axis and North is represented by Negative X axis. Figure 26, shows a flat panel which is tilted at 45^0 without any azimuth angle for the

collector. Figure 27 Shows a semi cylindrical panel tilted at 45^0 without any azimuth angle facing South.

Figure 28 and Figure 29 show flat panel and a semi-cylindrical surface tilted at 45^0 and also azimuth is 45^0 , which means the surface is towards east direction.

As surface normals were created for geometries lying flat on ground , normals can be created for tilted geometires and view factors can be obtained in the same way.Thus, using this modeling approach, any kind of surfaces can be tilted and given a certain azimuth and view factors can be obtained.

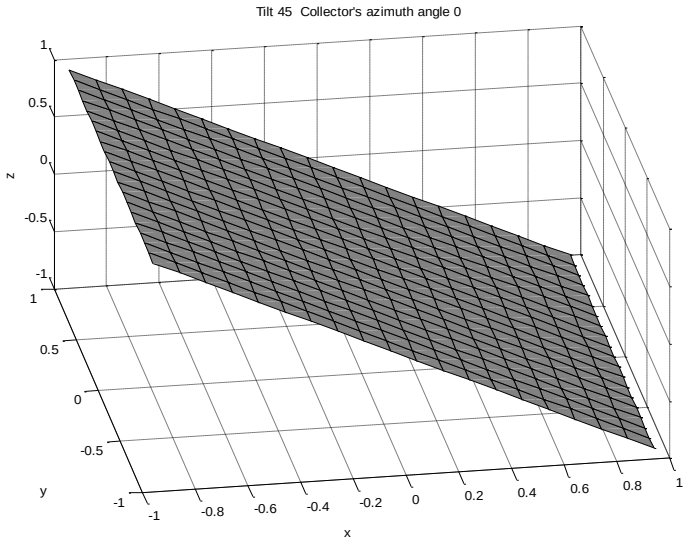

Figure 26: Flat surface tilted at 45 degs facing due south

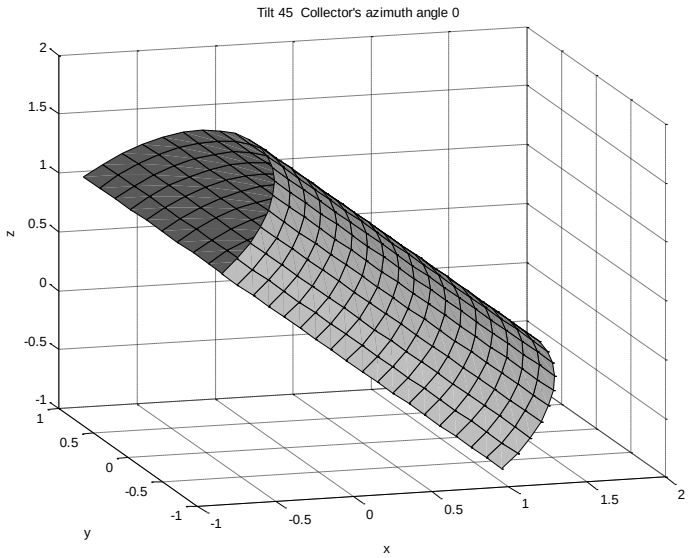

Figure 27: Semi-cylindrical surface tilted at 45 degs, facing due south.

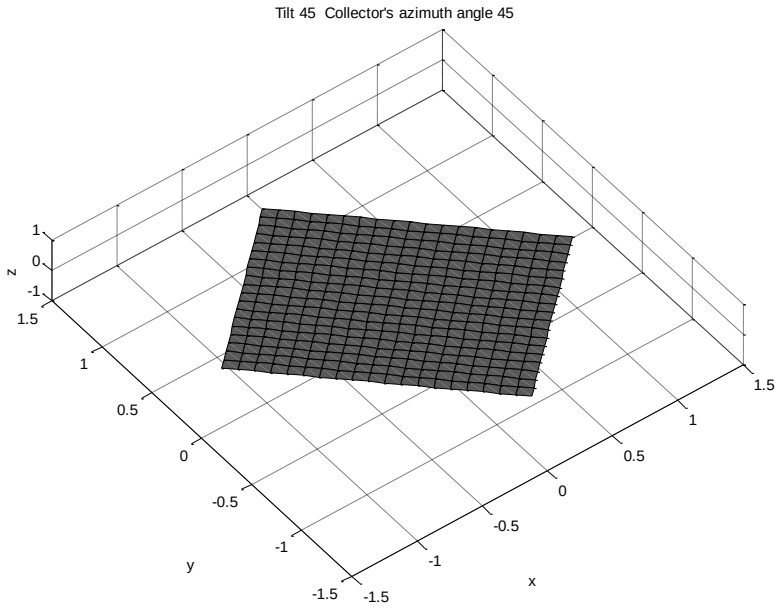

Figure 28: Flat plate tilted at 45 degs and azimuth is 45 degs, facing east-of-south

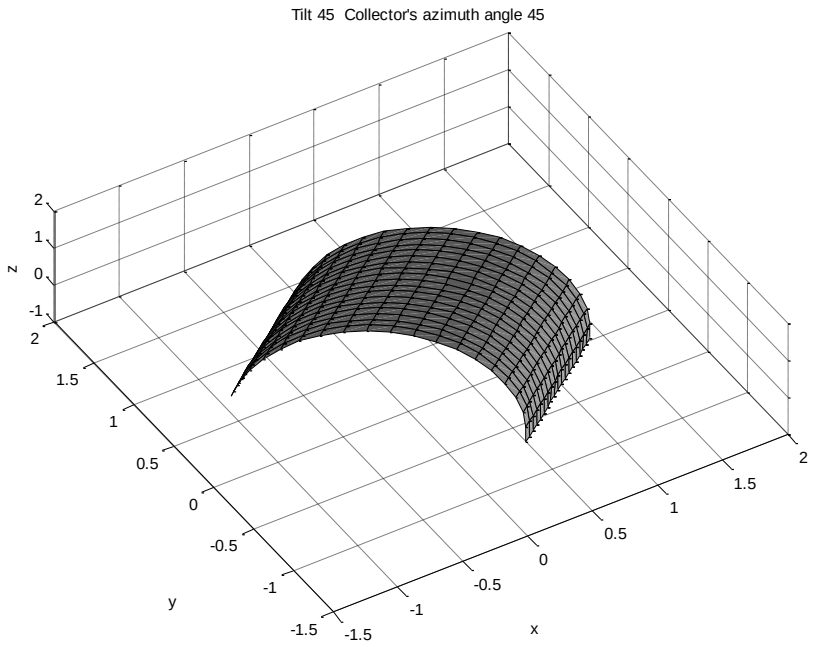

Figure 29: Semi-cylindrical surface tilted up at 45 degs and its azimuth is 45 degs, facing east-of-south

Chapter summary

This chapter outlines the modelling approach adopted to get the average view factor of various surface at every hour of the day. The following Figure 30 gives the flow chart that outlines the algorithm used to get the view factors for each surface.

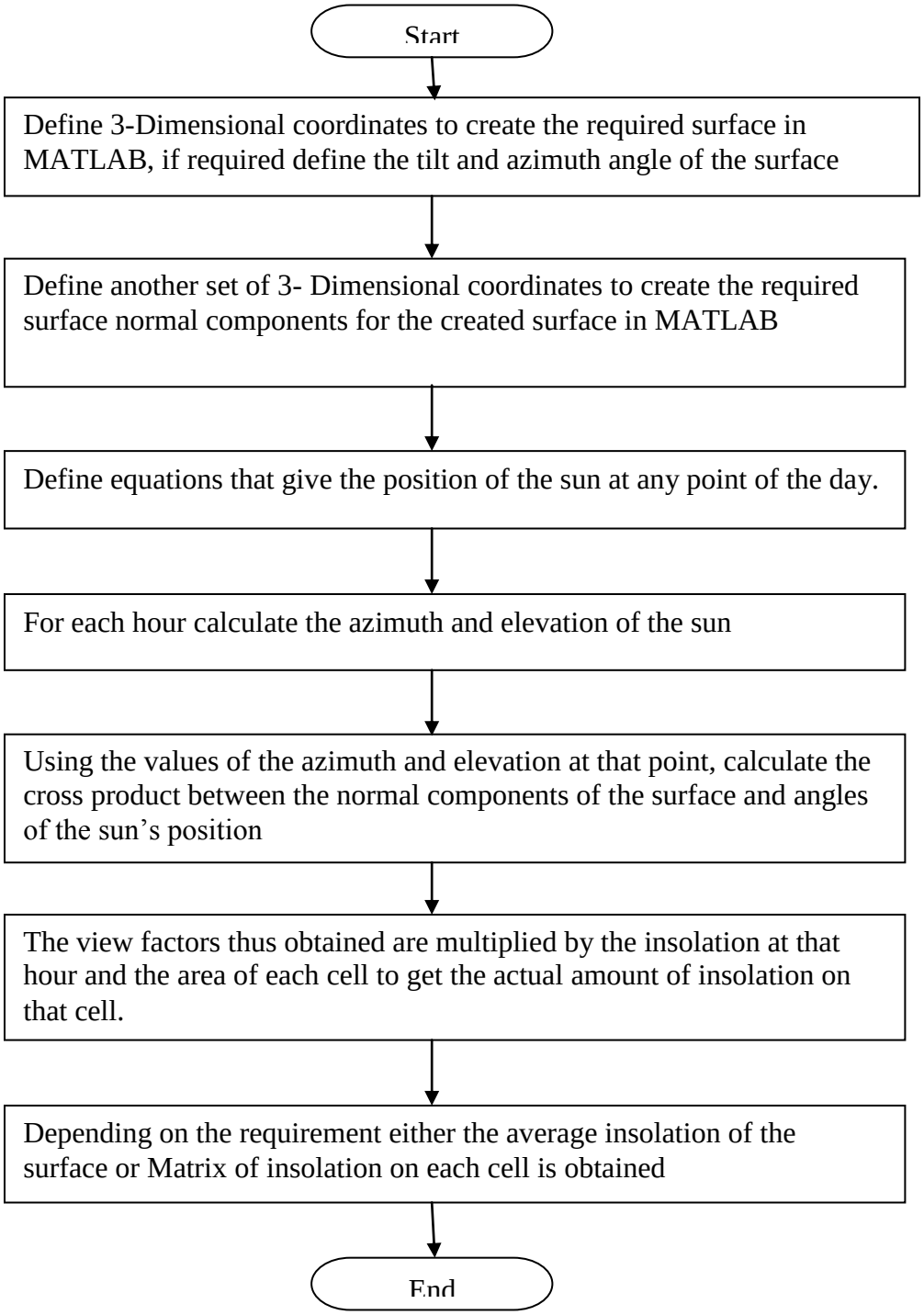

Figure 30: Flow chart summarizing the modeling approach

CHAPTER IV

VALIDATION OF THE APPROACH

This chapter outlines the validation of the modeling approach adopted to get the view factors of various non flat geometries of PV panel. Various surfaces are created and their view factor graphs are plotted in this chapter. The view factors plotted here is the average view factor of the entire surface, which is the effective area of the surface that is being exposed to sun at that hour. Since the view factor is the ration of projected area of the surface and actual area of the surface, the view factors take values in the closed set of real numbers [0, 1]. A value of '1' indicates that the entire surface is exposed but if the view factor is '0.5' only half the entire surface area is being exposed to sun at that point of the day. A common day of June Solstice 173 is chosen and Latitude of 23.5 deg because at this latitude and on that day we have the highest sun's altitude of 90 deg at noon and gives us a fair ground for comparison. Table 2 tabulates the elevation values of the sun on this particular day. It can be observed that at 12:00 PM the sun is at 90 deg in the horizon.

Table 2: Elevation angle of the sun on 173 day of the year

Hour of the day	Altitude angle of the sun
5	0
6	9.1297
7	22.1122
8	35.4037
9	48.9014
10	62.5338
11	76.2476
12	89.9480
13	76.2476
14	62.5338
15	48.9014
16	35.4037
17	22.1122
18	9.1297
19	0

Validation of the flat surface view factors

It can be seen from Figure 31 that during early morning and evening hours of the day there is very less view factor of flat surface i.e., the effective area exposed to sun is less but it peaks at the noon to maximum and drops down again in the evening.

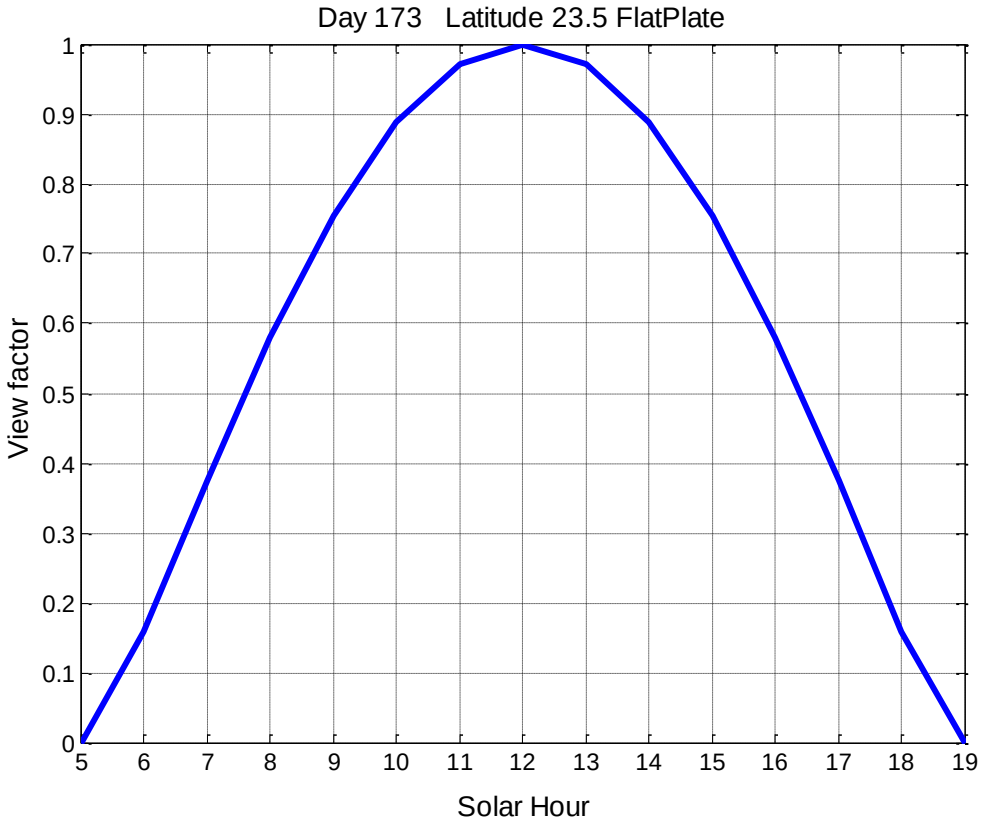

Figure 31: View factors of flat surface on a particular day

To validate that we have the correct view factors from the modeling approach the results from the modeling approach are compared with the results obtained from theoretical equation already present in the literature and mentioned in Chapter III and given below for reference [74].

$$\cos\theta = \cos\beta\cos(\phi_S - \phi_C)\sin\tau + \sin\beta\cos\tau \qquad \text{Eq.11}$$

where θ is the incidence angle of the solar panel, β is the altitude angle, Φ_S is the azimuth of the sun and the solar panel is tipped up at an angle τ and faces in a direction described by its azimuth angle Φ_C (measured relative to due south, with positive values

in the southeast direction and negative values in the southwest). The values from the equation are plotted along with the view factors obtained from modeling the flat plate, it can be seen from Figure 32 that they coincide perfectly. That is why the two lines overlap one on another and look like single one.

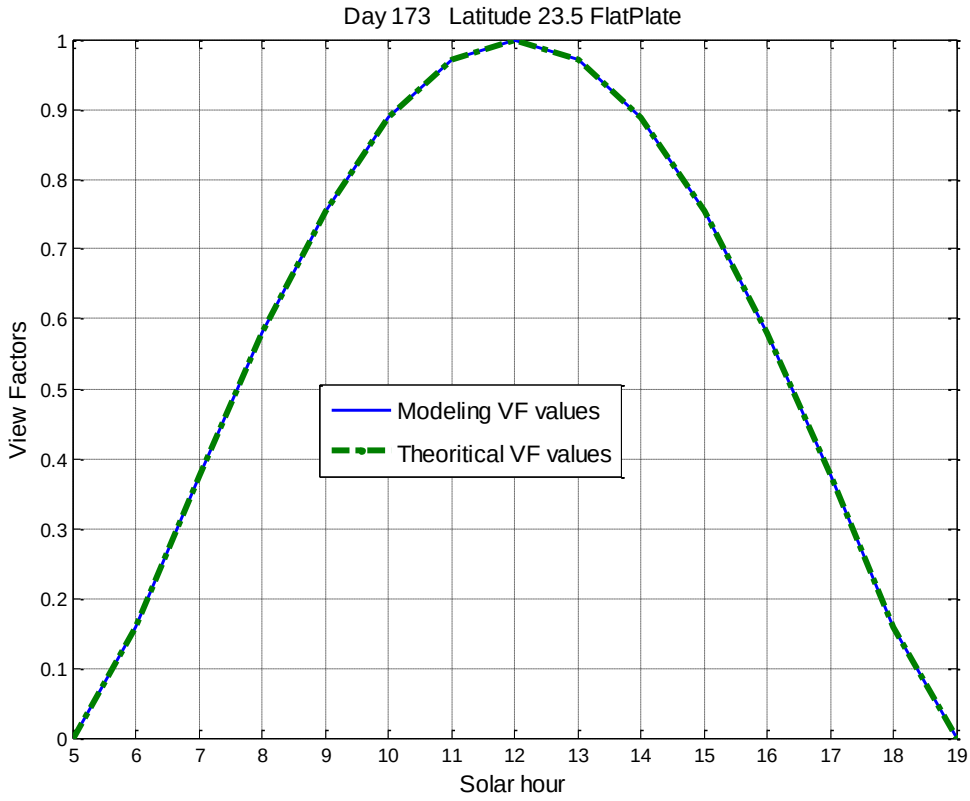

Figure 32: Validation of flat surface view factors with theoretical values

In the Figure 32, the validation of view factors for flat surface lying flat on ground i.e. tilt is 0^o and azimuth of collector 0^o was carried out. Since the surfaces can be tilted, it needs to be verified that we are still getting the correct view factors from modeling

approach even after tilting the surfaces. Plotting the view factors obtained from Modeling approach against view factors obtained from theoretical equation presented above we get the graph presented in Figure 33. It can be seen that when the surface is tilted at 45^{o} and its azimuth is at 45^{o} which is South-east direction we shift the peak to around 10:00 AM in the morning. The graph coincides perfectly with the theoretical values and validates the approach used for tilting the surfaces.

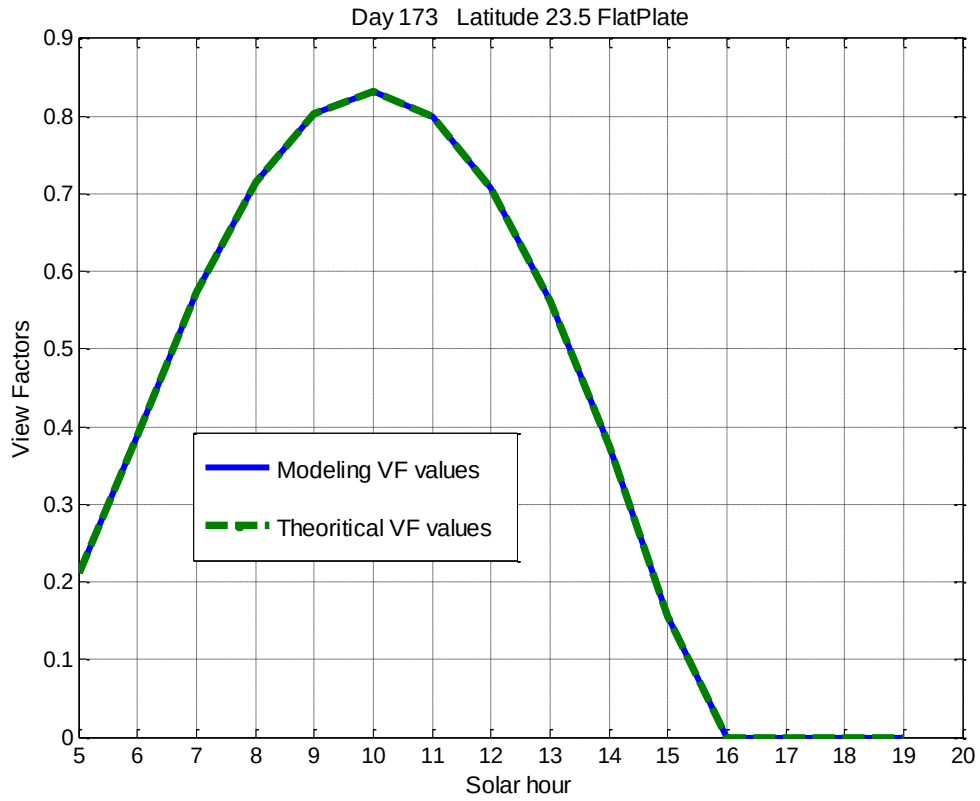

Figure 33: View factors of flat plate with 45° tilt and 45° azimuth

Validation of semi-cylindrical surface view factors

For a semi-cylindrical surface it can be observed from Figure 34 that during early morning and late evening hours the view factor is not less as was the case with flat panel. The effective area that is exposed sun is greater. For applications where availability of the energy during early hours is critical like telecommunications the semi cylindrical surface provides better results which will be proved in Chapter VI. The validity of the view factors obtained can be proved mathematically as shown below.

Consider a semi-cylinder with radius *r* and length *l*, the total surface area will be πrl and if we consider a flat plate of same length and breadth the area is $2rl$, now when looked at the semi-cylinder from top at noon we have projection of area πrl as a flat plate of area $2rl$ so the effective projection will be $\frac{2rl}{\pi rl} = 0.6366$ which is the view factor value at the peak obtained by the graph plotted from MATLAB as shown in Figure 34.

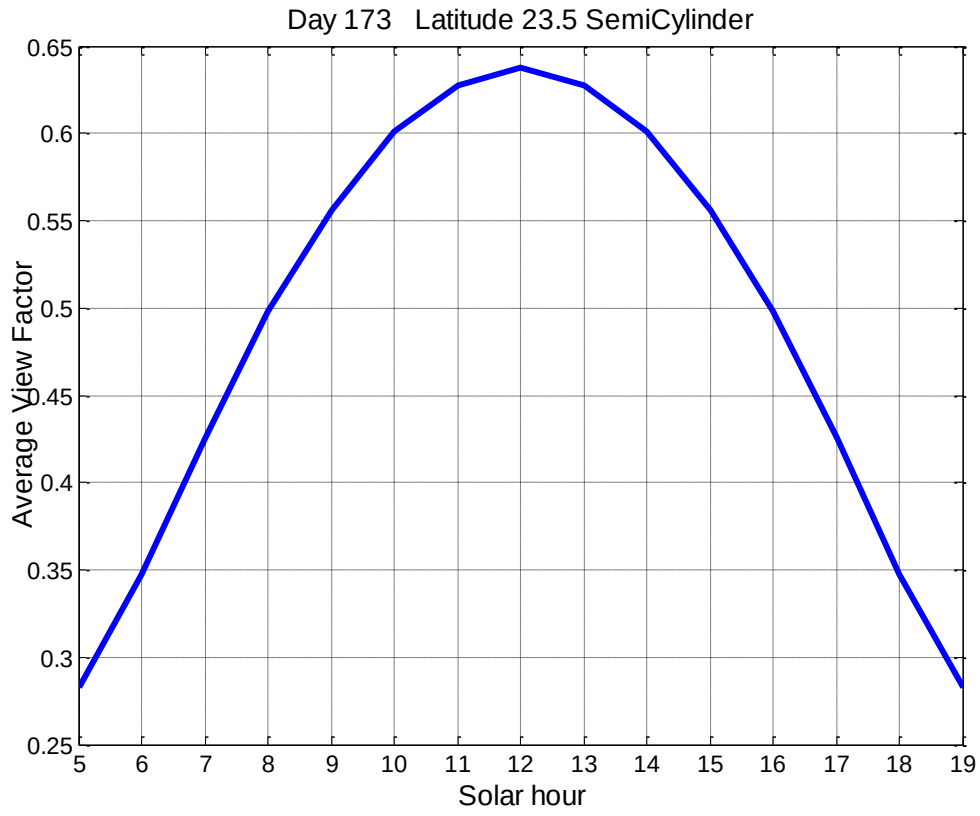

Figure 34: View factors for semi-cylindrical surface

Validation of cylindrical surface view factors

For a cylindrical surface due to the bottom part not being exposed to sun the total effective area exposed to sun at noon decreases but the effective area exposed to sun during early morning and evening hours is increased which is evident from the increase in view factor during those times. Another important observation that needs to be made is that the view factor variation of the surface throughout the day is not wide which means that effective surface area exposed to sun in a cylinder throughout the day is almost the same owing to its symmetry.

The proof for this cylindrical surface will be given in the same way given for semi-cylinder. Consider a cylinder with r radius and l length the total surface area will be $2\pi rl$ and if we consider a flat plate of same length and breadth the area is $2rl$, now when looked at the cylinder from top at noon we have projection of area $2\pi rl$ as a flat plate of area $2rl$ so the effect project will be $\frac{2rl}{2\pi rl}$ which is equal to 0.318 which is the value of the view factor at the peak obtained by the graph plotted from MATLAB shown in Figure 35.

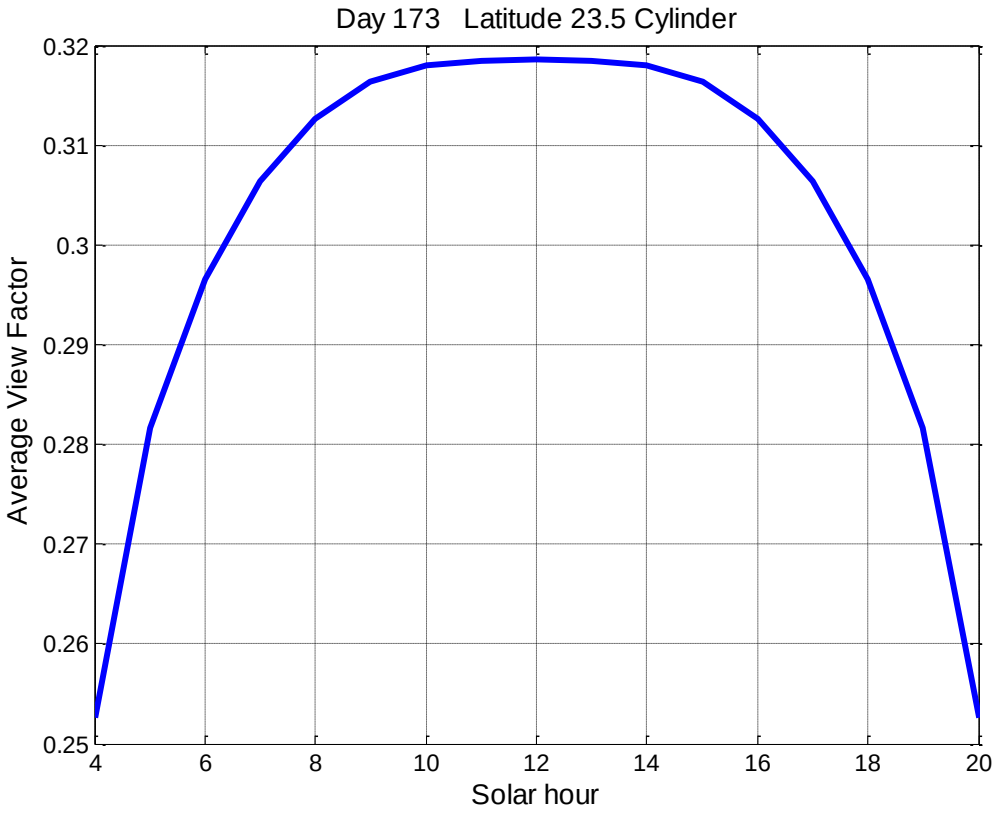

Figure 35: View factors of a cylindrical surface

Validation of sinusoidal surface view factors

It can be observed from the graph below shown in Figure 36 that there is a small amount of surface area exposed to sun during early and late evening hours but not as great as semi-cylinder but better than a flat plate. But as the sun rises in the horizon the effective area exposed to sun is increasing similar to the flat plate. The mathematical proof for the peak value of the curve is given below.

The curved length of the sine wave needs to be calculated, which can be found using the following equations. The formula for arc length of a function f(x) is,

$$\int_a^b \sqrt{(f'(x)^2 + 1)}dx \qquad \text{Eq.12}$$

In our case f(x) = sin(x).The derivative of sin(x) is cos(x). Squaring it, adding one, and taking the square root we get:

$$\sqrt{(\sin'(x)^2 + 1)} = \frac{\cos(x)^2 + 1}{2} \qquad \text{Eq.13}$$

Now integrating this expression from zero to π in our case gives the length which is equal to 3.8201. If we consider equal breadth, when looked from top at noon this surface will look like a flat surface with length equals to π (which is the base length). By dividing this effective area with actual area we have 0.833 which is the same value obtained from MATLAB simulation figure shown in Figure 36. It has to be observed that the surface created in the Chapter III has a base of 3.14 which is the value of π.

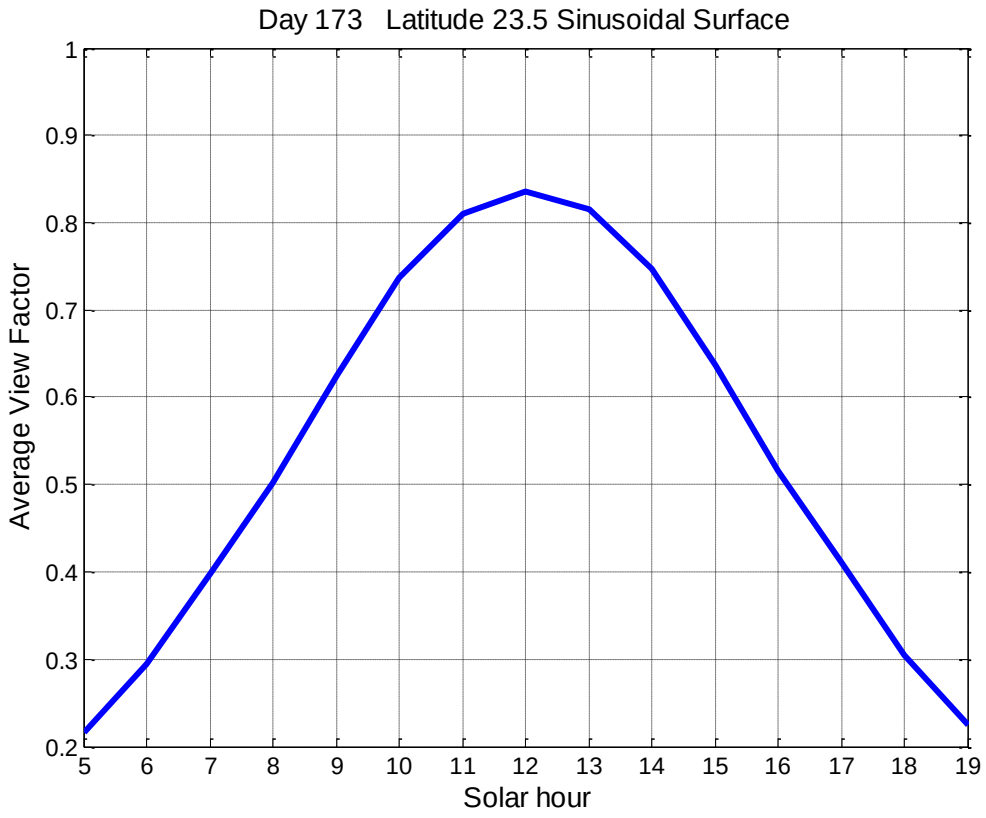

Figure 36: View factors for sinusoidal surface

Validation of hemispherical surface view factors

It can be observed from the graph shown in Figure 37 that similar to semi-cylinder the hemisphere also has larger effective area exposed to sun during early morning and late evening hours unlike flat plate but there is wide variation in the view factors owing to its geometry.

The following gives the mathematical proof for the peak value of the view factor obtained in the graph shown in Figure 37.

The total surface area of a hemisphere is given by $2\pi r^2$, when looked from the top at noon the effective area of the surface will be πr^2, a circle with radius of r. So the effective area exposed or the view factor at that point will be $\frac{\pi r^2}{2\pi r^2} = 0.5$, which is the same as the value obtained from modeling approach.

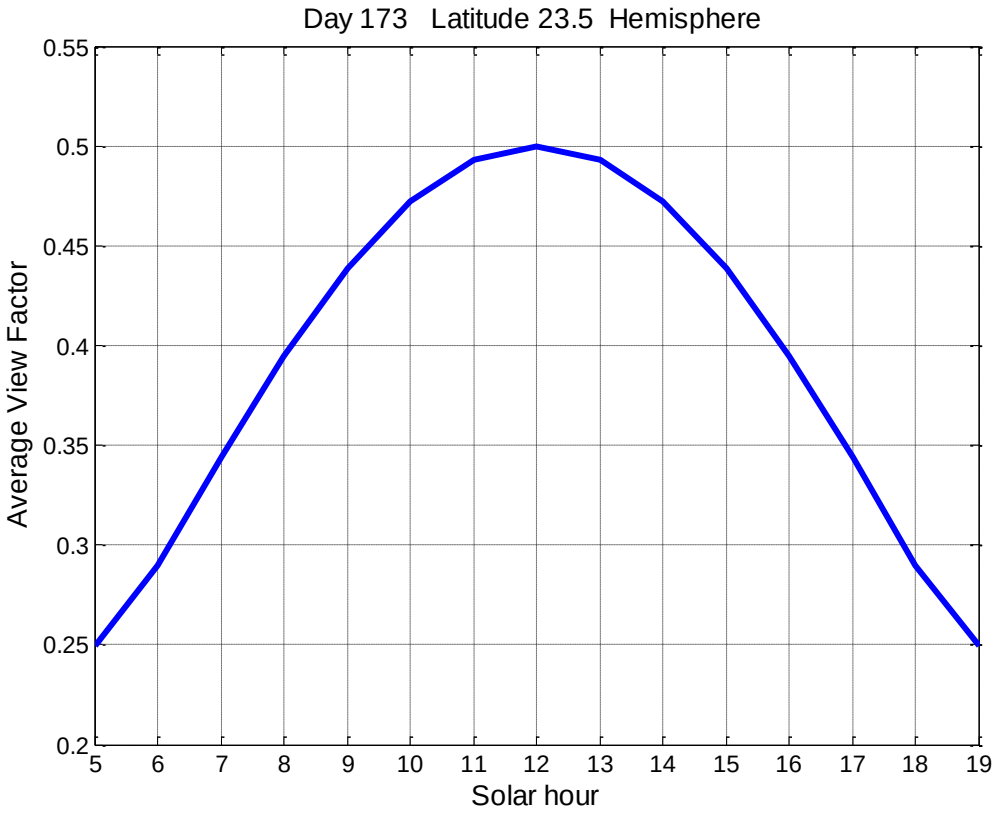

Figure 37: View factors of hemispherical surface

Chapter summary

Thus view factors obtained for various surfaces are validated using mathematical analysis, as it can be seen that to validate a single point on graph we require such extensive mathematical analysis. In order to derive the mathematical equations to get the view factors for these surfaces is very laborious and has not be done so far. This modeling approach helps us obtain accurate view factors of various surfaces at any given point of the time, day, and month of a year with respect to the position of the sun which is very critical in analyzing the variation in energy capture on the surface and thus the variations in energy generated.

CHAPTER V

APPLICATION: INCREASING THE ENERGY HARVEST

Chapter IV validated the view factors obtained from the modeling approach. These view factors can be obtained either in a matrix form in which each element will represent the view factor of individual cell on that surface or mean of that matrix can be calculated which will represent the view factor of the entire surface at that point of the day. This mean will represent the effective area of the surface that is being exposed to sun at that point of the day. This can be used to calculate the effective amount of insolation falling on that surface. But this still gives us value in $\frac{W}{m^2}$ which is the insolation. This needs to be multiplied by the area m^2 of the surface to get the total insolation in W on the surface. This chapter uses this approach to calculate the total amount of energy that is being captured by various surfaces throughout a day and presents a systematic comparison of these energy harvests to investigate which surface is better in harvesting the energy.

Comparison of cylindrical, semi-cylindrical and flat surfaces for energy harvest

When comparing the different surfaces it needed to be based on a common ground and here the surfaces with equal footprint i.e., with same base area are compared so that we get approximately same peak value for all the surfaces at noon. For semi-cylinder, cylinder and flat plate, assuming radius (r) and length (l) to be 1 meter each, Semi-cylinder with surface area πrl, cylinder of area $2\pi rl$ and flat surface of area $2rl$ are considered. The flat surface is taken to be of area $2rl$ because when seen from top at

noon in summer both the semi-cylinder and cylinder will be projected as a flat surface with an area of $2rl$

Common latitude of 23.5 deg north is taken for comparison and four particular days March equinox, summer solstice, September equinox and winter solstice are taken to give an overall comparison of the energy harvest across the whole year.

Table 3: Comparison of cylinder, semi-cylinder and flat plate energy capture

Day=173			
Hour of the Day	Cylinder with surface area $2\pi rl$	Semi-cylinder with surface area πrl	Flat Plate with surface area $2rl$
5	0	0	0
6	548.00	320.10	93.300
7	1205.9	839.70	471.50
8	1491.9	1187.3	880.10
9	1640.3	1442.9	1243.5
10	1718.5	1623.8	1526.1
11	1756.0	1729.5	1704.7
12	1767.0	1768.2	1765.8
13	1756.0	1729.5	1704.7
14	1718.5	1623.8	1526.1
15	1640.3	1442.9	1243.5
16	1491.9	1187.3	880.10
17	1205.9	839.70	471.50
18	548.00	320.10	93.300
19	0	0	0

The Table 3 and Figure 38 give the comparison for day 173 which is the summer solstice. These show that a cylindrical surface has the best energy capture during early morning and evening hours followed by semi-cylinder and flat surface when the area of the flat surface is $2rl$.

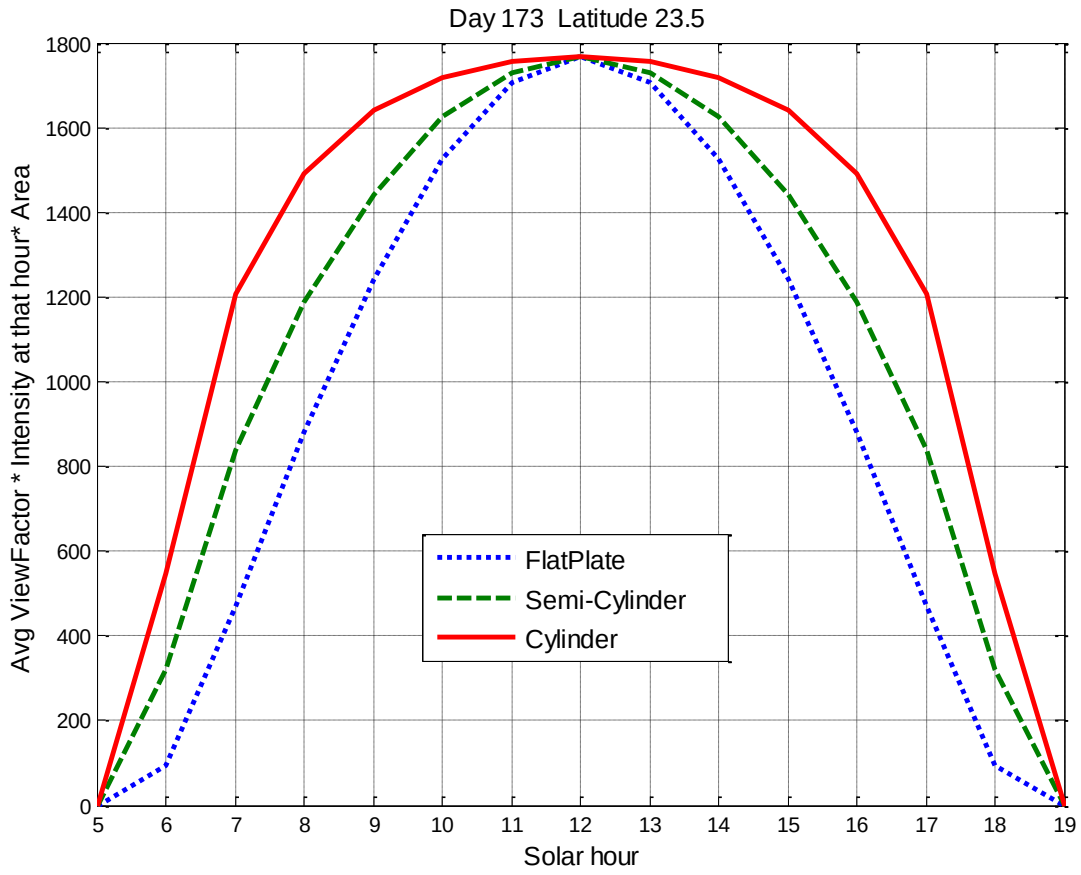

Figure 38: Comparison of cylinder, semi-cylinder and flat plate energy capture

It can be observed that cylindrical surface high energy capture and it is high right from 7:00 in the morning to 5:00 in the evening, whereas flat surface has comparable energy captures only from 10 am to 2:00 pm.

When the energy values are added for the typical four days of a year March equinox, summer solstice, September equinox and winter solstice and average is calculated, the following Table 4 gives the total energy values.

Table 4: Comparison of average energy captured in a day for a flat, semi-cylindrical and cylindrical surfaces

Surface	Average Total energy in a day (Wh)	Percentage increase in surface area
Flat	11575.2	
Semi-cylindrical	13992.675 (20.88%)	57%
Cylindrical	16394 (41.63%)	214%

It has to be observed that for a semi-cylindrical surface the total amount of energy harvested is 20.88% more than a flat plate and also for a cylindrical surface the total amount of energy harvested is 41.63% more than a flat plate in a particular day. It has to be noted that these comparisons are carried out for surfaces with equal footprints and also with regard to the amount of solar energy that is being captured on that surface. These results suggest that a cylindrical surface captures highest energy throughout the day but when we look at the amount of surface area that is increased from flat plate it is

a 214 % increase and for a semi-cylinder the percentage increase in surface area from a flat plate is 57% for which we are getting a 20.88% increase in energy harvest. Thus an optimization needs to be made when choosing a particular geometry depending on the operation.

Applications

In applications where the energy capture has to be maximized during early morning and evening hour's example for a residential household where the loads are high during morning and evening hours, a cylindrical geometry can be chosen. And applications where the cost of the system plays a critical role along with increased energy capture during early morning and evening hours a semi cylindrical geometry can be chosen.

Comparison of hemispherical and flat surfaces for energy harvest

Similar to the comparison between cylindrical, semi-cylindrical and flat surface, a comparison between flat plate and hemisphere can be done. Hemispherical geometry is a special case owing to its greater symmetry in its geometry when compared with cylinder or a semi-cylinder. And also when a hemisphere is projected on to ground it represents a circle instead of a rectangle which was the case with both cylindrical and semi-cylindrical surfaces.

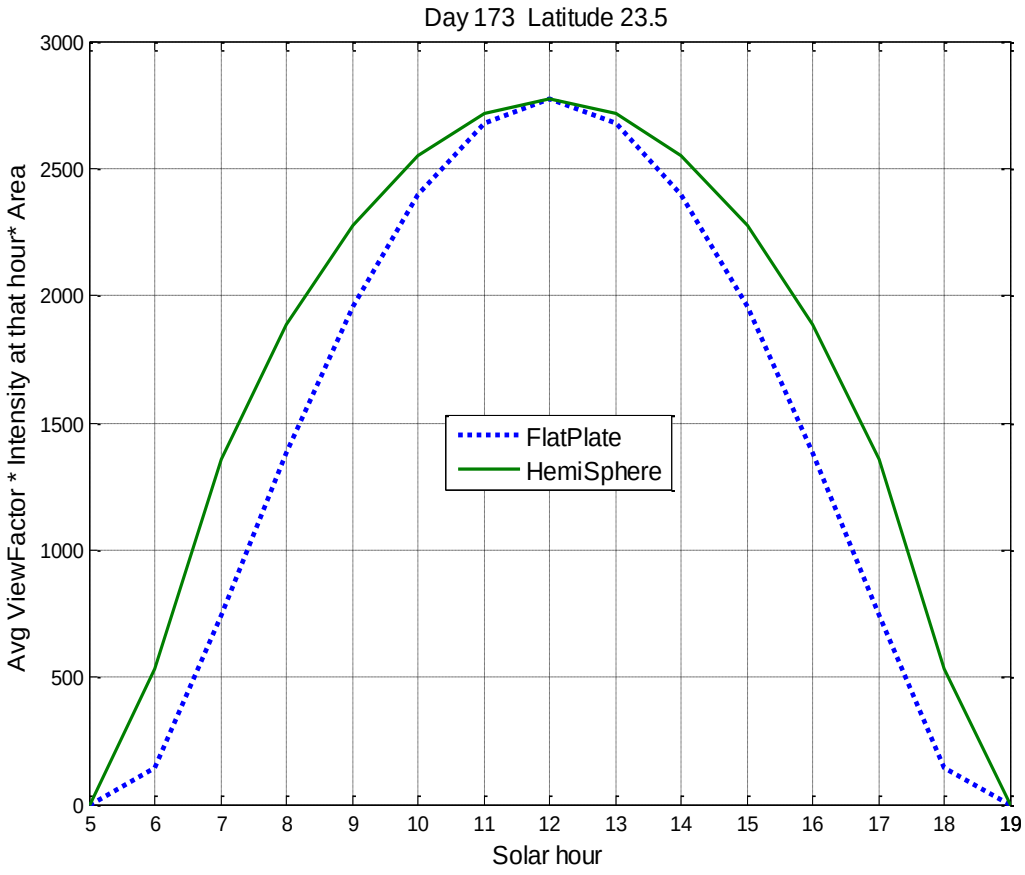

Figure 39: Comparison of hemispherical and flat surface

It can be seen from Figure 39 that hemisphere harvests more energy during early morning and evening hours as predicted. But the actual advantage of this kind of geometry can only be seen when we observe the view factor of this surface at North pole area. At North pole sun is present for 24 hours in a day for six months and sun moves in the horizon i.e, the altitude of the sun doesn't change as it changes at any other latitude. The following Table 5 gives the comparison of altitude of the sun on summer solstice at latitude 23.5 N and at latitude 90 N.

Table 5: Comparison of sun's altitude angle at L=23.5 and L=90

Day = 173		
Hour of the Day	Latitude 23.5 Altitude angle of the sun	Latitude 90 Altitude angle of the sun
5	0	23.4480
6	9.12970	23.4480
7	22.1122	23.4480
8	35.4037	23.4480
9	48.9014	23.4480
10	62.5338	23.4480
11	76.2476	23.4480
12	89.9480	23.4480
13	76.2476	23.4480
14	62.5338	23.4480
15	48.9014	23.4480
16	35.4037	23.4480
17	22.1122	23.4480
18	9.12970	23.4480
19	0	23.4480

Thus with a geometry like hemisphere we get equal amount of energy capture throughout the day. This gives a chance to once again validate the view factors that are obtained for hemisphere. The Figure 40 gives the view factor of the hemisphere when it is placed at Latitude 90 N and also to verify the view factors mathematically the altitude of the sun is made 0 i.e., the sun is now moving across the hemisphere at its bottom and it should see a semi circle of area $\frac{\pi r^2}{2}$ at any point of the time and that makes the view factor to be $\frac{\pi r^2 / 2}{2\pi r^2}$ = 0.25. It can be seen from Figure 40 that we are indeed getting a constant view factor of 0.25 throughout the day.

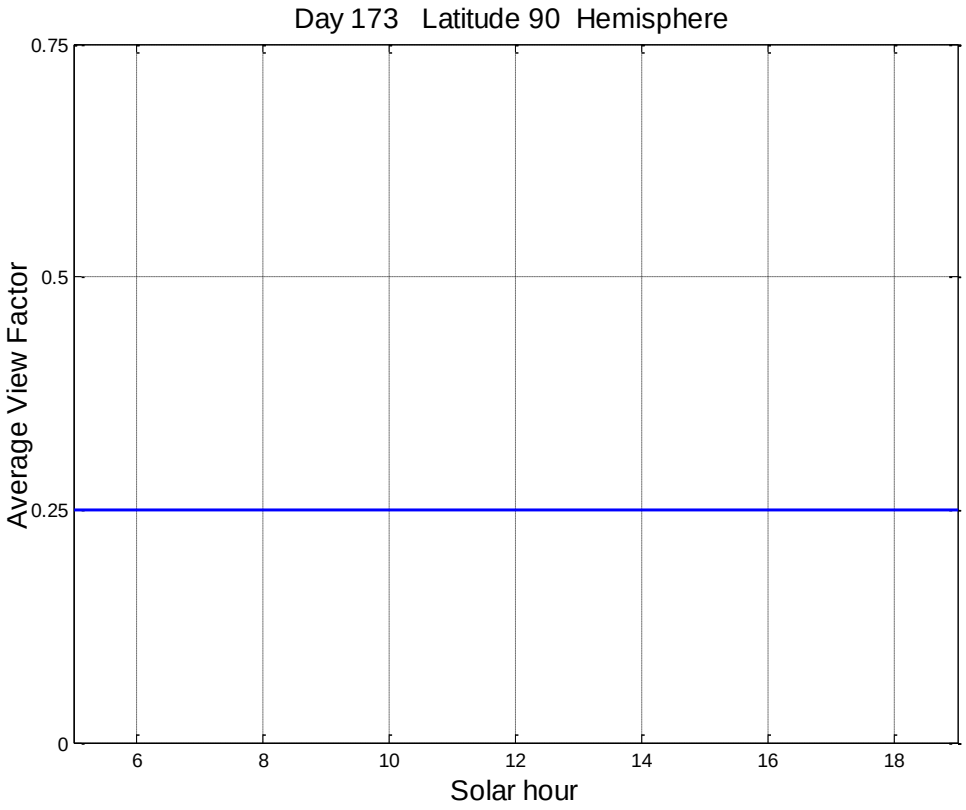

Figure 40: View factor for hemisphere at latitude 90 N and altitude of sun is made 0^o

The Figure 41 shows the amount of insolation that a hemisphere captures throughout the day when it is placed at latitude of 90 N. It can be seen that it is constant and energy capture for this geometry would be the highest.

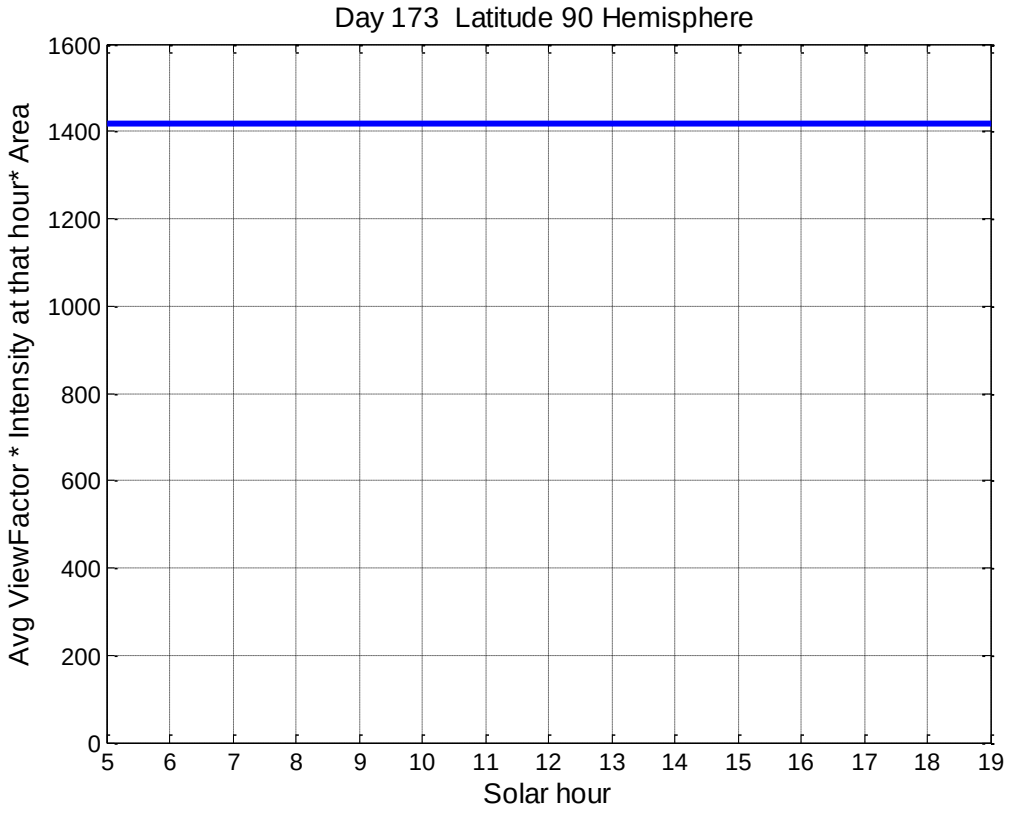

Figure 41: Energy capture of a hemispherical surface at latitude 90

Considering the similar case if we use a cylindrical or a semi cylindrical geometry, Figure 42 illustrates how it would be done. It needs to be observed as in how the energy capture varies as the sun moves in the horizon due to asymmetry in the cylindrical and semi cylindrical geometries. Thus it can be stated that hemispherical geometry is the best choice for this kind of application.

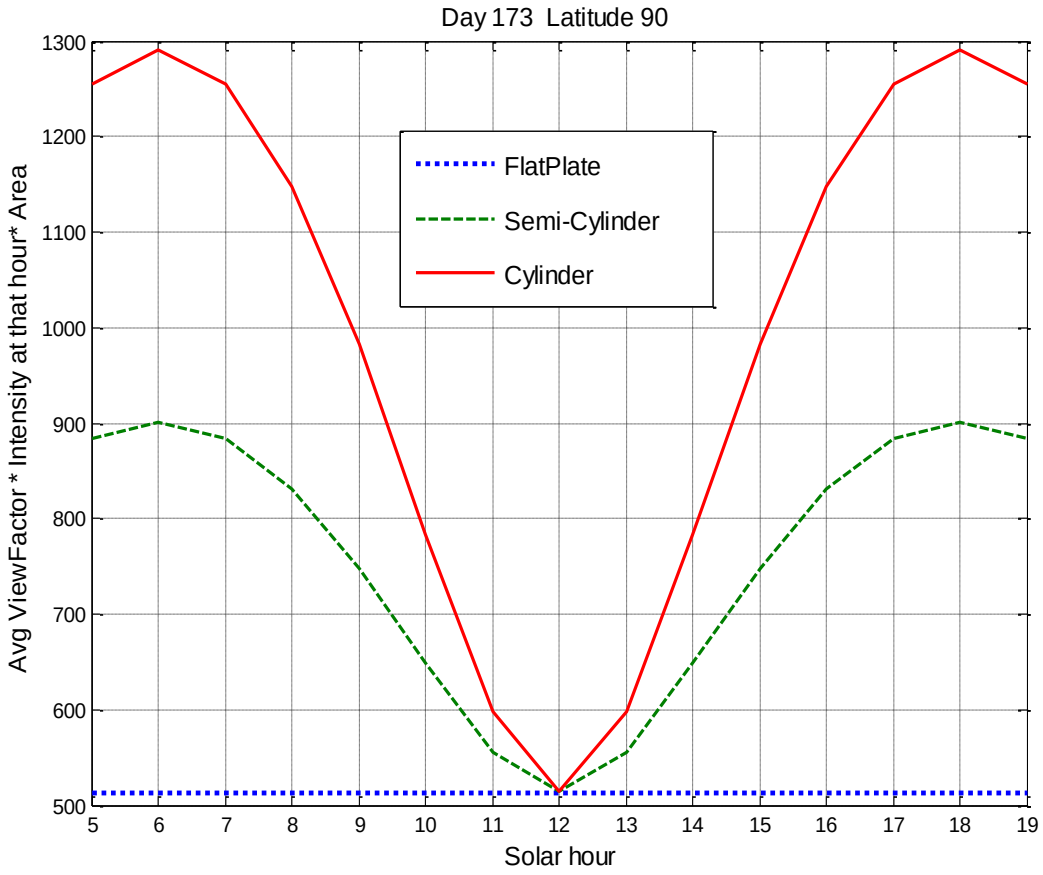

Figure 42: Comparison of energy harvest for cylindrical, semi-cylindrical and flat surfaces

Application

For scientific research expeditions that head out to Arctic and Antarctic area's can use a solar panels of hemispherical geometry for more energy capture instead of a flat plate and can get more energy for a given footprint and can maximize the energy harvest.

Also for extra terrestrial applications, the sensor with hemispherical panel can be dropped off from the space craft to collect data. Since the hemisphere is symmetrical it

need to aligned or tilted for maximum energy harvest unlike a flat panel. This can be used for defense applications for dropping off sensors on field from aircraft to collect data.

It has to be noted that in all comparisons that are done just the solar energy that is captured is taken into account and not the electrical energy that is obtained after the conversion which is dependent upon the design of appropriate power electronic circuitry. This shows that even though using different geometries provide advantages over flat plate in many applications to utilize this advantage efficient power electronic circuitry needs to be designed to gain the maximized energy output. Thus the results from this research can be utilized to obtain the variations in solar insolation falling on the surface and modeling the *v-i* characteristics to design the efficient circuitry.

Chapter summary

This chapter systematically compared various geometries and stated few applications where various geometries can perform better than a conventional flat plate. For applications where energy capture must be high during early morning and evening hours a cylindrical or semi-cylindrical geometry can be used. And in the applications where consistent energy capture is required like for Arctic and Antarctic expeditions, a solar panel of hemispherical geometry would be ideal.

CHAPTER VI

APPLICATION: OPTIMIZING ENERGY AVAILABILITY TO AUTONOMOUS STAND-ALONE POWER SYSTEM

Stand-alone power systems

A stand-alone power system supplies power to a load which is electrically isolated from the utility grid which is shown in Figure 43. It is custom designed to supply power to a specific load, based on its application. For present study stand-alone systems typically can be categorized into two types based on its scale.

1. Large scale stand-alone power systems supply power to remotely located homes, isolated light houses, unattended pumps, etc., for these systems the average power requirement maybe high but the necessity of the power system to continuously supply the load may be not be critical.
2. Small scale stand-alone power systems supply power to sign lighting, agricultural sensors and controls, geological and metrological sensors, broadband Internet hardware, sensors for monitoring gas level in pipelines across international borders, remotely located telecommunication transmitters and receivers etc. for these systems the average power required for the loads may be low, but the necessity of the power system to continuously supply the load is very critical.

For any kind of stand-alone system the common characteristic is the impracticality of feeding the load from a utility grid. The best source for generation of electricity for these kinds of stand-alone systems is a renewable energy source, but due to the intermittent

nature of the renewable energy sources it is required that the system contains a storage system to supply power whenever the renewable energy source will not be available.

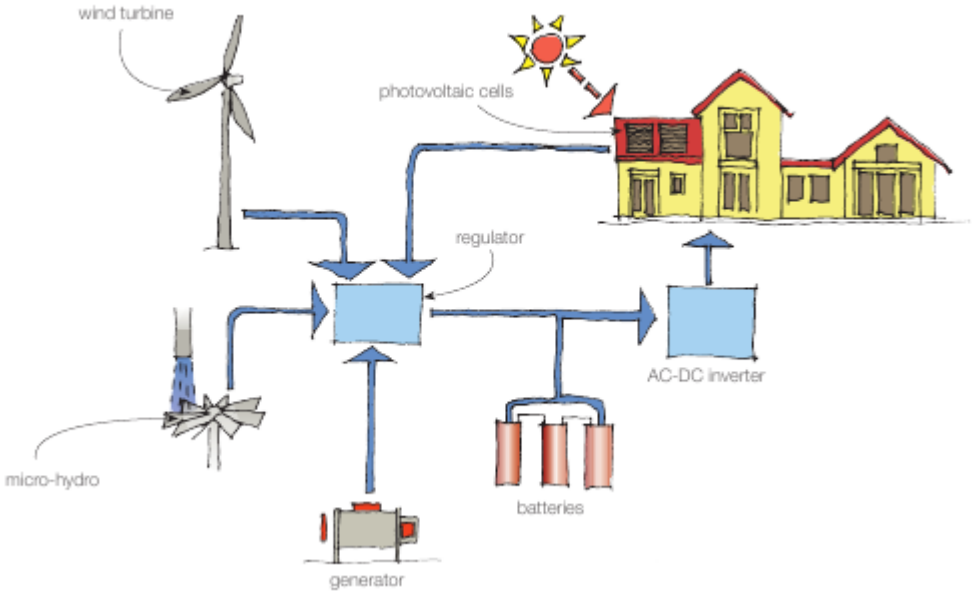

Figure 43: Stand-alone power generation system [75]

Electrical energy storage systems

The electrical energy storage systems in general are useful in power system applications to economically meet peak loads, quickly provide spinning reserve, improve power quality and stability, maintain reliability and security and sometimes to defer the installation of new transmission lines [76]. Also increasing integration of renewable energy sources into the grid is necessitating the use of electrical energy storage systems to stabilize the output from renewable energy sources. The storage systems can be of various kinds like pumped hydro, fuel cells, flywheels, super capacitors, etc., [77] but based on the availability of the resource, geographic

conditions, size of the load, its application etc., the choice of storage system varies. There are various applications which require the usage of electrical energy storage systems and their requirements differ widely. Table 6 summarizes various applications and their requirements.

For the stand-alone power system, that is being considered for the research, energy storage system is required for enabling renewable energy technologies but for small scale stand-alone applications. Table 7 compares various electrical energy generation technologies and their characteristics.

Table 6: Various applications and their energy storage requirements

Application	Matching Electricity Supply to Load Demand	Providing Backup Power to Prevent Outages	Enabling Renewable Technologies	Power Quality
Discharged Power	< 1MW to 100's of MW	1 – 200 MW	20kW to 10 MW	1 kW to 20MW
Response Time	< 10min	< 10ms (prompt) < 10 min (conventional)	< 1sec	< 20ms
Energy Stored	1 MWh to 1000 MWh	1 MWh to 1000 MWh	10 kWh to 200 MWh	50 to 500 kWh
Need for high efficiency	High	Medium	High	Low
Need long cycle or calendar life	High	High	High	Medium

Table 7: Comparison of various storage energy technologies

Storage Technology	Pumped Hydropower	Compressed Air Storage	Batteries	Flywheels	SMES	Capacitors
Energy Storage Capacity	<24,000 MWh	400 - 7200 MWh	<200 MWh	< 100 kWh	0.6 kWh	0.3 kWh
Duration of Discharge at maximum power level	~ 12 hours	4 – 24 hours	1 – 8 hours	Minutes to 1 hour	10 s	10 s
Power Level	< 2000MW	100-300 MW	<30 MW	<100kW	200 kW	100 kW
Response Time	30 ms	3 -15 min (large scale)	30 ms	5 ms	5 ms	5 ms
Cycle Efficiency	0.87	0.8	0.70 - 0.85	0.93	0.95	0.95
Lifetime	40 yrs	30 yrs	2-10 yrs	20 yrs	40 yrs	40 yrs

It can be observed from Table 6 and Table 7 that for small scale stand-alone renewable energy applications to provide power to remotely located sensors, batteries are best suited as energy storage systems owing to their quick response time, portability, scalability and duration of discharge.

Energy sources for small scale stand-alone power systems

Different types of sources for energy generation have been proposed in literature for such small scale autonomous systems which power a remotely located sensor like, mechanical vibration [78-81], ambient radio frequency energy [82, 83], wind [84-87], and solar energy[88-90]. Each kind of source has its own advantages and disadvantages. Solar energy has the most advantages and the least disadvantages, when compared with

other energy sources and is the energy source considered for the system described in the coming sections. These kinds of applications need very high power density which is obtained through solar energy as noted in [90]. These energy harvesting systems need to be optimized such that there is minimal amount of storage required to supply the load continuously.

Solar energy harvesting systems for remote loads

Coming to solar energy harvesting systems for remotely located sensor loads, there is one system that is designed and present in the paper [29]. The system design – energy flow diagram for such system is shown in the Figure 44.

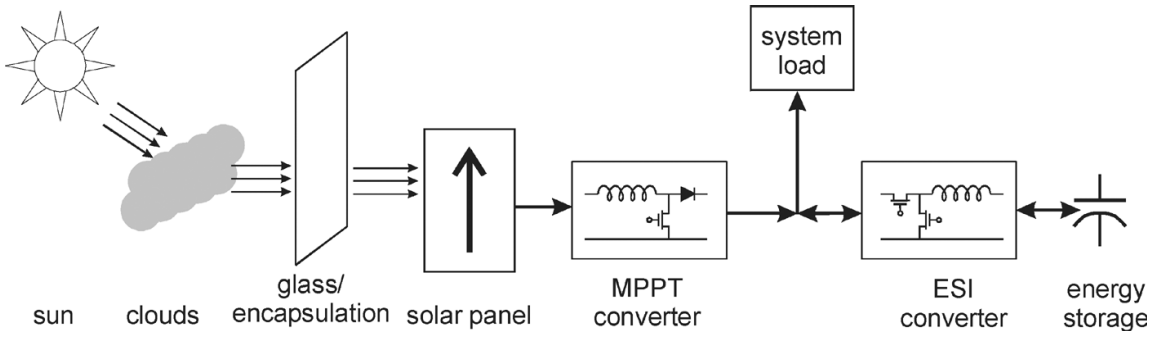

Figure 44: System design- energy flow diagram [29].

The system presented in the Figure 44 generates the regulated DC voltage for the load by drawing energy from the sun. All practical considerations like sun's energy passing through atmosphere, then passing through the glass encapsulation to solar panel are taken into account. To harvest maximum solar energy available from the solar panel and to minimize the size of solar panel required to supply the power the input converter

an is designed as a MPPT converter [31]. To store excess energy that is gathered during daylight hours and to deliver it to the load at night or on days when there is no adequate amount of solar energy to power the load, a bidirectional power electronic circuit the energy storage interface (ESI), is used [91]. The system presented in Figure 44 represents the important functions that are needed in a remotely located, autonomous power system. The energy generation system, storage system, and load are isolated through different power converters which is an important advantage of the topology in Figure 44, unlike, topologies such as [92] and [93], which are isolated through a transformer, and are effective where either a galvanic isolation or substantial voltage gain is required for the load. The following are the functions any remote power source should include the [29]:

1) Source of energy;
2) Maximization of power generation;
3) Monitoring and management of energy flow;
4) Conditioning of storage device for prolonged life;
5) Regulation of voltage at the output;
6) Protection from faults;
7) Fault tolerance.

This paper [29] with this energy system as a model presents a system availability simulation methodology which calculated the overall availability of the power system in a day which is averaged over 30 years. Availability is defined as the percentage of the time when energy is present to power the load. It is required to clearly differentiate

reliability and availability. Reliability is the system's capability to function without failure and availability is the system's ability to power the load continuously. An exceptionally reliable system, which is prone to failures, may have less availability if during night or during an overcast day there is no enough storage capacity to support the power requirements of the load, or if there is no sufficient generation of energy to recharge the system. Table 8 gives numerical values of system availability in percentages and the resultant unavailability in time over a thirty-year period for the availability calculations in this research. To simulate real-time environmental conditions this methodology uses historical insolation data, present at the NSRDB over a 30-year period, from 1961 to 1990, [94]. Model is constructed to approximately calculate the comprehensive availability of the system using the hourly incident solar insolation data from the NSRDB. The algorithm, shown below in pseudo-code [29], computes the number of hours when the net energy generated and stored falls to zero, making the system unable to provide power to the load. This number of hours is then converted to availability of the system over the 30 years period of time.

```
// intialize model
I=0              // increment over hourly datapoints in dataset
Bad_Hours =0     // counting the number of bad hours detected
Stored_Energy = Max_Avail_Stored   // begin full

// loop over all hours in dataset
WHILE (Not end_of_the_dataset)
      I=I+1
      Input_Energy = Insolation*Area*Efficiency
      Net_Energy = Input_Energy-Load_Energy-losses //can be +or -
      Stored_Energy_New = Stored_Energy_Last+Net_Energy

      IF (Stored_Energy > Max_Avail_Stored)
            Stored_Energy = Max_Avail_Stored
      END IF

      IF (Stored_Energy < 0)    // no stored energy remaining
           Stored_Energy= 0      // dont allow stored energy to go
      // negative
            Bad_Hours = Bad_Hours+1   // count the bad hours
      END IF
END WHILE

// Compute Availability
Availability =1 - Bad_Hours/I
```

Figure 45: Pseudo code for calculating the availability of the power system

Table 8: Unavailable time in 30 years

Availability	Unavailable time in 30 years
99.999%	2.63 hours
99.99%	26.3 hours
99.9%	11 days
99%	15.6 weeks
90%	36.5 months

If the system is available for 90% of the time it would not be able to supply power to the load for 36.5 months in a 30 year period.

The model of the system in Figure 44 was used in conjunction with the 30-year hourly solar insolation data [94] for Tucson to determine the availability of this solar energy harvesting system in a day by using a constant load and constant energy storage. The results presented in the paper indicate that the availability of the system drops during the early morning and evening hours. The proposed system in the paper uses a flat solar panel for the power generation. With the energy harvesting results obtained for various geometries so far, as shown in previous chapters, using the same modeling approach, instead of conventional flat plate geometry for the panel non flat geometries can be used to increase the availability during early morning and evening hours. So the model uses the same methodology as presented in the paper [29] but uses various other geometries to increase the availability of the system. The view factors for the various geometries are obtained from the modeling approach presented in chapter 3 and the insolation values for 30 years are taken from the National Solar Radiation Data Base (NSRDB) [94] to get the availability curve for the system. The following section presents the validation of the approach by comparing the values obtained from the flat plate model presented in chapter 3 with the NREL data that is collected over 30 years period.

Validation of the results

The National Solar Radiation Data Base (NSRDB) contains complete collection of hourly values of the three most common measurements of solar radiation (global horizontal, direct normal, and diffuse horizontal) over a 30 year period of time for 236

sites across the United States. The following are the definitions for the various measurements of solar radiation that are collected by NSRDB [94] :

- Global horizontal irradiance: Irradiance produced by solar radiation on a horizontal surface on the earth. This measurement of irradiance takes into account the view factor of the flat plate placed on ground.
- Direct normal irradiance: Principal component of sunshine, directly from the sun
- Diffuse normal irradiance: Secondary component of sun shine scattered by sky

The Figure 46 gives the various components of solar irradiance. These irradiance values in the database are collected values by placing pyranometers and pyrheliometers at various sites. The global horizontal irradiance obtained from the database must be approximately equal to

$$\text{Direct normal irradiance} * \text{View factor of the flat plate} + \text{Diffuse normal irradiance} \quad \text{Eq.14}$$

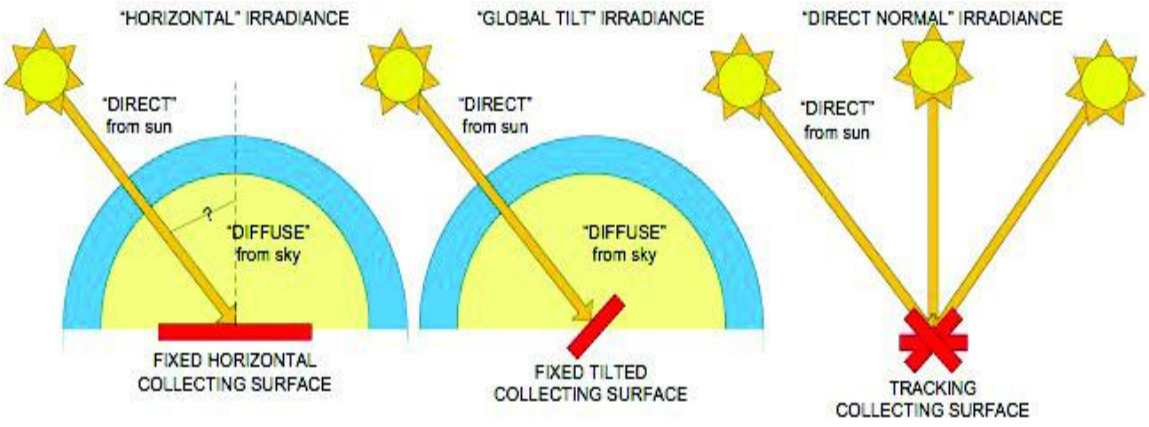

Figure 46: Components of solar irradiance

The modeling approach used to obtain the view factors for flat plate is used to get the view factor at every hour and it is multiplied by the direct normal irradiance and diffuse component which are also taken from NSRDB is added to it. The resultant value obtained must be approximately equal to the actual measured global horizontal irradiance data from NSRDB. The Figure 47 gives the comparison. It can be observed that there is discrepancy between the actual NSRDB values and values obtained from modeling approach. The reason for this discrepancy was investigated and it has been observed that the NSRDB values for iraadiance are the radiant energy elements integrated over the hour preceding the designated time in the data base and hence when the view factor is calculated at every hour is used, there is discrepancy and hence the view factor exactly at the half hour is taken and the resultant values are replotted. i.e, instead of view factor at 8:00 am and 9:00 am the view factor is calculated at 8:30 am and the values are mulitplied.

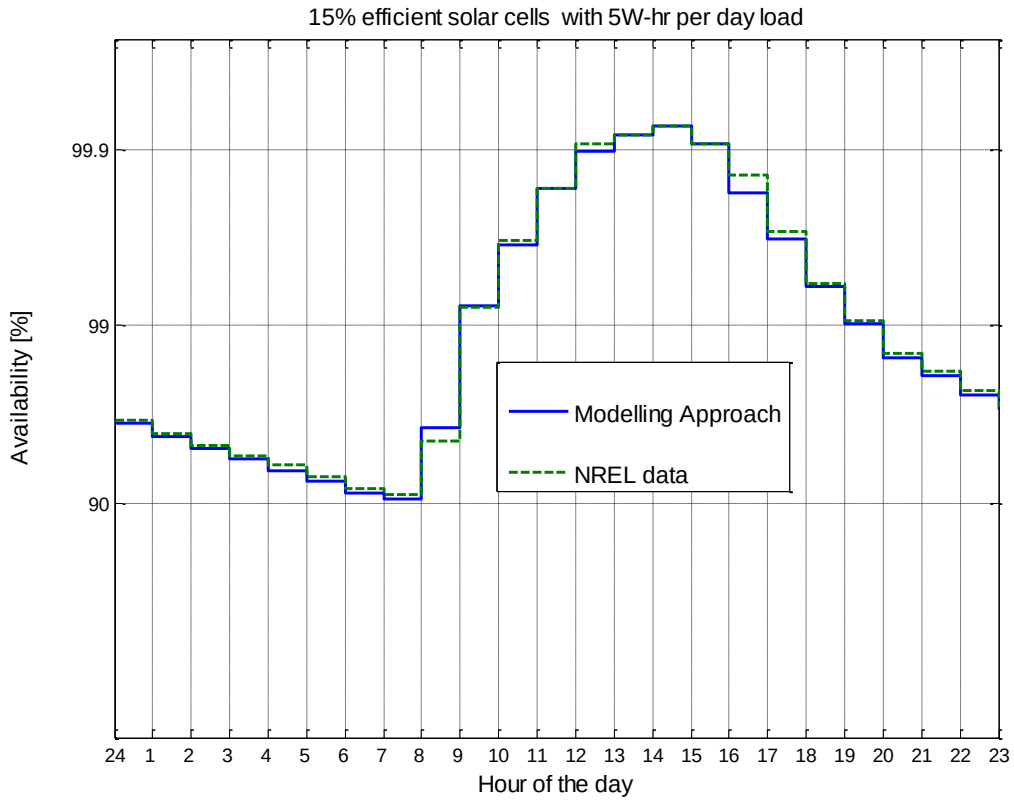

Figure 47: Comparison of values calculated from modeling approach and NREL data with discrepancy

It can be seen from Figure 47 that, during the morning hours, the availability calculated using the data from the model has higher values than the data from the NSRDB database [94]. This can be explained by considering that the value of insolation data that the data base stores is the *average value* of the total insolation from the *hour preceding* the data point..

For instance, if we consider the value of insolation given at 8:00 am it is the average value of the insolation obtained from 7:00 to 8:00 am and not the value collected at 8:00 am. At first to calculate the availability, the view factors for flat plate are calculated every hour at 7:00, 8:00 , 9:00 and so on. Let us consider a case during morning hours from 6:00 to 7:00 am, the average value of insolation calculated would be less than what it would be at 7:00 am. So when we consider view factor at 7:00 am and multiply it with average insolation we get higher values than the actual values, hence the data obtained from modeling has higher availability during morning hours and less during evening hours. Hence to correct this discrepancy and get correct values the view factors are taken in between the hours 7:30, 8:30 and 9:30 so on to get the average value and hence the correct insolation. The Figure 48 shows the comaprison between availability obtained from modeling approach and NSRDB data and it can be seen that the values are almost coincident with a maximum deviation of 0.002373 from original data at hour 9.

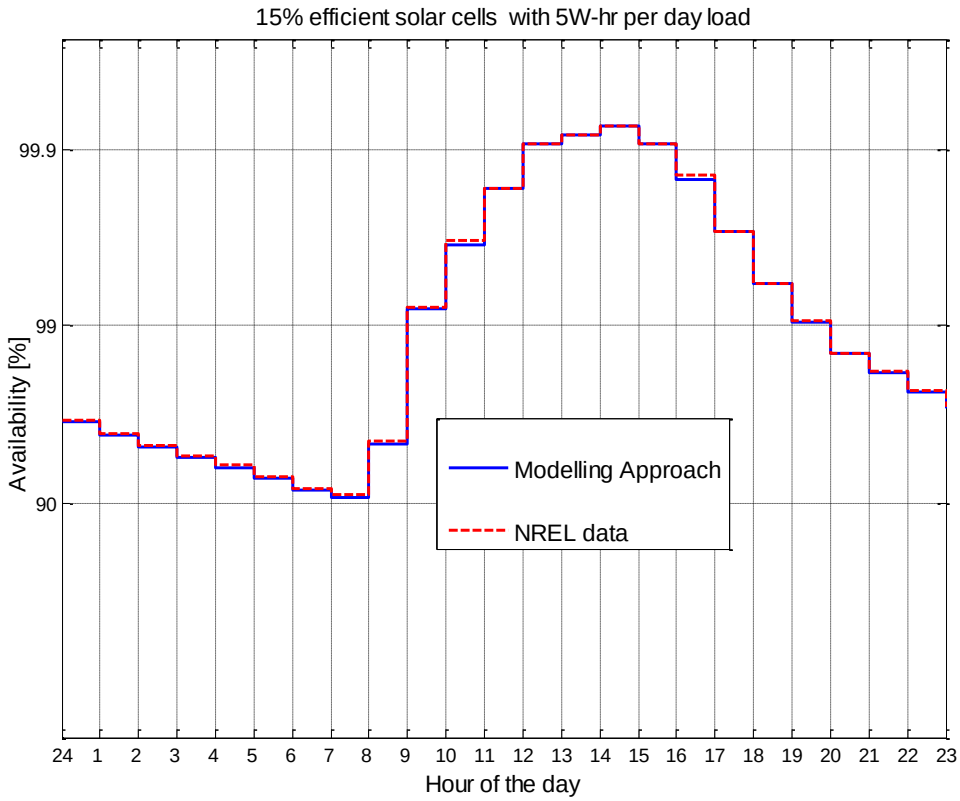

Figure 48: Comparison of values calculated from modeling approach and NSRDB data without discrepancy

To give a clear understanding of how the data is calculated and validated,Table 9: Calculation of insolation data from modeling approach and comparing it with NSRDB data presents an example picking day 1 i.e, January 1st data of Tucson from the NSRDB. The view factors for that particular day are calculated using the modeling approach and total insolation is obtained by

Total insolation= View factor* Direct normal insolation + Diffuse insolation

The direct normal and diffuse insolations are obtained form NSRDB. These values are compared against the global horizontal insolation obtained from NSRDB.

Table 9: Calculation of insolation data from modeling approach and comparing it with NSRDB data

View Factors	Direct Normal Insolation from NSRDB	Diffuse Insolation from NSRDB	Total Insolation obtained by multiplying the view factors and direct insolation +diffuse insolation	Global horizontal insolation from NSRDB
0	0	0		0
0	0	0	0	0
0	0	0	0	0
0	0	0	0	0
0	0	0	0	0
0	0	0	0	0
0	0	0	0	0
0	39.0	22.0	22.000	26.0
0.1820	440	58.0	138.080	143
0.3434	730	81.0	331.682	337
0.4673	843	92.0	485.933	492
0.5452	951	62.0	580.485	583
0.5718	968	64.0	617.502	617
0.5452	799	104	539.614	537
0.4673	729	100	440.661	437
0.3434	561	85.0	277.647	271
0.1820	452	45.0	127.264	123
0	119	11.0	11.000	24.0
0	0	0	0	0
0	0	0	0	0
0	0	0	0	0
0	0	0	0	0
0	0	0	0	0
0	0	0	0	0
	total		3571.871	3590

It can be seen that the values are almost coincident with a maximum deviation of 7 W-hr at 9:00 in the morning and we obtained perfect data. Figure 49 gives the comparison of data for a single day and it is perfectly coincident with the NSRDB data.

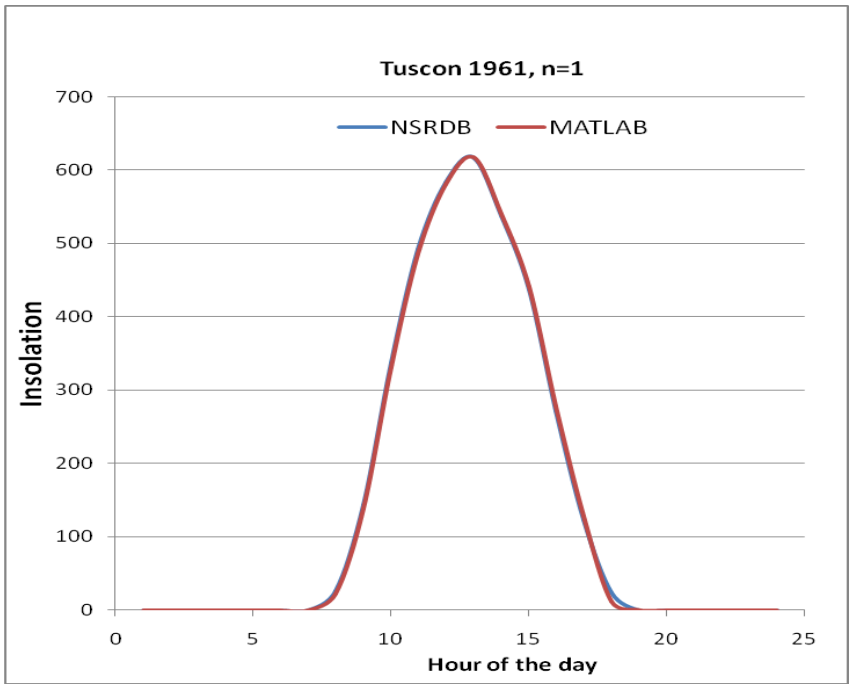

Figure 49: Comparison of insolation data for a single day.

This insolation values are then multiplied with the area of the cell and efficiency to get the energy generated. Thus the modeling approach is validated again, against the real time data from NSRDB. This approach is taken forward and availability for different geometries is compared against flat plate in the next section.

Comparison and results

The view factors from results obtained from the modeling approach are taken and put in the remote and unattended system model to get the availability for a constant footprint but for different geometries. The important parameters that can be varied for optimized output for this modeling approach are

1. Area of the footprint for the panel.

2. Storage capacity available.

Also the simulations are done for both a losses less system and system with realistic losses. A loss less system assumes that after the conversion from solar energy to electrical energy by the panels, all the energy is used with no losses elsewhere in the system. In a system with realistic losses in the MPPT controller, ESI converter and storage system are considered lossy with a given efficiency and also are assumed to consume base power to run the equipment and also glass transmission efficiency is considered. The Net energy obtained is then calculated by subtracting these losses from generated energy and availability of the system is obtained.

Comparison of availability with a lossless system and with a realistic system

The Figure 50 gives the comparison of availability for a flat plate, semi-cylinder and a cylindrical solar panel for a loss less system. It can be seen that the energy availability increases for a semi-cylinder and then increases further for a cylindrical surface. But this system is not realistic and over estimates the availability so losses in the system need to be considered. Figure 51 gives the availability comparison but using a realistic system.

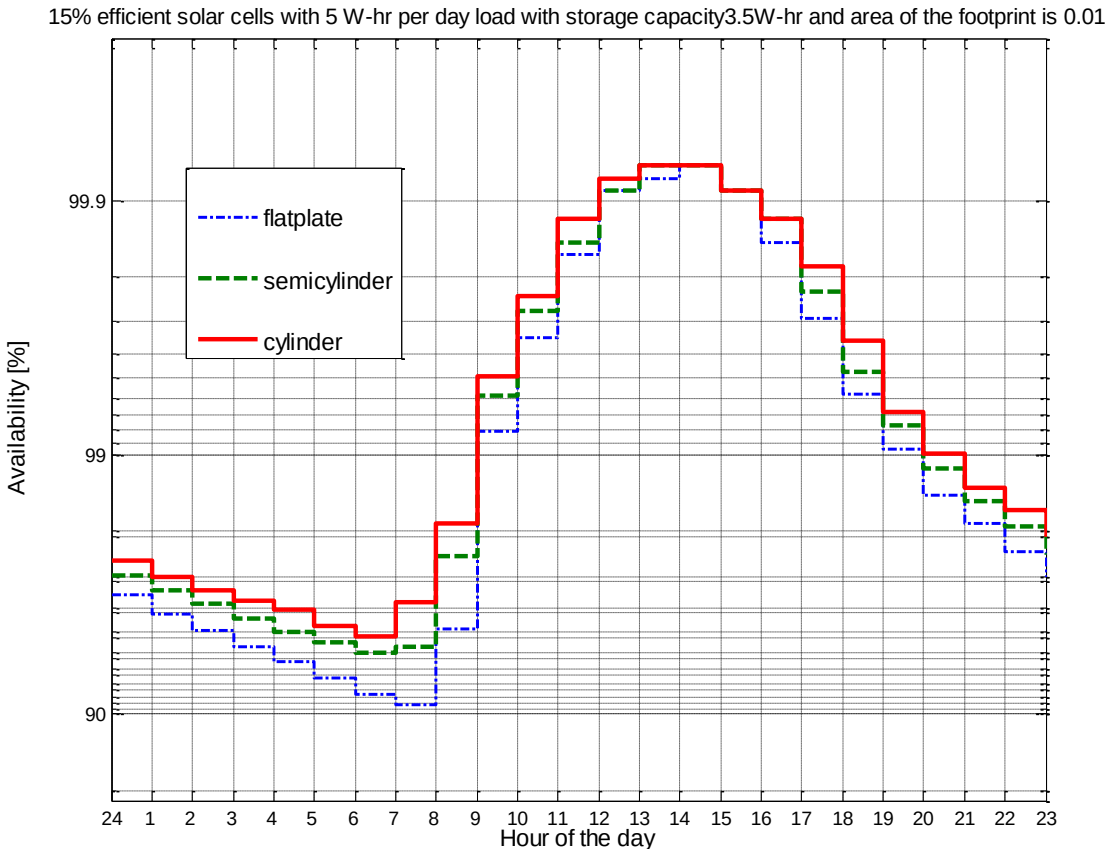

Figure 50: Comparison of energy availability in a loss less ideal system

It can be seen that availability of the system is more for a lossless system than a lossy system. But when we consider the increase in availability between different geometries it is evident from the lossy system comparison that, the system is now more available when moved to a semi-cylinder or a cylinder. This is because, if we consider the increase in energy obtained, when a semi-cylinder or cylindrical geometry is used, is little more than a flat plate. And when a lossless system was considered the flat plate was able to supply the load equivalent to a semi-cylinder or cylindrical geometry. But when the losses are considered, the flat plate was not able to generate that extra energy needed to

make the system available but a cylindrical or a semi-cylindrical geometry was able to supply the load. Thus, the full advantage of using geometry other than a flat plate can be made when a realistic system is taken into consideration.

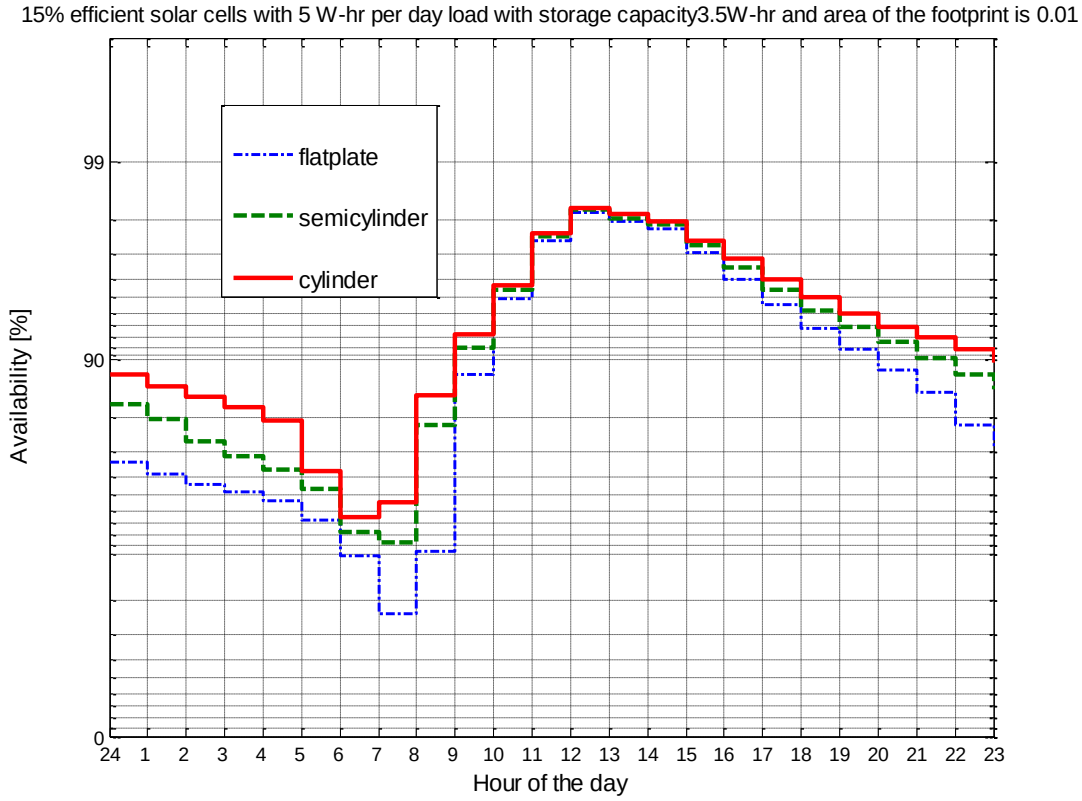

Figure 51: Comparison of energy availability in system including losses

Effect of variation of footprint of the panel on the availability

The Figure 52 and Figure 53 show how the availability of the system changes when the footprint of the panel used is increased. It can be seen that as the footprint is increased the availability increased.

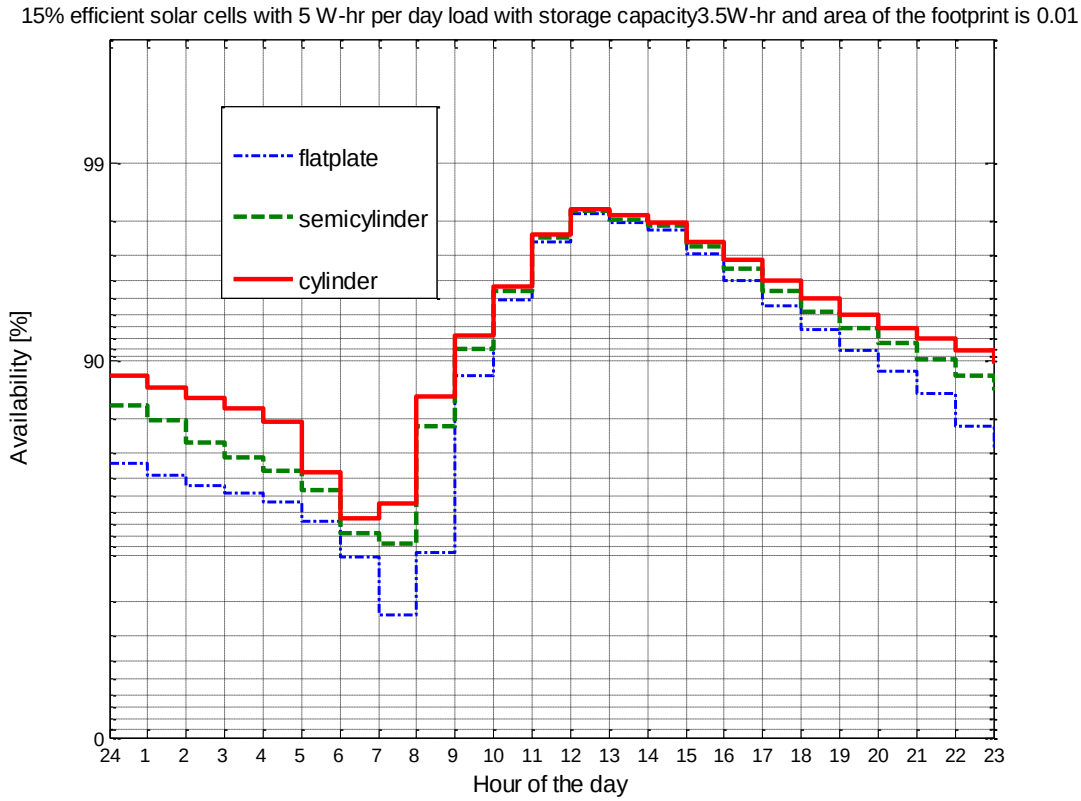

Figure 52: Availability comparison for 0.01 m^2 area of footprint

Important observation that needs to be made here is that, when the footprint is increasing as the day progresses the flat plate, semi-cylinder and cylindrical geometries have the same availability and the inherent advantage of using a different geometry other than a flat plate is lost. So for a given smallest possible footprint of area the comparison has to be made.

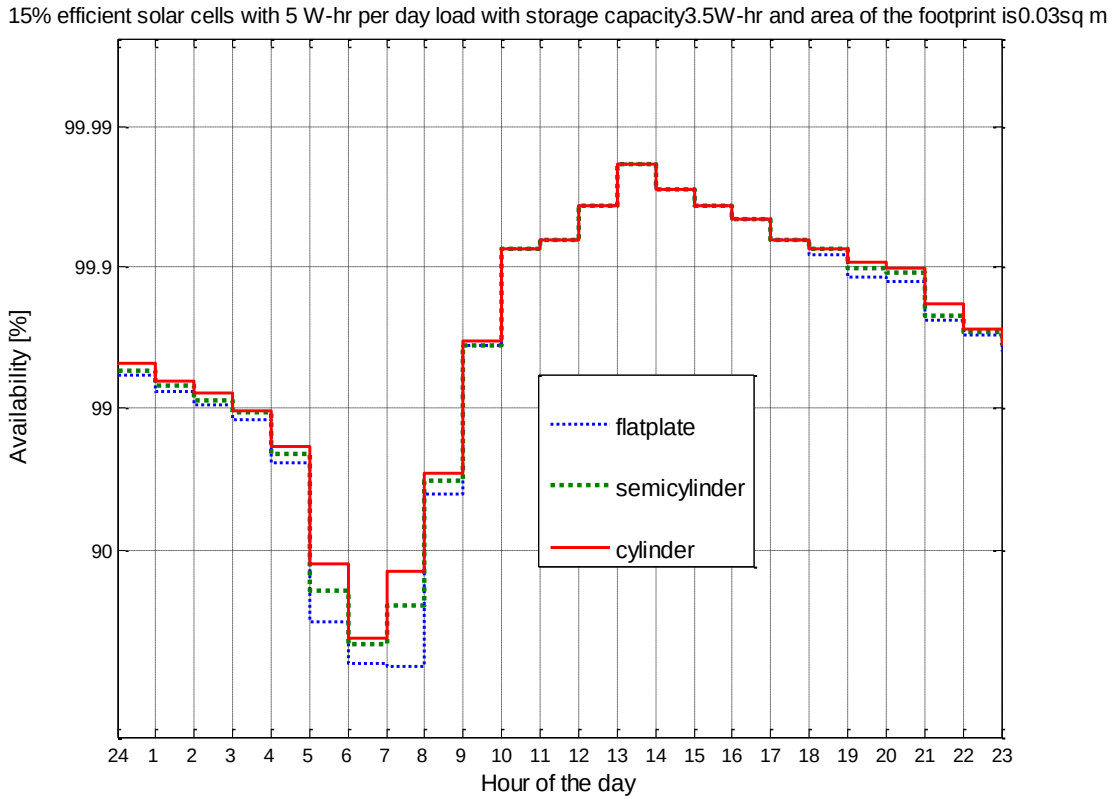

Figure 53: Availability comparison for 0.03 m^2 area of footprint

Effect of variation of storage capacity of the power system on the availability

The Figure 54 and Figure 55 show how the availability of the system changes when the footprint of the panel used is increased. It can be seen that in general as the storage capacity increased the availability increased. But when the availability increase is considered over the day the cylindrical geometry is more available than a semi-cylindrical geometry, which is more available than a flat plate.

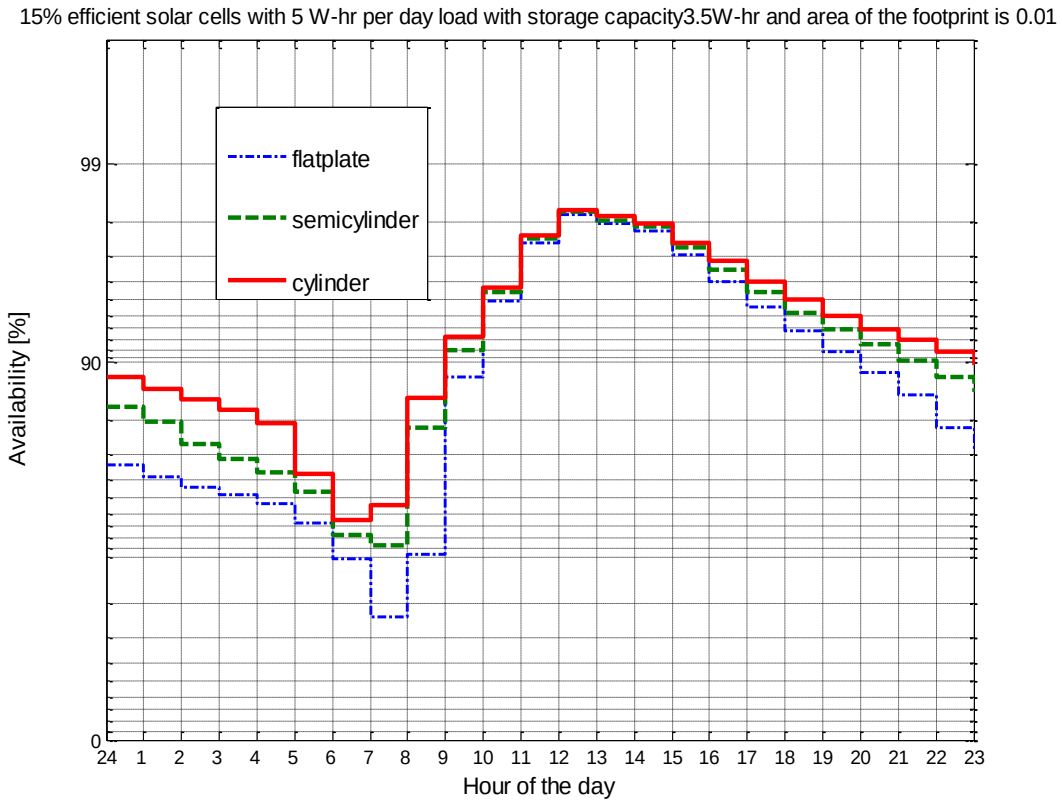

Figure 54: Availability comparison for 3.5 W-hr storage capacities

This is so because when the storage is limited to 3.5 W-hr the excess energy that is generated by the non flat geometries is going waste due to lack of storage in evening hours. But when the storage capacity is increased it can be seen that a non flat geometry indeed generates more energy which when stored increases the availability of the system throughout the day. Hence the non flat geometry best performs when an optimal storage and an optimal footprint is considered, taking all these observations into account.

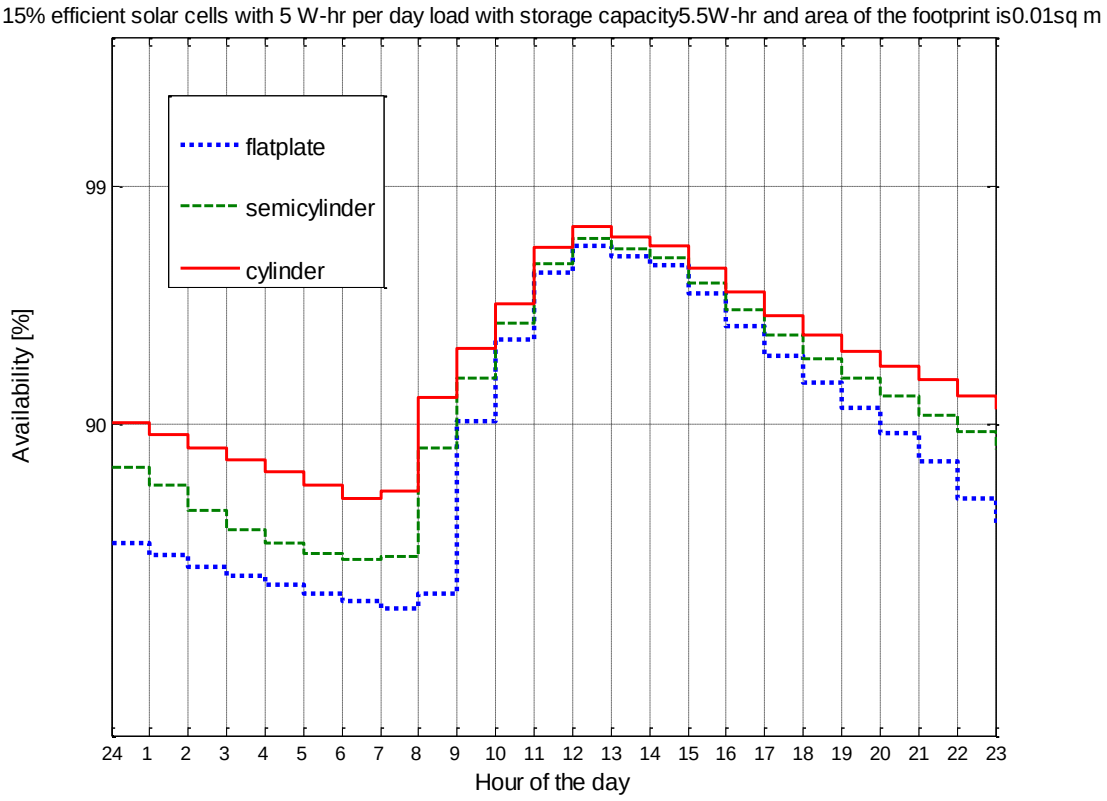

Figure 55: Availability comparison for 5.5 W-hr storage capacities

Analyzing the results obtained

Until now whenever the availability was compared it was just done qualitatively by looking at the graph and its increase. But in order to appreciate the increase the quantitative analysis of the results needs to be done which is presented in this section. First the analysis is carried out for a hemispherical geometry and a flat geometry and then the same analysis is applied for comparing the semi cylindrical and flat plate geometries for a constant footprint.

The Figure 56 gives the availability graph comparison between a hemisphere and flat plate with footprint of area $0.0314m^2$, for a load of 5 W-hr and storage of 3.5 W-hr and the system is assumed to have no losses for calculations. It can be seen that availability for a hemisphere is greater than a flat plate throughout the day.

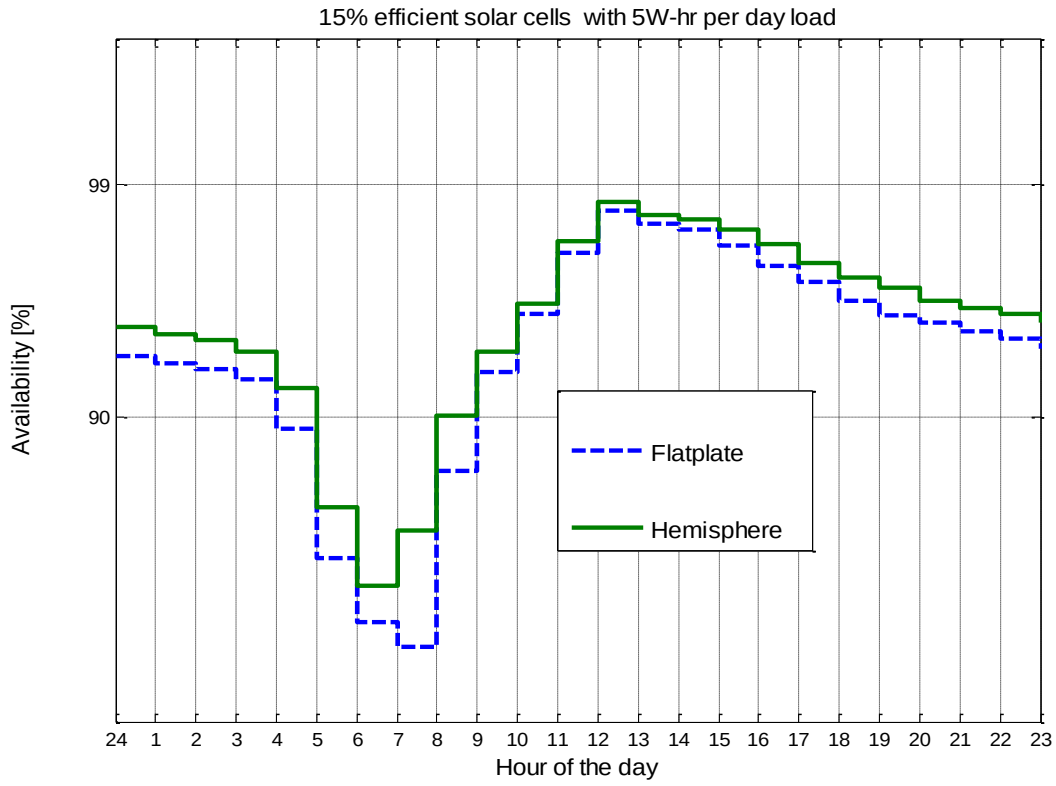

Figure 56: Comparison of the availability between a hemispherical PV module and a flat PV module

The following Table 10 gives the difference between percentage availability for thirty years normalized for each year at each hour. The difference in the percentage is converted into no. of days per year for a reasonable comparison of increase in

availability. It can be seen that availability of the system is increased during early morning hours and specifically by 138 days per year at 7:00 AM.

Table 10: Increase in the availability for hemispherical PV module

Hour	% Diff	No. Of Days/year	Hour	% Diff	No. of Days/year	Hour	% Diff	No. of Days/year
1	1.4603	5.3	9	1.1226	4.1	17	0.4381	1.6
2	1.6245	5.9	10	0.3194	1.1	18	0.6754	2.4
3	1.6519	6.0	11	0.2008	0.7	19	0.8853	3.2
4	3.5867	13.0	12	0.1004	0.3	20	0.7940	2.9
5	12.348	45.1	13	0.1278	0.4	21	0.8853	3.2
6	12.522	45.7	14	0.1643	0.5	22	0.9674	3.5
7	37.839	138.2	15	0.2647	0.9	23	1.1499	4.1
8	6.6442	24.2	16	0.4472	1.6	24	1.3598	4.9

Similarly, Figure 57 gives the availability comparison for semi-cylinder and flat plate. The footprint is constant at $0.01m^2$ for a load of 5 W-hr and constant storage of 3.5 W-hr. The system is a non ideal with losses considered for calculations. It can be seen that availability for semi-cylinder is greater than a flat plate especially during early morning and evening hours.

The following Table 11 gives the difference between availability for thirty years normalized for each year at each hour; the difference in the percentage is converted into no. of days for a reasonable comparison of increase in availability. It can be observed that there is huge increase in the availability during early morning hours and a maximum of increase of availability of the system for 158 days per year at 8:00 AM.

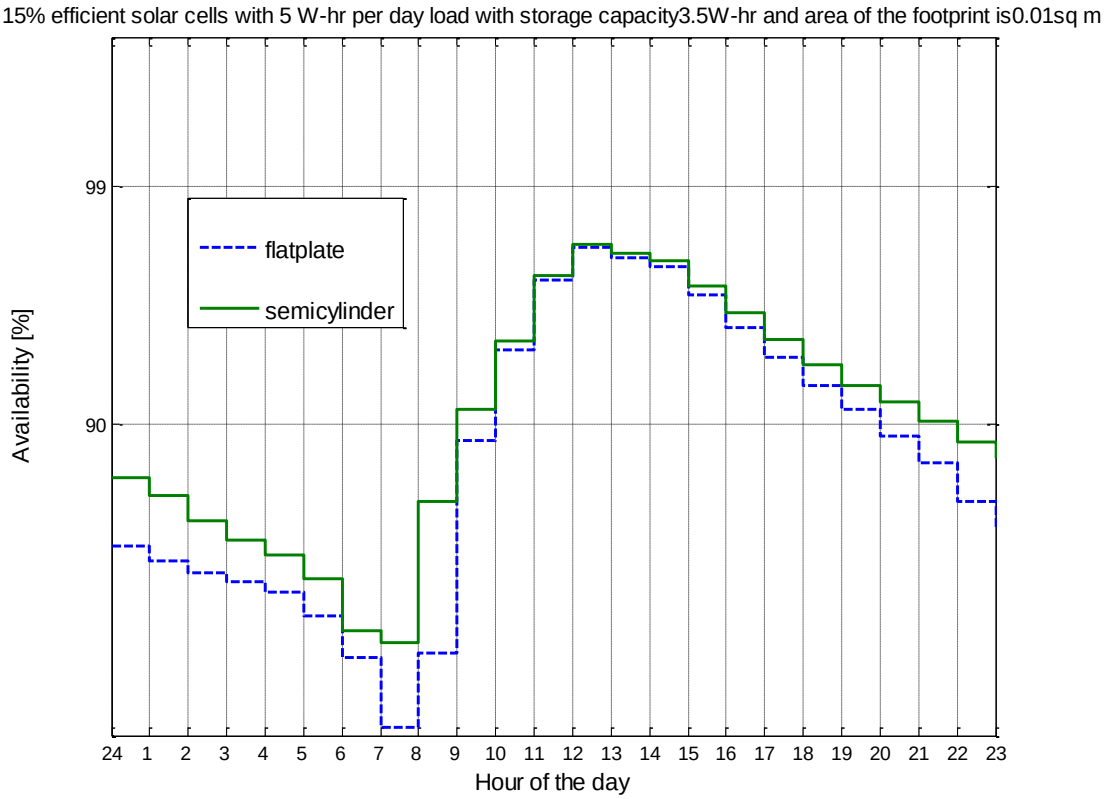

Figure 57: Comparison of the availability between a semi-cylindrical PV module and a flat PV module

Table 11: Increase in the availability for semi-cylindrical PV module

Hour	% Diff	No. Of Days/year	Hour	% Diff	No. of Days/year	Hour	% Diff	No. of Days/year
1	14.228	51.9	9	3.0392	11.0	17	0.8305	3.0
2	12.759	46.5	10	0.4107	1.4	18	1.2412	4.5
3	11.262	41.1	11	0.1095	0.3	19	1.8618	6.7
4	10.778	39.3	12	0.0639	0.2	20	3.0209	11.0
5	11.992	43.8	13	0.0730	0.2	21	4.6454	16.9
6	9.7746	35.6	14	0.1004	0.3	22	8.5242	31.1
7	28.137	102.7	15	0.2464	0.9	23	11.983	43.7
8	43.671	159.5	16	0.5020	1.8	24	13.498	49.3

Similar results can be analyzed for various areas and storage options to increase the availability. It needs to be noted that if the storage capacity and footprint is increased the availability increases but the main aim of the remotely located system is to minimize this energy storage and footprint by increasing the energy generation through non flat geometries.

Chapter summary

This chapter presents an autonomous energy harvesting system for a remotely located load and uses a methodology presented in paper [29] to calculate the availability of the system. It is shown that using a non flat geometry for a PV panel for a same footprint, the availability can be improved. If the same availability needs to be obtained, using a non flat geometry will in fact reduce the amount of storage and also the footprint of the panel required to supply the load.

CHAPTER VII

FUTURE WORK AND CONCLUSION

Emerging PV cell technologies no longer impose the requirement for a rigid flat PV module. This research presents a method and analysis technique to determine the impact of arbitrary non-flat geometries on energy harvest and the implications for the power electronics circuitry and controls for maximum power point tracking. This thesis illustrates the modeling approach to determine the view factors for any surface so that the amount of energy captured by the various parts of the surface can be studied. This also led to an interesting result that more energy can be captured by moving towards novel geometries for a given footprint. Also the research has studied the modeling approach to calculate the availability of a stand-alone power system supplying power to load using conventional flat PV panel. Then, using the same methodology, it has proved that by using a non flat geometry for a PV module the availability of the system can be increased by greater extent. This research concludes that to be able to effectively capture the energy harvested by these novel geometries, power electronics engineers should move away from conventional circuitry design to more sophisticated and efficient design. This research presents the first step towards that goal by giving a modeling approach to understand the variations in energy capture of various geometries and thereby the ground work to design better electronic circuitry to maximize the energy generation. This research can be taken forward in various directions as proposed in the subsequent sections.

Potential future work

Non-Flat geometries offer new opportunities for conformal and flexible PV modules, but have significant implications for the cell interconnection and power electronics needed to collect and convert the electricity generated to a useful form. An intentionally non-flat PV module exhibits a varying view factor to the sun, creating gradients in total incident solar radiation (insolation) across the surface of the module. This causes non-uniform current density, leading to locally circulating currents which reduces efficiency. When the module is partitioned into smaller cells to minimize variation in current density, each cell can generate different currents which limit the ability to arbitrarily interconnect these cells (such as the common series-connection) without adding bypass diode or extra circuitry. Cell-level maximum power point tracking is required to ensure maximum energy harvest when cells are interconnected within the PV module [25]. This impacts requirements for the power electronics circuitry and control algorithms.

A PV pixel may be comprised of numerous PV cells, in which the cells are optimized for electrical conversion efficiency, and other processing requirements. Cells that experience similar operating characteristics (not necessarily physically adjacent) can be wired in series/parallel combinations. Assuming that PV cell fabrication technology can produce cells of any size, it is essential to develop a top-down, application-driven mathematical approach to determine the optimal pixel size, PV cell size, the modes of integrating these cells into pixels for maximizing energy harvest and requirements for the balance of the autonomous energy generation system. Mathematical modeling

approach presented in this research will quantify the variations in electrical generation due to arbitrarily curved PV modules by obtaining the view factors across the surface and operating conditions (insolation and thermal gradients). The result will enable new applications in which the energy harvest is not limited by existing form factors, or existing integration methods.

Proposal 1

Consider the cell structure shown in the Figure 58. Let us assume that we have a non flat geometry for PV module like a wavy surface which represents the solar fabric. The Modeling approach presented in this thesis will give a matrix containing the view factors and thus the insolation at every point on the surface. The cells with same insolation capture are marked with same color thus, once we have this matrix and information about which cells have same insolation capture, those cells can be connected in series as shown in Figure 58. Thus appropriate power electronic circuitry can be designed to get maximum energy generation.

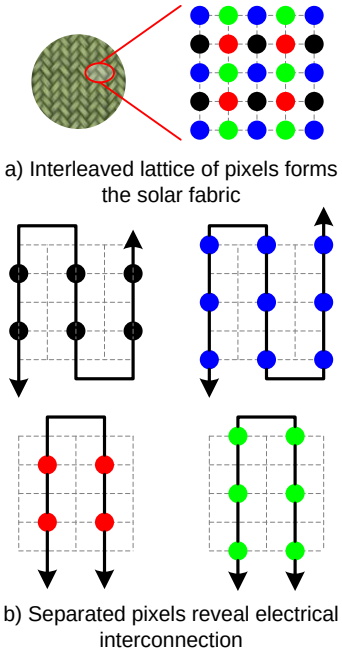

Figure 58: Cell structure for a solar fabric

Proposal 2

In Chapter VI, a non flat PV module was used in place of conventional flat plate module to increase the availability of the power system; it assumed the two module geometries to have same footprint. The hypothesis of this research proposal is to do the opposite of what has been done in this research, that is, the footprint of the PV collector can be reduced by using non-flat 3-D geometries that more effectively capture the available solar energy over the course of the entire daily and seasonal solar patterns. The expected outcome is the ability to reduce the size of the sensor footprint while still maintaining the same sensor energy availability. An optimal geometry that aligns the rate of energy generation (i.e., increased harvest in the early morning and later afternoon) with the rate it is consumed is expected to reduce the amount of energy

storage required while still providing the same energy availability. Considering the preliminary results for the semi-cylindrical shape, the feasibility of other geometries can be explored such as a semi-cylinder with a flatter top surface or different side-wall characteristics such as an inverted parabola.

REFERENCES

[1] U. S. Energy Information Administration, "International Energy Outlook 2010," Washington D.C, DC, Rep. DOE/EIA-0484(2010), Jul. 2010.

[2] R.Priddle, *World Energy Outlook*, Paris, France, International Energy Agency Press, 2008.

[3] G. Conibeer, "Third Generation Photovoltaics," *Materials Today,* Vol. 10, pp. 42-50, Nov. 2007.

[4] P. Frankl and S.Nowak, *Technology Roadmaps: Solar photovoltaic energy*, Paris, France, International Energy Agency Press,2010.

[5] E. Cartlidge. (2007). *Bright outlook for solar cells* [Online]. Available: http://physicsworld.com/cws/article/print/30345

[6] School of Photovoltaic and Renewable Energy Engineering. (2008). *Third generation photovoltaics* [Online]. Available: http://www.pv.unsw.edu.au/Research/3gp.asp

[7] T. Juvonen, J. Harkonen and R. Kuivalainen, "High efficiency single crystalline silicon solar cells," *Physica Scripta,* vol. T101, pp. 96-98, 2002.

[8] M. A. Green, "Silicon solar cells- evolution, high-efficiency design and efficiency enhancements," *Semiconductor Science and Technology,* vol. 8, pp. 1-12, Jan. 1993.

[9] M. A. Green, K. Emery, Y. Hishikawa and W. Warta, "Solar cell efficiency tables (version 36)," *Progress in Photovoltaics*, vol. 18, pp. 346-352, Aug. 2010.

[10] T. J. Gillespie, C. H. Marshall, M. Contreras and J. Keane, "Copper indium diselenide (CIS) process, control and manufacturing," *Solar Energy Materials and Solar Cells,* vol. 59, pp. 27-34, Sep. 1999.

[11] J. Britt and C. Ferekides, "Thin-film CdS/CdTe solar-cell with 15.8% efficiency," *Applied Physics Letters,* vol. 62, pp. 2851-2852, May 1993.

[12] F. Kessler and D. Rudmann, "Technological aspects of flexible CIGS solar cells and modules," *Solar Energy,* vol. 77, pp. 685-695, 2004.

[13] C. S. Ferekides, D. Marinskiy, V. Viswanathan, B. Tetali, V. Palekis, *et al.*, "High efficiency CSSCdTe solar cells," *Thin Solid Films,* vol. 361, pp. 520-526, Feb. 2000.

[14] B. Dimmler and R. Wachter, "Manufacturing and application of CIS solar modules," *Thin Solid Films,* vol. 515, pp. 5973-5978, May 2007.

[15] F. C. Krebs, T.Tromholt and M. Jorgensen, "Upscaling of polymer solar cell fabrication using full roll-to-roll processing," *Nanoscale,* vol. 2, pp. 873-886, 2010.

[16] B. R. Saunders and M. L. Turner, "Nanoparticle-polymer photovoltaic cells," *Advances in Colloid and Interface Science,* vol. 138, pp. 1-23, Apr. 2008.

[17] W. U. Huynh, J. J. Dittmer and A. P. Alivisatos, "Hybrid nanorod-polymer solar cells," *Science,* vol. 295, pp. 2425-2427, Mar. 2002.

[18] A. C. Arango, L. R. Johnson and V. N. Bliznyuk, "Efficient titanium oxide/conjugated polymer photovoltaics for solar energy conversion," *Advanced Materials,* vol. 12, pp. 1689, Nov. 2000.

[19] M. Gratzel, "Solar energy conversion by dye-sensitized photovoltaic cells," *Inorganic Chemistry,* vol. 44, pp. 6841-6851, Oct. 2005.

[20] Department of Energy. (2008). *Solar energy technologies program* [Online]. Available: http://www1.eere.energy.gov/solar/pdfs/solar_program_overview.pdf

[21] SolarBuzz (2011, May 5), *Module pricing* [Online]. Available: http://solarbuzz.com/facts-and-figures/retail-price-environment/module-prices

[22] Y. Hamakawa, "Recent advances of thin film solar cells and their technologies," in *Conf. Rec. of the 24th IEEE Photovoltaic Specialists Conf. on Photovoltaic Energy Conversion,* Waikoloa, HI, 1994, pp. 34-41, vol.1.

[23] A. A. D. T. Adikaari, D.M.N.M. Dissanayake and S.R.P. Silva, "Organic & inorganic solar cells: Recent developments and outlook," *Selected Topics in IEEE J. of Quantum Electron.,* vol. 16, pp. 1595-1606, 2010.

[24] J. Plastow, "Progress in building integrated PV technologies," in *Conf. Rec. of the IEEE 4th World Conf. on Photovoltaic Energy Conversion,* Waikoloa, HI, May 7-12, 2006, pp. 2316-2318.

[25] I. Caluianu, G. Notton, I. Colda, S Caluianu and A. Damian,, "Photovoltaic energy generation under partially shading conditions," in *8th Int. Symp. on Advanced Electromechanical Motion Systems & Electric Drives,* Lille, France, Jul. 1-3, 2009, pp. 1-6.

[26] G. M. Masters, *Renewable and Efficient Electric Power Systems*. Hoboken, NJ: John Wiley & Sons, 2004.

[27] A. F. Mills, *Heat Transfer,* 2nd ed. Upper Saddle River, N.J., Prentice Hall, 1999.

[28] P. J. Wolfs and L. Tang, "A single cell maximum power point tracking converter without a current sensor for high performance vehicle solar arrays," in *Power Electronics Specialists Conf.,* Recife, Brazil, 2005, pp. 165-171.

[29] J.W. Kimball, B.T. Kuhn and R.S. Balog; "A system design approach for unattended solar energy harvesting supply", *IEEE Trans. on Power Electron.*, vol. 24, no. 4, pp. 952-962, Apr. 2009.

[30] S. Kazmi, H. Goto, O. Ichinokura and Hai-Jiao Guo, "An improved and very efficient MPPT controller for PV systems subjected to rapidly varying atmospheric conditions and partial shading," in *Australasian Universities Power Engineering Conf.,* Adelaide, Australia, 2009, pp. 1-6.

[31] A. Durgadevi, S Arulselvi and S.P.Natarajan, "Study and implementation of Maximum Power Point Tracking (MPPT) algorithm for photovoltaic systems," in *1st Int. Conf. on Electrical Energy Systems,* Chennai, India, Jan. 3-5, 2011, pp. 240-245.

[32] D. Hohm and M. Ropp, "Comparative study of maximum power point tracking algorithms using an experimental, programmable, maximum power point tracking test," *in Proc. 28th IEEE Conf. Rec. Photovoltaic Specialists.*, Anchorage, Alaska, Sep. 17-22, 2000, pp. 1699–1702

[33] S. Jain and V. Agarwal, "Comparison of the performance of maximum power point tracking schemes applied to single-stage grid-connected photovoltaic systems," *Electric Power Applications,* vol. 1, pp. 753-762, 2007.

[34] M. S. Ngan and C. W. Tan, "A study of maximum power point tracking algorithms for stand-alone Photovoltaic Systems," in *IEEE Applied Power Electronics Colloq.,* Johor Bharu, Malaysia, April 18-19, 2011, pp. 22-27.

[35] R. Gules, J. De Pellegrin Pacheco, H. L. Hey, and J. Rnhoff, "A maximum power point tracking system with parallel connection for PV stand alone applications," *IEEE Trans. Ind. Electron.*, vol. 55, no. 7, pp. 2674–2683, Jul. 2008.

[36] L. Gao, R. A. Dougal, S. Liu and A. P. Iotova, "Parallel-connected solar PV system to address partial and rapidly fluctuating shadow conditions," *IEEE Trans. Ind. Electron.*, vol. 56, no. 5, pp. 1548–1556, May 2009.

[37] E. Román, R. Alonso, P. Ibañez, S. Elorduizapatarietxe, and D. Goitia, "Intelligent PV module for grid-connected PV systems," *IEEE Trans. Ind. Electron.*, vol. 53, no. 4, pp. 1066–1073, Jun. 2006

[38] W. Xiao, N. Ozog, and W. Dunford, "Topology study of photovoltaic interface for maximum power point tracking," *IEEE Trans. Ind. Electron.*,vol. 54, no. 3, pp. 1696–1704, Jun. 2007.

[39] A. Kajihara and T. Harakawa, "Model of photovoltaic cell circuit under partial shading," in *IEEE Int. Conf. on Industrial Technology,* Hong Kong, Dec. 15-18, 2005, pp. 866-87

[40] F. Liu, S. Duan, F. Liu, B. Liu, and Y. Kang, "A variable step size INC MPPT method for PV systems," *IEEE Trans. Ind. Electron.*, vol. 55, no. 7, pp. 2622–2628, Jul. 2008

[41] M.-L. Chiang, C.-C. Hua, and J.-R. Lin, "Direct power control for distributed PV power system," in *Proc. Power Conversion Conf.*, Osaka, Japan, 2002, pp. 311–315.

[42] W. Xiao and W. G. Dunford, "A modified adaptive hill climbing MPPT method for photovoltaic power systems," in *Proc. IEEE Power Electronics Specialists Conf.*, Aachen, Germany, Jun. 20-24, 2004, pp. 1957–1963.

[43] A. Pandey, N. Dasgupta, and A. K. Mukerjee, "Design issues in implementing MPPT for improved tracking and dynamic performance," in *Proc. IEEE Industrial Electronics Society Conf.*, Paris, France, Nov 7-10, 2006, pp. 4387–4395.

[44] N. Femia, D. Granozio, G. Petrone, G. Spagnuolo, and M. Vitelli, "Predictive & adaptive MPPT perturb and observe method," *IEEE Trans. Aerosp. Electron. Syst.*, vol. 43, no. 3, pp. 934–950, Jul. 2007.

[45] K. Irisawa, T. Saito, L. Takano, and Y. Sawada, "Maximum power point tracking control of photovoltaic generation system under non-uniform insolation by means of monitoring cells," in *Proc. IEEE 28th Photovoltaic Specialists Conf.*, Anchorage, AK, Sep. 15–22, 2000, pp. 1707–1717

[46] T. Noguchi, S. Togashi, and R. Nakamoto, "Short-current pulse-based maximum-power-point tracking method for multiple photovoltaic-and converter module system," *IEEE Trans. Ind. Electron.*, vol. 49, no. 1,pp. 217–223, Feb. 2002

[47] D. Sera, R. Teodorescu, J. Hantschel, and M. Knoll, "Optimized maximum power point tracker for fast-changing environmental conditions," *IEEE Trans. Ind. Electron.*, vol. 55, no. 7, pp. 2629-2637, Jul. 2008.

[48] H.-J. Chiu, H.-M. Huang, L.-W. Lin, and M.-H. Tseng, "A multiple-input dc/dc converter for renewable energy systems," in *Proc. Int. Conf. on Industrial Technology*, Hong Kong, China, Dec. 14–17, 2005, pp. 1304–1308.

[49] A. Kwasinski, “Identification of feasible topologies for multiple-input dcdc converters,” *IEEE Trans. Power Electron.*, vol. 24, no. 3, pp. 856–861,Mar. 2009

[50] Y. M. Chen, Y. C. Liu, and T. F. Wu, “Multi-input converter with power factor correction, maximum power point tracking, and ripple-free input currents,” *IEEE Trans. Power Electron.*, vol. 19, no. 3, pp. 631–639, May 2004

[51] J. J. Bzura, "The AC module: An overview and update on self-contained modular PV systems," in *IEEE Power and Energy Society General Meeting,* Minneapolis, MN, July 24-29, 2010, pp. 1-3.

[52] L. E. de Graaf and T. C. J. van der Weiden, “Characteristics and performance of a PV-system consisting of 20 AC modules,” in *Proc. IEEE World Conf. Exhibition Photovolt. Solar Energy Conversion,* Waikoloa, HI, 1994, pp.921–924.

[53] A. Hunter Fanney, B.P. Dougherty and M.W. Davis, "Performance and characterization of building integrated photovoltaic panels," in *Conf. Rec. of the 29th IEEE Photovoltaic Specialists Conf.*, New Orleans, LA, May 20-24, 2002, pp. 1493-1496.

[54] A. Kyritsis, N. Papanicolaou and E. Tatakis, “A novel parallel active filter for current pulsation smoothing on single stage grid-connected acpv modules,” in *European Conf. on Power Electronics and Applications,* Aalborg, Denmark, Sept. 2007, pp. 1 –10.

[55] T. Shimizu, K. Wada and N. Nakamura, ”Flyback type single-phase utility interactive inverter with power pulsation decoupling on the DC input for an AC photovoltaic module system” *IEEE Trans. on Power Electron*., Vol. 21, no. 5, pp.1264 - 127, Sept. 2006.

[56] R. H. Wills, S. Krauthamer, A. Bulawka and J.P. Posbic, "The AC photovoltaic module concept," in *Proc. of the 32nd Intersociety Energy Conversion Engineering Conf. (IECEC),* Honolulu, HI, Jul. 27- Aug. 1, 1997, pp. 1562-1563, vol.3.

[57] L. Battistelli, E. Chiodo and D. Lauria, "Bayes assessment of photovoltaic inverter system reliability and availability," in *Int. Symp. on Power Electronics*

Electrical Drives Automation and Motion (SPEEDAM), Pisa, Italy, Jun.14-16, 2010, pp. 628-634.

[58] J. M. Fife, M. Scharf, S.G. Hummel and R.W.Morris, "Field reliability analysis methods for photovoltaic inverters," in *35th IEEE Photovoltaic Specialists Conf. (PVSC),* Honolulu, HI, Jun., 2010, pp. 2767-2772.

[59] G. Graditi, D. Colonnese and N. Femia, "Efficiency and reliability comparison of DC-DC converters for single phase grid connected photovoltaic inverters," in *Int. Symp. on Power Electronics Electrical Drives Automation and Motion (SPEEDAM),* Pisa, Italy, Jun.14-16, 2010, pp. 140-147.

[60] Z. J. Ma and S. Thomas, "Reliability and maintainability in photovoltaic inverter design," in *Reliability and Maintainability Symp. (RAMS),* Buena Vista, FL, 2011, pp. 1-5.

[61] C. J. Muray, A. Davoudi and P.L. Chapman, "Reliability analysis for single-phase photovoltaic inverters with reactive power support," in *IEEE Power and Energy Conf. at Illinois (PECI),* Urbana-Champaign, IL, 2011, pp. 1-6.

[62] W. Bower, R. West and A. Dickerson, "Innovative PV microinverter topology eliminates electrolytic capacitors for longer lifetime," in *Proc. IEEE World Conf. Photovoltaic Energy Conversion*, Waikoloa, HI, May 7-12, 2006, pp.2038–2041.

[63] H. Hu, S. Harb, N. Kutkut, I. Batarseh and Z. J. Shen, "Power decoupling techniques for microinverters in PV systems-a review", in *IEEE Energy Conversion Congr. and Expo.,* Atlanta, GA, Sept. 12-16, 2010, pp. 3235 - 3240.

[64] S. Harb, Haibing Hu, N. Kutkut, I. Batarseh and Z.J. Shen, "A three-port photovoltaic (PV) microinverter with power decoupling capability," in *26th Annual IEEE Applied Power Electronics Conf. and Expo. (APEC),* Fort Worth, TX, 2011, pp. 203-208.

[65] B. Burger and D. Kranzer, "Extreme high efficiency PV-power converters," in *Proc. 13th European Conf. on Power Electronics and Applications EPE*, Barcelona, Spain,Oct. 2009 , pp. 1-13.

[66] J. H. R. Enslin and D. B. Snyman, "Combined low-cost, high-efficient inverter, peak power tracker and regulator for PV applications," *IEEE Trans. on Power Electron.,* vol. 6, pp. 73-82, 1991.

[67] J. Kwon, W. Choi and B. Kwon, "Multi-mode MPPT control for improved efficiency," in *Proc. of IEEE Int. Conf. on Sustainable Energy Technologies*, Singapore, Singapore, Nov. 2008, pp.140-143.

[68] J.M.Kwon, B.H.Kwon and K.H.Nam," High-efficiency moduleintegrated photovoltaic power conditioning system". *IEEE Trans. on Power Electron.,*vol. 2, pp 410-420, 2009

[69] A. Karavadi, R. S. Balog, "Novel non-flat photovoltaic module geometries and implications to power conversion," *presented at the Energy Conversion Congress & Exposition*, Phoenix, AZ, 2011.

[70] R. Nave. (2005). *Heat radiation* [Online]. Available: http://hyperphysics.phy-astr.gsu.edu/hbase/hframe.html

[71] J. R. Howell.(1982). *A catalog of radiation heat transfer configuration factors* [Online]. Available: http://www.engr.uky.edu/rtl/Catalog/

[72] G. Nellis and S. Klein, *Heat Transfer*. New York: Cambridge University Press, 2009.

[73] Electropaedia. (2005). *Solar Power* [Online]. Available: http://www.mpoweruk.com/solar_power.htm

[74] G. M. Masters, Ed.2, *Renewable and Efficient Electric Power Systems*. Hoboken, NJ John Wiley & Sons,, 2004,

[75] J. Branz. (2007). *Stand alone systems* [Online]. Available: http://www.level.org.nz/fileadmin/downloads/Energy/LevelDiagram43.pdf .

[76] S. Yeleti and F. Yong, "Impacts of energy storage on the future power system," in *North American Power Symp. (NAPS),* Arlington, TX, 2010, pp. 1-7.

[77] R. B. Schainker, "Executive overview: Energy storage options for a sustainable energy future," in *IEEE Power Engineering Society General Meeting*, Denver, CO, 2004, pp. 2309-2314 Vol.2.

[78] S. Meninger, J. O. Mur-Miranda, R. Amirtharajah, A. P. Chandrakasan, and J. H. Lang, "Vibration-to-electric energy conversion," *IEEE Trans. Very Large Scale Integr. (VLSI) Syst.*, vol. 9, no. 1, pp. 64– 76, Feb. 2001.

[79] P. D. Mitcheson , T. C. Green, E. M. Yeatman, and A. S. Holmes,"Architectures for vibration-driven micropower generator ," *J. Microelectromech. Syst.*, vol. 13, pp. 429 –440, Jun. 2004.

[80] T.-K. Chung, D.-G. Lee, M. Ujihara, and G. P. Carman, "Design, simulation, and fabrication of a novel vibration-based magnetic energy harvesting device," in *Proc. Int. Solid-State Sensors, Actuators and Microsystems Conf.* , Lyon, France, Jun. 10–14, 2007, pp. 867 –870.

[81] R. N. Torah, M. J. Tudor, K. Patel, I. N. Garcia, and S. P. Beeby, "Autonomous low power microsystem powered by vibration energy harvesting," in *Proc. IEEE Sensors Conf.*, Atlanta, GA,Oct. 28-31, 2007, pp. 264–267.

[82] T. Le, K. Mayaram, and T. Fiez, "Efficient far-field radio frequency energy harvesting for passively powered sensor networks," *IEEE J. Solid-State Circuits*, vol. 43, no. 5, pp. 1287–1302, May 2008.

[83] T. S. Paing and R. Zane, "Resistor emulation approach to low-power energy harvesting," in *Proc. IEEE Power Electronics Specialists Conf.*, Jeju, South Korea, Jun.18–22, 2006, pp. 1–7.

[84] P. Chulsung and P. H. Chou, "AmbiMax: Autonomous energy harvesting platform for multi-supply wireless sensor nodes," in *Proc. IEEE Communications Society Conf. on Sensor, Mesh and Ad Hoc Communications and Networks*, Reston, VA, Sep. 28, 2006,vol. 1, pp. 168–177 .

[85] R. Myers, M. Vickers, H. Kim, and S. Priya, "Small scale windmill," *Applied Physics Letters*, vol. 90, pp. 54106-54109, 2007.

[86] M. A. Weimer, T. S. Paing and R. A. Zane, "Remote area wind energy harvesting for low-power autonomous sensors," in *Proc. IEEE Power Electronics Speialists Conf.*, Jeju, Korea, Jun. 18--22, 2006, pp. 1–5.

[87] Y. K. Tan and S. K. Panda, "A novel piezoelectric based wind energy harvester for low-power autonomous wind speed sensor," in *Proc. 33rd Annu. Conf. IEEE Industrial Electronics Society,* Taipei, Taiwan,Nov. 5–8, 2007, pp. 2175–2180.

[88] B. T. Kuhn and R. S. Balog, "Design considerations for long-term remote photovoltaic-based power supply," in *Proc. IEEE Appl. Power Electron. Conf.*, Austin, TX, Feb. 24–28, 2008, pp. 154–159.

[89] F. I. Simjee and P. H. Chou, "Efficient charging of supercapacitors for extended lifetime of wireless sensor nodes," *IEEE Trans. on Power Electron.,* vol. 23, pp. 1526-1536, 2008.

[90] Raghunathan Vijay, A. Kansal, J. Hsu, J. Friedman and Srivastava Mani, "Design considerations for solar energy harvesting wireless embedded systems," in *Proc. 4th Int. Symp. Information Processing in Sensor Networks,* Piscataway, NJ, 2005, pp. 457–462.

[91] L. M. Tolbert, W. A. Peterson, C. P.White, T. J. Theiss and M. B. Scudiere, "A bi-directional DC-DC converter with minimum energy storage elements," in *Conf. Rec. IEEE Industrial Applications Conf. and Annu. Meeting,* Pittsburgh , PA , 2002, pp. 1572–1577.

[92] H.Al-Atrash, F.Tian and I.Batarseh, "Tri-modal half-bridge converter topology for three-port interface," *IEEE Trans. on Power Electron.,* vol. 22, pp. 341-345, 2007.

[93] D. Liu and L. Hui, "A ZVS bi-directional DC-DC converter for multiple energy storage elements," *IEEE Trans. on Power Electron.,* vol. 21, pp. 1513-1517, 2006.

[94] National Renewable Energy Laboratories (NREL). (2009, March 10). *National Solar Radiation Data Base (NSRDB) 1961–1990* [Online]. Available: http://rredc.nrel.gov/solar/old_data/nsrdb/tmy2/

APPENDIX

Chapter III

Program to create various surfaces and drawing normals at center of each cell

```
% For every 3D surface X,Y and Z coordinates must be
specified in the form of a
%  matrix for MATLAB to create the surface. The matlab in
built function surfnorm     % creates normals on the
surface at vertices instead of the center. So, another
surface is % created by shifting the existing surface so
that this surface's vertices are in the centre % of
original surface and surfnorm is used to draw the surfaces

clc
clear all
close all

% Various Surfaces are created for comparison

%FlatPlate
surface='FlatPlate';
xsize=1;
xstep=0.1;
ysize=1;
ystep=0.1;
%for Surface
[X,Y]   = meshgrid(-xsize:xstep:xsize,-ysize:ystep:ysize);
Z = 0*ones(size(X));
%for Normals
[nX,nY] = meshgrid((-xsize+xstep/2):xstep:xsize-xstep/2,(-
ysize+ystep/2):ystep:ysize-ystep/2);
nZ = 0*ones(size(nX));

%SemiCylindrical Surface
surface='SemiCylinder';
ns =20;
R = ones(20,1);
m = length(R);
theta = (0:ns)/ns*pi;
Y = (R*cos(theta));
```

```
Z = (R*sin(theta));
X = ((-(m-1)/2:(m-1)/2)'*ones(1,((ns+1))))/10;
 %for creation of normals which are in between the patch
nR=ones(19,1);
thetan = (0.5:(ns-0.5))/ns*pi;
nY = (nR*cos(thetan));
nZ = (nR*sin(thetan));
%to cut the amplitude of the semi-cylinder
%nZ = min((nR*sin(thetan)),0.5);
nX = ((-(m-1)/2:(m-2)/2)'*ones(1,((ns)))+0.5)/10;


%Cylindrical Surface
surface='Cylinder';
ns =50;
R = ones(20,1);
m = length(R);
theta = (0:ns)/ns*2*pi;
Y = (R*cos(theta));
Z = (R*sin(theta));
X = (-(m-1)/2:(m-1)/2)'*ones(1,((ns+1)));
 % for creation of normals whcih are in between the patch
nR=ones(19,1);
thetan = (0.5:(ns-0.5))/ns*2*pi;
nY = (nR*cos(thetan));
nZ = (nR*sin(thetan))+2;
nX = (-(m-1)/2:(m-2)/2)'*ones(1,((ns)))+0.5;


%Half SineWave in Yaxis
surface='SineWaveinY';
xsize=3.1416;
xstep=0.1;
ysize=3.1416;
ystep=0.1;
% for Surface
[X,Y]   = meshgrid(0:xstep:xsize,0:ystep:ysize);
Z =min(sin(Y),1);
%for creation of normals whcih are in between the patch
[nX,nY] = meshgrid((0+xstep/2):xstep:xsize-
xstep/2,(0+ystep/2):ystep:ysize-ystep/2);
 nZ=min(sin(nY),1);

%hemisphere
```

```
surface='Hemisphere';
n = 12;
theta = (-n:1:n)/n*pi;
%phi=0*ones(2*n+1,1);
phi = (0:0.5:n)'/n*pi/2;
X = cos(phi)*cos(theta);
Y = cos(phi)*sin(theta);
Z = sin(phi)*ones(1,2*n+1);
%  X = ones(2*n+1,1)*cos(theta);
%  Y = ones(2*n+1,1)*sin(theta);
%  Z = phi*ones(1,2*n+1);
 %for creation of normals whcih are in between the patch
thetan = (-n+0.5:1:(n-0.5))/n*pi;
%phin=0*ones(2*n,1);
phin = (0.25:0.5:n-0.25)'/n*pi/2;
nX = cos(phin)*cos(thetan);
nY = cos(phin)*sin(thetan);
nZ = sin(phin)*ones(1,2*n);


% Wavy Surface
xsize=20;
xstep=2;
ysize=20;
ystep=2;

% Surface creation
[X,Y]   = meshgrid(-xsize:xstep:xsize,-ysize:ystep:ysize);
Z = sin((X*pi/xsize)*2) + sin((Y*pi/ysize)*2);


% Normals creation
[nX,nY] = meshgrid((-xsize+xstep/2):xstep:xsize-xstep/2,(-
ysize+ystep/2):ystep:ysize-ystep/2);
nZ=  sin((nX*pi/xsize)*2) + sin((nY*pi/ysize)*2);


% creation of the surface along with normals

hsurf=surfl(X,Y,Z);                % creates the surface
surfnorm(nX,nY,nZ);                % creates the normals
colormap gray;
title(sprintf('%s',surface));
xlabel('x'); ylabel('y');zlabel('z')
```

The following program creates various surfaces with certain tilt and phi angle

```
clc
clear all
close all
% Various Surfaces are created for comparison

xsize=1;
xstep=0.1;
ysize=1;
ystep=0.1;
[X,Y]   = meshgrid(-xsize:xstep:xsize,-ysize:ystep:ysize);
[nX,nY] = meshgrid((-xsize+xstep/2):xstep:xsize-xstep/2,(-
ysize+ystep/2):ystep:ysize-ystep/2);
Z = 0*ones(size(X));
nZ = 0*ones(size(nX));

% tilt of the solar panel
 tilt=45;

%Direction of the solar panel
 phic = 45;

%**Flat Plate
 z = Z-tand(tilt)*X;
 nzf = nZ-tand(tilt)*nX;

 x=cosd(phic)*X-sind(phic)*Y;
 nxf=cosd(phic)*nX-sind(phic)*nY;

 y=sind(phic)*X+cosd(phic)*Y;
 nyf=sind(phic)*nX+cosd(phic)*nY;

%SemiCylindrical Surface
ns1 =20;
R1 = ones(20,1);
m1 = length(R1);
theta1 = (0:ns1)/ns1*pi;
Ys = (R1*cos(theta1));
Zs = (R1*sin(theta1));
% to cut the amplitude of the semi-cylinder
```

```
%Z = min((R*sin(theta)),0.5);
Xs = ((-(m1-1)/2:(m1-1)/2)'*ones(1,((ns1+1))))/10;

% for creation of normals whcih are in between the patch
nR1=ones(19,1);
thetan1 = (0.5:(ns1-0.5))/ns1*pi;
nYs = (nR1*cos(thetan1));
nZs = (nR1*sin(thetan1));
% to cut the amplitude of the semi-cylinder
%nZ = min((nR*sin(thetan)),0.5);
nXs = ((-(m1-1)/2:(m1-2)/2)'*ones(1,((ns1)))+0.5)/10;



zs = -tand(tilt)*Xs+Zs*cosd(tilt);
nzs2 = -tand(tilt)*nXs+nZs*cosd(tilt);

xs_i=Xs+Zs*sind(tilt);
nxs_i=nXs+nZs*sind(tilt);

xs=cosd(phic)*xs_i-sind(phic)*Ys;
nxs2=cosd(phic)*nxs_i-sind(phic)*nYs;

ys=sind(phic)*xs_i+cosd(phic)*Ys;
nys2=sind(phic)*nxs_i+cosd(phic)*nYs;



%Cylindrical Surface
% surface='Cylinder';
ns =50;
R = ones(20,1);
m = length(R);
theta = (0:ns)/ns*2*pi;
Yc = (R*cos(theta));
Zc = (R*sin(theta));
Xc = (-(m-1)/2:(m-1)/2)'*ones(1,((ns+1)));

% for creation of normals whcih are in between the patch
nR=ones(19,1);
thetan = (0.5:(ns-0.5))/ns*2*pi;
nYc = (nR*cos(thetan));
nZc = (nR*sin(thetan));
nXc = (-(m-1)/2:(m-2)/2)'*ones(1,((ns)))+0.5;
```

```
zc = -tand(tilt)*Xc+Zc*cosd(tilt);
nzc2 = -tand(tilt)*nXc+nZc*cosd(tilt);

xc_i=Xc+Zc*sind(tilt);
nxc_i=nXc+nZc*sind(tilt);

xc=cosd(phic)*xc_i-sind(phic)*Yc;
nxc2=cosd(phic)*nxc_i-sind(phic)*nYc;

yc=sind(phic)*xc_i+cosd(phic)*Yc;
nyc2=sind(phic)*nxc_i+cosd(phic)*nYc;



surfl(nxf,nyf,nzf);
title(sprintf('Tilt %g  Collector''s azimuth angle %g
',tilt,phic));
colormap('gray');
xlabel('x'); ylabel('y');zlabel('z')
figure;
surfl(nxs2,nys2,nzs2);
title(sprintf('Tilt %g  Collector''s azimuth angle %g
',tilt,phic));
colormap('gray');
xlabel('x'); ylabel('y');zlabel('z')
figure;
surfl(nxc2,nyc2,nzc2);
colormap('gray');
```

Chapter IV

The following sets of programs are used to calculate the view factors of the various surfaces for a given specific day for validation.

1. **Flat plate view factor**

```
%Amulya Karavadi
clc
clear all
close all

xsize=1;
xstep=0.1;
ysize=1;
ystep=0.1;
[X,Y]   = meshgrid(-xsize:xstep:xsize,-ysize:ystep:ysize);
[X1,Y1] = meshgrid((-xsize+xstep/2):xstep:xsize-xstep/2,(-
ysize+ystep/2):ystep:ysize-ystep/2);

% tilt of the solar panel
 tilt=0;

%Direction of the solar panel
 phic = 0;

%**Flat Plate
 z = 0*ones(size(X))-tand(tilt)*X;
 z1 = 0*ones(size(X1))-tand(tilt)*X1;

 x=cosd(phic)*X-sind(phic)*Y;
 x1=cosd(phic)*X1-sind(phic)*Y1;

 y=sind(phic)*X+cosd(phic)*Y;
 y1=sind(phic)*X1+cosd(phic)*Y1;

 % the number of day
 n=173;

 % Latitude
 L=23.5;
```

```
 % declination angle
 d=23.45*sind((360/365)*(n-81));

 % constants to evaluate the solar intensity
 A=1160+(75*sind((360/365)*(n-275)));
 k=0.174+ (0.035*sind((360/365)*(n-100)));

 i=1;

 % variable to compute total energy output
 TE=0;

 W= tand(d)/tand(L); % constant to check the condition for
correct azimuth

 for t= 7:-1:-7

      c=t+0;

      % hour angle
      H(i)=(15*c);
 % Elevation to eliminate conditions where the sun is below
the % horizon and has negative angles.

B(i)=max(asind((cosd(L)*cosd(d)*cosd(H(i)))+(sind(L)*sind(d
))),0);

      Ba(i)=B(i);
      %azimuth
      phis(i)=asind((cosd(d)*sind(H(i)))/cosd(B(i)));

 % during spring and summer in early mornings and late
afternoons
 % the azimuth tends to go above 90 deg to take into
account the
% correct azimuth the following condition is checked.

      if(cosd(H(i))<W && t>0)
          phis(i)=180-phis(i);
      elseif(cosd(H(i))<W && t<0)
```

```
          phis(i)=180-phis(i)-360;
      end

% since the MATLAB corordinates are placed 90 degs ahead of
solar
% coordinates to be able to accomodate that change we add
90 to the
% above obtained azimuth angle.

      phisa(i)=phis(i)+90;
      m(i)=1/sind((B(i)));
      %Solar insolation at that hour
      I(i)=A*exp(-(k*m(i)));

      % the viewfactor
      thetha(i)=max((cosd(B(i))*cosd((phis(i)-
phic))*sind(tilt))+(sind(B(i))*cosd(tilt)),0);

      %the actual insolation on solar panel
      Ic(i)= max(I(i)*(thetha(i)),0);

 % Passing the matlab azimuth and elevation into surface to
get the % actual lighting effect.
       s=[phisa(i) Ba(i)];
       k1 = [0, 1, 0, 10];
      % Convert to radians
      az = s(1)*pi/180; el = s(2)*pi/180;
      s = zeros(1,3);
      s(1) =  sin(az)*cos(el);
      s(2) = -cos(az)*cos(el);
      s(3) =  sin(el);

      [nx,ny,nz] = surfnorm(x1,y1,z1);

      R1 = (k1(2)*diffuse(nx,ny,nz,s));

      Mean(i) = mean2(R1);

      Ic(i)=I(i)*Mean(i);

      %total energy calculation
```

```
      TE = TE+I(i)*Mean(i);

      Ia(i)=Ic(i);

      TOD(i) = 12-t;

      i=i+1;
 end
 Mean';
 plot(TOD,Mean,TOD,thetha);
 legend('Modeling VF values','Theoritical VF values');
 title(sprintf('Day %g   Latitude %g FlatPlate',n,L));
 xlabel('Solar hour');
 ylabel('View Factors');
 grid on
```

2. View factors for semi cylindrical surface

```
% Important note:-
% The matlab coordinates for azimuth
% are 0 with respect to (negative)-Y-axis and it moves in
counter clockwise
% direction to 90 deg at positive X-axis and 180 deg at
positive Y-axis and if the
% angle of azimuth is negative it moves in clockwise
direction from
% negative Y-axis towards negative X-axis.
% The Masters book coordinates are -90 deg at negative Y-
axis and 0 degs
% at Positive X-axis and +90 degs at Positive Y axis. To
map these
% coordinate system an extra 90 is added to Masters azimuth
angle.

%Amulya Karavadi
clc
clear all
close all

tilt1=0;
```

```
ns =20;
R = ones(20,1);
m = length(R);
theta = (0:ns)/ns*pi;
Y = (R*cos(theta));
Z = (R*sin(theta));
% to cut the amplitude of the semi-cylinder
%Z = min((R*sin(theta)),0.5);
X = (-(m-1)/2:(m-1)/2)'*ones(1,((ns+1)));

% for creation of normals whcih are in between the patch
nR=ones(19,1);
thetan = (0.5:(ns-0.5))/ns*pi;
nY = (nR*cos(thetan));
nZ = (nR*sin(thetan));
% to cut the amplitude of the semi-cylinder
%nZ = min((nR*sin(thetan)),0.5);
nX = (-(m-1)/2:(m-2)/2)'*ones(1,((ns)))+0.5;

% the number of day
 n=173;

 % Latitude
 L=23.5;

 %Direction of the solar panel
 phic = 0;

 % tilt of the solar panel
 tilt=0;

 % declination angle
 d=23.45*sind((360/365)*(n-81));

 % constants to evaluate the solar intensity
 A=1160+(75*sind((360/365)*(n-275)));
 k=0.174+ (0.035*sind((360/365)*(n-100)));

 i=1;
```

```
 % variable to compute total energy output
 TE=0;

 W= tand(d)/tand(L); % constant to check the condition for
correct azimuth

 for j=7:-1:-7

      c=j;
      % hour angle
      H(i)=(15*c);

 % Elevation to eliminate conditions where the sun is below
the
 % horizon and has negative angles.

B(i)=max(asind((cosd(L)*cosd(d)*cosd(H(i)))+(sind(L)*sind(d
))),0);

      Ba(i)=B(i);

      %azimuth

      phis(i)=asind((cosd(d)*sind(H(i)))/cosd(B(i)));

% during spring and summer in early mornings and late
afternoons
% the azimuth tends to go above 90 deg to take into account
the
% correct azimuth the following condition is checked.

      if(cosd(H(i))<W && j>0)
          phis(i)=180-phis(i);
      elseif(cosd(H(i))<W && j<0)
          phis(i)=180-phis(i)-360;
      end



% since the MATLAB coordinates are placed 90 degs ahead of
solar
```

```
% coordinates to be able to accommodate that change we add
90 to the % above obtained azimuth angle.

      phisa(i)=phis(i)+90;
      m(i)=1/sind((B(i)));
     %Solar insolation at that hour
      I(i)=A*exp(-(k*m(i)));

% Passing the matlab azimuth and elevation into surface to
get the
      % actual lighting effect.
      s=[phisa(i) Ba(i)];
      k1 = [0, 1, 0, 10];
      % Convert to radians
      az = s(1)*pi/180; el = s(2)*pi/180;
      s = zeros(1,3);
      s(1) =  sin(az)*cos(el);
      s(2) = -cos(az)*cos(el);
      s(3) =  sin(el);

      cax=gca;
      a = [get(cax,'xlim')get(cax,'ylim')get(cax,'zlim')];
      Sx = a(2)-a(1);
      Sy = a(4)-a(3);
      Sz = a(6)-a(5);
      scale = max([Sx,Sy,Sz]);
      Sx = Sx/scale; Sy = Sy/scale; Sz = Sz/scale;

      xx = nX/Sx; yy = nY/Sy; zz = nZ/Sz;
      [nx,ny,nz] = surfnorm(xx,yy,zz);
      %[nx,ny,nz] = surfnorm(nX,nY,nZ);

      R1 = (k1(2)*diffuse(nx,ny,nz,s));
      Mean(i) = mean2(R1);

      Ic(i)=I(i)*Mean(i);
      %total energy calculation
      TE = TE+I(i)*Mean(i);

      VF(i)= Mean(i)*pi/2;
      TOD(i) = 12-j;
```

```
      Ia(i)=Ic(i)*pi;

      i=i+1;
 end
 VF'
 Mean';
 Ia';
 plot(TOD,Mean);
 title(sprintf('Day %g   Latitude %g SemiCylinder',n,L));
 xlabel(' Solar hour');
 ylabel('Average View Factor');
 grid on
```

3. Cylindrical surface view factors

```
clc
clear all
close all
tilt1=0;

%Cylindrical Surface
ns =50;
R = ones(20,1);
m = length(R);
theta = (0:ns)/ns*2*pi;
Y = (R*cos(theta));
X = (-(m-1)/2:(m-1)/2)'*ones(1,((ns+1)));
Z = (R*sin(theta))-tand(tilt1)*X;
nR=ones(19,1);
thetan = (0.5:(ns-0.5))/ns*2*pi;
nY = (nR*cos(thetan));
nX = (-(m-1)/2:(m-2)/2)'*ones(1,((ns)))+0.5;
nZ = (nR*sin(thetan))-tand(tilt1)*nX;

% the number of day
 n=173;

 % Latitude
 L=23.5;

 %Direction of the solar panel
```

```
phic = 0;

% tilt of the solar panel
tilt=0;

% declination angle
d=23.45*sind((360/365)*(n-81));

% constants to evaluate the solar intensity
A=1160+(75*sind((360/365)*(n-275)));
k=0.174+ (0.035*sind((360/365)*(n-100)));

i=1;

% variable to compute total energy output
TE=0;

% constant to check the condition for correct azimuth
W= tand(d)/tand(L);

for j=8:-1:-8

     c= j+0;
     % hour angle
     H(i)=(15*c);

% Elevation to eliminate conditions where the sun is below
the % horizon and has negative angles.

B(i)=max(asind((cosd(L)*cosd(d)*cosd(H(i)))+(sind(L)*sind(d
))),0);

     Ba(i)=B(i);

     %azimuth

     phis(i)=asind((cosd(d)*sind(H(i)))/cosd(B(i)));

% during spring and summer in early mornings and late
afternoons
```

```
% the azimuth tends to go above 90 deg to take into account
the
% correct azimuth the following condition is checked.

      if(cosd(H(i))<W && j>0)
          phis(i)=180-phis(i);
      elseif(cosd(H(i))<W && j<0)
          phis(i)=180-phis(i)-360;
      end



% since the MATLAB coordinates are placed 90 degs ahead of
solar
% coordinates to be able to accommodate that change we add
90 to the % above obtained azimuth angle.

      phisa(i)=phis(i)+90;
      %phisa(i)=0;



      m(i)=1/sind((B(i)));
     %Solar insolation at that hour
      I(i)=A*exp(-(k*m(i)));

      % the viewfactor
      thetha(i)=((cosd(B(i))*cosd((phis(i)-
phic))*sind(tilt))+(sind(B(i))*cosd(tilt)));

      %the actual insolation on solar panel
      Ic(i)= max(I(i)*(thetha(i)),0);

% Passing the matlab azimuth and elevation into surface to
get the
      % actual lighting effect.
      s=[phisa(i) Ba(i)];
      k1 = [0, 1, 0, 10];
      % Convert to radians
      az = s(1)*pi/180; el = s(2)*pi/180;
      s = zeros(1,3);
      s(1) =  sin(az)*cos(el);
      s(2) = -cos(az)*cos(el);
      s(3) =  sin(el);
```

```
      cax=gca;
      a = [get(cax,'xlim')get(cax,'ylim')get(cax,'zlim')];
      Sx = a(2)-a(1);
      Sy = a(4)-a(3);
      Sz = a(6)-a(5);
      scale = max([Sx,Sy,Sz]);
      Sx = Sx/scale; Sy = Sy/scale; Sz = Sz/scale;
      xx = nX/Sx; yy = nY/Sy; zz = nZ/Sz;
      [nx,ny,nz] = surfnorm(xx,yy,zz);

      R1 = (k1(2)*diffuse(nx,ny,nz,s));
      Mean(i) = mean2(R1);
      Ic(i)=I(i)*Mean(i);
      %total energy calculation
      TE = TE+I(i)*Mean(i);
      VF(i)= Mean(i)*pi;
      Ia(i)=Ic(i)*2*pi;
      TOD(i) = 12-j;
      i=i+1;
end
VF'
plot(TOD,Mean);
title(sprintf('Day %g   Latitude %g Cylinder',n,L));
xlabel('Solar hour');
ylabel(' Average View Factor');
grid on
```

4. Hemi-spherical surface view factors

```
% Important note:-
% The matlab coordinates for azimuth
% are 0 with respect to (negative)-Y-axis and it moves in
counter clockwise
% direction to 90 deg at positive X-axis and 180 deg at
positive Y-axis and if the
% angle of azimuth is negative it moves in clockwise
direction from
% negative Y-axis towards negative X-axis.
% The Masters book coordinates are  -90 deg at negative Y-
axis and 0 degs
```

```
% at Positive X-axis and +90 degs at Positive Y axis. To
map these
% coordinate system an extra 90 is added to Masters azimuth
angle.
%Amulya Karavadi

clc
clear all
close all

%hemisphere
nh = 30;
theta = (-nh:1:nh)/nh*pi;
phi = (0:0.5:nh)'/nh*pi/2;
Xh = cos(phi)*cos(theta);
Yh = cos(phi)*sin(theta);
Zh = sin(phi)*ones(1,2*nh+1);

thetan = (-nh+0.5:1:(nh-0.5))/nh*pi;
phin = (0.25:0.5:nh-0.25)'/nh*pi/2;
nXh = cos(phin)*cos(thetan);
nYh = cos(phin)*sin(thetan);
nZh = sin(phin)*ones(1,2*nh);
Area=(sin(phi)*(pi/2/2/nh)*(pi/nh)*ones(1,2*nh+1));
Area2=Area(1:2*nh,1:2*nh);
f=((1/4)*(pi*pi/(nh*nh)))*sqrt(1-(nXh.*nXh+nYh.*nYh));
for i=1:1:2*nh
Area3(i,:)=f(((2*nh)+1)-i,:);
end

% the number of day
 n=173;

 % Latitude
 L=90;

 %Direction of the solar panel
 phic = 0;

 % tilt of the solar panel
 tilt=0;
```

```
 % declination angle
 d=23.45*sind((360/365)*(n-81));

 % constants to evaluate the solar intensity
 A=1160+(75*sind((360/365)*(n-275)));
 k=0.174+ (0.035*sind((360/365)*(n-100)));

 i=1;

 % variable to compute total energy output
 TE=0;

 % constant to check the condition for correct azimuth
 W= tand(d)/tand(L);
 for j=7:-1:-7

      % hour angle
      H(i)=(15*j);

% Elevation to eliminate conditions where the sun is below
the
% horizon and has negative angles.

B(i)=max(asind((cosd(L)*cosd(d)*cosd(H(i)))+(sind(L)*sind(d
))),0);

      Ba(i)=B(i);

      %azimuth

      phis(i)=asind((cosd(d)*sind(H(i)))/cosd(B(i)));

 % during spring and summer in early mornings and late
afternoons
 % the azimuth tends to go above 90 deg to take into
account the
 % correct azimuth the following condition is checked.

      if(cosd(H(i))<W && j>0)
          phis(i)=180-phis(i);
      elseif(cosd(H(i))<W && j<0)
```

```
          phis(i)=180-phis(i)-360;
      end


      % since the MATLAB corordinates are placed 90 degs
ahead of solar
      % coordinates to be able to accomodate that change we
add 90 to the
      % above obtained azimuth angle.

      phisa(i)=phis(i)+90;
      m(i)=1/sind((B(i)));
     %Solar insolation at that hour
      I(i)=A*exp(-(k*m(i)));

      % the viewfactor
      thetha(i)=((cosd(B(i))*cosd((phis(i)-
phic))*sind(tilt))+(sind(B(i))*cosd(tilt)));

      %the actual insolation on solar panel
      Ic(i)= max(I(i)*(thetha(i)),0);

      % Passing the matlab azimuth and elevation into
surface to get the
      % actual lighting effect.
      s=[phisa(i) Ba(i)];
      k1 = [0, 1, 0, 10];
      % Convert to radians
      az = s(1)*pi/180; el = s(2)*pi/180;
      s = zeros(1,3);
      s(1) =  sin(az)*cos(el);
      s(2) = -cos(az)*cos(el);
      s(3) =  sin(el);
      [nxh,nyh,nzh] = surfnorm(nXh,nYh,nZh);

      R1 = (diffuse(nxh,nyh,nzh,s));
      R2 = sum(sum(Area3.*R1))/sum(sum(Area3));

      Mean(i) = R2;

      Ic(i)=I(i)*Mean(i);
      %total energy calculation
```

```
      TE = TE+I(i)*Mean(i);

      TOD(i) = 12-j;

      i=i+1;
 end
 Mean';
 B'
 TOD'
 plot(TOD,Mean);
 title(sprintf('Day %g   Latitude %g  Hemisphere %g',n,L));
 xlabel('Solar hour');
 ylabel('Average View Factor');
 grid on;
```

5. Sinusoidal surface view factors

```
clc
clear all
close all
xsize=3.1416;
xstep=0.05;
xvector=-xsize:xstep:xsize;
ysize=3.1416;
ystep=0.05;
yvector=-ysize:ystep:ysize;

[X,Y]   = meshgrid(0:xstep:xsize,0:ystep:ysize);
[X1,Y1] = meshgrid((0+xstep/2):xstep:xsize-
xstep/2,(0+ystep/2):ystep:ysize-ystep/2);
Z =sin(Y);
Z1=sin(Y1);

% the number of day
 n=173;

 % Latitude
 L=23.5;

 %Direction of the solar panel
 phic = 0;
```

```
 % tilt of the solar panel
 tilt=0;

 % declination angle
 d=23.45*sind((360/365)*(n-81));

 % constants to evaluate the solar intensity
 A=1160+(75*sind((360/365)*(n-275)));
 k=0.174+ (0.035*sind((360/365)*(n-100)));

 i=1;

 % variable to compute total energy output
 TE=0;

% constant to check the condition for correct azimuth
 W= tand(d)/tand(L);
 for j=7:-1:-7

      % hour angle
      H(i)=(15*j);
% Elevation to eliminate conditions where the sun is below
the
% horizon and has negative angles.

B(i)=max(asind((cosd(L)*cosd(d)*cosd(H(i)))+(sind(L)*sind(d
))),0);
      Ba(i)=B(i);
      %azimuth
      phis(i)=asind((cosd(d)*sind(H(i)))/cosd(B(i)));

% during spring and summer in early mornings and late
afternoons
% the azimuth tends to go above 90 deg to take into account
the
% correct azimuth the following condition is checked.

      if(cosd(H(i))<W && j>0)
          phis(i)=180-phis(i);
      elseif(cosd(H(i))<W && j<0)
          phis(i)=180-phis(i)-360;
      end
```

```
% since the MATLAB corordinates are placed 90 degs ahead of
solar
% coordinates to be able to accomodate that change we add
90 to the
% above obtained azimuth angle.

      phisa(i)=phis(i)+90;

      m(i)=1/sind((B(i)));
     %Solar insolation at that hour
      I(i)=A*exp(-(k*m(i)));

      % the viewfactor
      thetha(i)=((cosd(B(i))*cosd((phis(i)-
phic))*sind(tilt))+(sind(B(i))*cosd(tilt)));

      %the actual insolation on solar panel
      Ic(i)= max(I(i)*(thetha(i)),0);

% Passing the matlab azimuth and elevation into surface to
get the
      % actual lighting effect.
      s=[phisa(i) Ba(i)];
      k1 = [0, 1, 0, 10];
      % Convert to radians
      az = s(1)*pi/180; el = s(2)*pi/180;
      s = zeros(1,3);
      s(1) =  sin(az)*cos(el);
      s(2) = -cos(az)*cos(el);
      s(3) =  sin(el);

      cax=gca;
      a = [get(cax,'xlim')get(cax,'ylim')get(cax,'zlim')];
      Sx = a(2)-a(1);
      Sy = a(4)-a(3);
      Sz = a(6)-a(5);
      scale = max([Sx,Sy,Sz]);
      Sx = Sx/scale; Sy = Sy/scale; Sz = Sz/scale;

      xx = X1/Sx; yy = Y1/Sy; zz = Z1/Sz;
      [nx,ny,nz] = surfnorm(xx,yy,zz);
```

```
      R1 = (k1(2)*diffuse(nx,ny,nz,s));
      Mean(i) = mean2(R1);

      Ic(i)=I(i)*Mean(i);
      %total energy calculation
      TE = TE+I(i)*Mean(i);

      TOD(i) = 12-j;

      i=i+1;
 end
 Mean'
 plot(TOD,Mean);
 title(sprintf('Day %g Latitude %g Sinusoidal
Surface',n,L));
 xlabel(' Solar hour');
 ylabel('Average View Factor');
 grid on;
```

Chapter V

Program to plot the total energy harvest by various surfaces in a single plot for a particular day.

This program plots the comparison between semi-cylinder, cylinder and a flat plate on a same graph with equal footprint and comparison of hemisphere and flat plate on another graph in a single program.

```
% Important note:-
% The matlab coordinates for azimuth
% are 0 with respect to (negative)-Y-axis and it moves in
counter clockwise
% direction to 90 deg at positive X-axis and 180 deg at
positive Y-axis and if the
% angle of azimuth is negative it moves in clockwise
direction from
% negative Y-axis towards negative X-axis.
% The Masters book coordinates are  -90 deg at negative Y-
axis and 0 degs
% at Positive X-axis and +90 degs at Positive Y axis. To
map tehse
% coordinate system an extra 90 is added to Masters azimuth
angle.

%Amulya Karavadi
clc
clear all
close all
% Various Surfaces are created for comparison

%FlatPlate
xsize=1;
xstep=0.1;
ysize=1;
ystep=0.1;
%for Surface
[X,Y]   = meshgrid(-xsize:xstep:xsize,-ysize:ystep:ysize);
Z = 0*ones(size(X));
%for Normals
[nX,nY] = meshgrid((-xsize+xstep/2):xstep:xsize-xstep/2,(-
ysize+ystep/2):ystep:ysize-ystep/2);
nZ = 0*ones(size(nX));
```

```
%SemiCylindrical Surface
ns1 =20;
R1 = ones(20,1);
m1 = length(R1);
theta1 = (0:ns1)/ns1*pi;
Ys = (R1*cos(theta1));
Zs = (R1*sin(theta1));
Xs = (-(m1-1)/2:(m1-1)/2)'*ones(1,((ns1+1)));

% for creation of normals which are in between the patch
nR1=ones(19,1);
thetan1 = (0.5:(ns1-0.5))/ns1*pi;
nYs = (nR1*cos(thetan1));
nZs = (nR1*sin(thetan1));
nXs = (-(m1-1)/2:(m1-2)/2)'*ones(1,((ns1)))+0.5;

%Cylindrical Surface

ns =50;
R = ones(20,1);
m = length(R);
theta = (0:ns)/ns*2*pi;
Yc = (R*cos(theta));
Zc = (R*sin(theta))+2;
Xc = (-(m-1)/2:(m-1)/2)'*ones(1,((ns+1)));

% for creation of normals whcih are in between the patch
nR=ones(19,1);
thetan = (0.5:(ns-0.5))/ns*2*pi;
nYc = (nR*cos(thetan));
nZc = (nR*sin(thetan))+2;
nXc = (-(m-1)/2:(m-2)/2)'*ones(1,((ns)))+0.5;

%hemisphere
nh = 30;
theta = (-nh:1:nh)/nh*pi;
phi = (0:0.5:nh)'/nh*pi/2;
Xh = cos(phi)*cos(theta);
Yh = cos(phi)*sin(theta);
Zh = sin(phi)*ones(1,2*nh+1);
```

```
thetan = (-nh+0.5:1:(nh-0.5))/nh*pi;
phin = (0.25:0.5:nh-0.25)'/nh*pi/2;
nXh = cos(phin)*cos(thetan);
nYh = cos(phin)*sin(thetan);
nZh = sin(phin)*ones(1,2*nh);
Area=(sin(phi)*(pi/2/2/nh)*(pi/nh)*ones(1,2*nh+1));
Area2=Area(1:2*nh,1:2*nh);
f=((1/4)*(pi*pi/(nh*nh)))*sqrt(1-(nXh.*nXh+nYh.*nYh));
for i=1:1:2*nh
Area3(i,:)=f(((2*nh)+1)-i,:);
end

% the number of day
 n=173;

 % Latitude
 L=23.5;

 %Direction of the solar panel
 phic = 0;

 % tilt of the solar panel
 tilt=0;

 % declination angle
 d=23.45*sind((360/365)*(n-81));

 % constants to evaluate the solar intensity
 A=1160+(75*sind((360/365)*(n-275)));
 k=0.174+ (0.035*sind((360/365)*(n-100)));

 i=1;

 % variable to compute total energy output
 TE_F=0;
 TE_S=0;
 TE_C=0;
 TE_H=0;
 TE_Fh=0;
 % constant to check the condition for correct azimuth
 W= tand(d)/tand(L);
 for j=7:-1:-7
```

```
      % hour angle
      H(i)=(15*j);
 % Elevation to eliminate conditions where the sun is below
the
 % horizon and has negative angles.

B(i)=max(asind((cosd(L)*cosd(d)*cosd(H(i)))+(sind(L)*sind(d
))),0);

      Ba(i)=B(i);
      %azimuth
      phis(i)=asind((cosd(d)*sind(H(i)))/cosd(B(i)));
% during spring and summer in early mornings and late
afternoons
% the azimuth tends to go above 90 deg to take into account
the
% correct azimuth the following condition is checked.

      if(cosd(H(i))<W && j>0)
          phis(i)=180-phis(i);
      elseif(cosd(H(i))<W && j<0)
          phis(i)=180-phis(i)-360;
      end



% since the MATLAB corordinates are placed 90 degs ahead of
solar
% coordinates to be able to accomodate that change we add
90 to the
% above obtained azimuth angle.

      phisa(i)=phis(i)+90;



      m(i)=1/sind((B(i)));

     %Solar insolation at that hour
      I(i)=A*exp(-(k*m(i)));
```

```
% Passing the matlab azimuth and elevation into surface to
get the
      % actual lighting effect.
      s=[phisa(i) Ba(i)];
      k1 = [0, 1, 0, 10];
      % Convert to radians
      az = s(1)*pi/180; el = s(2)*pi/180;
      s = zeros(1,3);
%converting the az and el to polar coordinates to
facilitate the dot
%product with the normals
      s(1) =  sin(az)*cos(el);
      s(2) = -cos(az)*cos(el);
      s(3) =  sin(el);

%creating the surface normals at the centre of the patchs
using
%surfnormfunction

      [nx,ny,nz] = surfnorm(nX,nY,nZ);
      [nxs,nys,nzs] = surfnorm(nXs,nYs,nZs);
      [nxc,nyc,nzc] = surfnorm(nXc,nYc,nZc);
      [nxh,nyh,nzh] = surfnorm(nXh,nYh,nZh);



%passing these normals and the angle of sun into diffuse
function to
%calculate the  viewfactors at every normal for that patch

      R1 = (k1(2)*diffuse(nx,ny,nz,s));
      R2 = (k1(2)*diffuse(nxs,nys,nzs,s));
      R3 = (k1(2)*diffuse(nxc,nyc,nzc,s));
      R4 = (diffuse(nxh,nyh,nzh,s));
      R5 = sum(sum(Area3.*R4))/sum(sum(Area3));


  %taking the mean of these viewfactors to get the average
      Mean1(i) = mean2(R1);
      Mean2(i) = mean2(R2);
      Mean3(i) = mean2(R3);
      Mean4(i) = (R5);

%multiplying the mean to get the average insolation that is
falling
```

```
%on the surface.

      Ic1(i)=I(i)*Mean1(i);
      Ic2(i)=I(i)*Mean2(i);
      Ic3(i)=I(i)*Mean3(i);
      Ic4(i)=I(i)*Mean4(i);

%actual intensity multiplied by the area with radius and
length being
%1m meter each
      Ia1(i)=Ic1(i)*2;
      Ia2(i)=Ic1(i)*pi;
      Ia3(i)=Ic1(i)*2*pi;
      Ias(i)=Ic2(i)*pi;
      Iac(i)=Ic3(i)*2*pi;
      Iah(i)=Ic4(i)*2*pi;

 %time of the day
      TOD(i) = 12-j;
 %total energy calculation
      TE_F = TE_F+Ia1(i);
      TE_S = TE_S+Ias(i);
      TE_C = TE_C+Iac(i);
      TE_H = TE_H+Iah(i);
      TE_Fh= TE_Fh+Ia2(i);

      i=i+1;
 end
 TE_F
 TE_S
 TE_C
 TE_H
 TE_Fh
 Ba'
 plot(TOD,Ia1,TOD,Ias,TOD,Iac);
 legend('FlatPlate','Semi-Cylinder','Cylinder');
 title(sprintf('Day %g  Latitude %g ',n,L));
 xlabel(' Solar hour');
 ylabel('Avg ViewFactor * Intensity at that hour* Area');
 grid on;
 figure;
 plot(TOD,Ia2,TOD,Iah);
 legend('FlatPlate','HemiSphere');
```

```
title(sprintf('Day %g  Latitude %g ',n,L));
xlabel('Solar hour');
ylabel('Avg ViewFactor * Intensity at that hour* Area');
grid on;
```

Chapter VI

Program to calculate the number of bad hours in a given time frame

```
function [bad_hours, Energy] = sys_model2(S, area, Eload,
Emax, cell_eff)

%function [bad_hours, minUSE_wh] = sys_model(S, area,
Eload, Emax, cell_eff);
%USDA system energy model
%Computes the number of hours w/o energy based on energy
storage approach
%INPUT:
%   S         = insolation data (W/m^2)
%   area      = panel area in m^2
%   Eload     = energy requiement of the load (Wh)
%   Emax      = maximum stored energy (Wh)
%   cell_eff  = conversion efficiency of the solar cells
%OUTPUT:
%   bad_hours = number of hours w/o sufficienct energy
storage (scalar)
%   Energy
%     .min    = minimum residual stored energy [Wh]
(scalar)
%     .excess = excess energy not stored [Wh] (vector)
%     .stored = hourly stored energy
%     .badhour= hourly availability
%
***********************************


if nargin <5
  beep
  disp('wrong number of input arguments')
  bad_hours =-1e6;
  return
end

%*** Parameters
*************************************************
%Load / losses in the system
Pload = Eload/24;                %Output Power [(WH/day) /
(24 H/day)]
```

```
%MPPT RCC
rcc_base  = 0.042;                %Watts
rcc_eff   = 0.95;                 %Efficiency as a % of
transmitted power

%ESI SCM
esi_effic = 0.95;
esi_base  = 0.060;                %Watts

%Battery Equilizer
eq_base   = 0.045;                %Watts

%Glass transmission coefficient
glass_trans = 0.9;

%Efficiency of energy storage
storage_eff = 0.90;

%estimate the ultracapacitor losses as a fixed amount
divided over the day:
storage_loss_power = 0.25/24;     %0.25 W-hr over 24 hours

%initial conditions
USE_last = Emax;

%create empty vectors to store variables
USE             = zeros(size(S)); %usable stored energy
Energy.stored   = zeros(size(S)); %stored energy
Energy.badhour  = zeros(size(S)); %badhours
Energy.excess   = zeros(size(S)); %excess energy
Energy.net      = zeros(size(S)); %Net energy



%*** Algorithm
*****************************************************
for i = 1:length(S)
    %power generated from solar PV
    EG = max(0, S(i)*area*cell_eff*glass_trans-rcc_base-
eq_base); %W*hr
    EG = EG*rcc_eff; %W*hr
```

```
    netE = EG - esi_base - storage_loss_power - Pload*1.0;
%*1.0 is for 1 hour

  if netE > 0
        %store extra energy
        USE(i) = USE_last + netE;
    else
        %withdraw defecit energy from storage
        USE(i) = USE_last + netE;
    end

    %maintain the stored energy limits
    if USE(i) > Emax
        USE(i) = Emax;

    Energy.excess(i) = USE(i) - Emax;
    elseif USE(i) < 0
        USE(i) = 0;
    end

    USE_last = USE(i);

  Energy.net(i) = netE; %net  energy
end %i loop

bad_hours  = sum(USE == 0);
Energy.min = min(USE);
Energy.stored = USE;
Energy.badhour = Energy.stored == 0;
```

Program to calculate the availability for a flat plate

```
%hours
clc;
clear all;
[file,fdir]=uigetfile('insolation_*.mat');
if file ~= 0
  disp(sprintf('Time of study: %s\n',datestr(now)));
  disp(sprintf('Dataset: %s',file));
  load([fdir,file])
```

```
  disp(sprintf('\tcontains %g hours of insolation
data',length(T)));
  disp(sprintf('\tStarting on %s and ending
%s.\n',datestr(T(1),2),datestr(T(end),2)));
else
  disp('no file selected')
  break
end

[file,fdir]=uigetfile('insolation_*.mat');
if file ~= 0
  disp(sprintf('Time of study: %s\n',datestr(now)));
  disp(sprintf('Dataset: %s',file));
  load([fdir,file])
  disp(sprintf('\tcontains %g hours of insolation
data',length(T)));
  disp(sprintf('\tStarting on %s and ending %s.\n',...
    datestr(T(1),2),datestr(T(end),2)));
else
  disp('no file selected')
  break
end

[file,fdir]=uigetfile('viewfactors_*.mat');
if file ~= 0
  load([fdir,file])
  disp(sprintf('\tcontains %g hours of View Factor
data',length(VF_FlatPlate)));
 else
  disp('no file selected')
  break
end

S_F =SD.*VF_FlatPlate+SDf;



PV.area=0.01;
E_load= 5;
E_storage=3.5;
[num_hours_F,Energy_F] = sys_model_nolosses(S_F, PV.area,
E_load, E_storage, 0.15);
[num_hours,Energy] = sys_model_nolosses(S, PV.area, E_load,
E_storage, 0.15);
```

```
S_F(262968)=0;
S_Diff=(S_F-S);

%total=sum(S_Diff)

[y,m,d,h,mi,s]=datevec(T);        %decompose date vector
H=h;
H(find(h==0)) = 24;               %rename 24th hour from 0
to 24

%Compute start of a day
H_day = mod(h-1,24);
IND_H = H_day==0;                 %Indicies of start of the
day

%Adjust for daylight savings time (DST)
dst = f_isDST_modified(T');                %determine if
hour is in DST
IND_dst = find(dst);              %Indicies of hrs in DST
H_dst = H;                        %hour vector corrected
for DST
H_dst(IND_dst) = H(IND_dst)+1;    %subtract 1 hour to
correct for DST
H_dst(find(H_dst==25)) = 1;
%%
%*** Compute hourly availabilty
**********************************
for k = 1:24;
  hour_F(k).ind   = find(H_dst ==k);  %indicies for each
ith hour
  disp(sprintf('Length of hour %2g record:
%g',k,length(hour_F(k).ind)));
  hour_F(k).data  = Energy_F.stored(hour_F(k).ind);
  hourlyavail_F(k)= 1 -
sum(Energy_F.badhour(hour_F(k).ind)) / 10957;
  Shourdata_F(k)  = sum(SD(hour_F(k).ind)) ;  %hourly
insolation
  Ehourdata_F(k)  = sum(Energy_F.stored(hour_F(k).ind)) /
10957 ;  %hourly insolation
end

for k = 1:24;
```

```
  hour(k).ind   = find(H_dst ==k);  %indicies for each ith
hour
  disp(sprintf('Length of hour %2g record:
%g',k,length(hour(k).ind)));
  hour(k).data  = Energy.stored(hour(k).ind);
  hourlyavail(k)= 1 - sum(Energy.badhour(hour(k).ind)) /
10957;
  Shourdata(k)  = sum(SD(hour(k).ind)) ;  %hourly
insolation
  Ehourdata(k)  = sum(Energy.stored(hour(k).ind)) / 10957 ;
%hourly insolation
end


%availability increments
avail_inc=[ 0.9, 0.99, 0.999, 0.9999, 0.99999, 0.999999,...
            0.9999999, 0.99999999];
logavail_inc=log10(avail_inc);
avail_label=num2str(avail_inc'*100,8);
avail_label(end,:)=char('      100');


%logarithm format
loghourlyavail1_F=log10(hourlyavail_F);
loghourlyavail_F=loghourlyavail1_F;             %because
avail is a matrix
loghourlyavail_F(find(loghourlyavail_F==0))=log10(avail_inc
(end));  %lim value


%logarithm format
loghourlyavail1=log10(hourlyavail);
loghourlyavail=loghourlyavail1;             %because avail
is a matrix
loghourlyavail(find(loghourlyavail==0))=log10(avail_inc(end
));  %lim value


%%
%***
Plotting************************************************
****
hr=1:24;                                      %hour of the
day
[hrs_F,ys_F]=stairs(hr-1,loghourlyavail_F);         %'-1'
adjusts to pre steps
loghourlyavail2_F=[loghourlyavail_F(end),loghourlyavail_F];
```

```
%%
%***
Plotting**************************************************
****
hr=1:24;                                          %hour of the
day
[hrs,ys]=stairs(hr-1,loghourlyavail);          %'-1' adjusts
to pre steps
loghourlyavail2=[loghourlyavail(end),loghourlyavail];

hr2=[0,hr];

%%
figure
%semilogy(hr2,loghourlyavail2_F,'*',hrs_F,ys_F,'r');
semilogy(hr2,loghourlyavail2_F,'*',hrs_F,ys_F,'r',hr2,logho
urlyavail2,'*',hrs,ys,'b');
set(gca,'xlim',[0 24],'xtick',0:24,'xticklabel',[24,1:24])
set(gca,'ytick',logavail_inc,'yticklabel',avail_label)
set(gca,'ylim',[-1,-10^-9])
xlabel('Hour of the day')
ylabel('Availability [%]');
title(['15% efficient PV cells  with ',...
  num2str(E_load),'W-hr per day load'])
grid on
legend ('Modelling Approach','Modelling Approach','NREL
data','NREL data')
%%
```

Program to calculate the availability for a semi cylindrical, cylindrical and flat plate and plotting them in a same graph for comparison.

```
%hours
clear all;

[file,fdir]=uigetfile('insolation_*.mat');
if file ~= 0
%  diary([file(1:end-4),'.txt'])
  disp(sprintf('Time of study: %s\n',datestr(now)));
  disp(sprintf('Dataset: %s',file));
  load([fdir,file])
```

```
  disp(sprintf('\tcontains %g hours of insolation
data',length(T)));
  disp(sprintf('\tStarting on %s and ending %s.\n',...
    datestr(T(1),2),datestr(T(end),2)));
else
  disp('no file selected')
  break
end

[file,fdir]=uigetfile('viewfactors_*.mat');
if file ~= 0
  load([fdir,file])
  disp(sprintf('\tcontains %g hours of View Factor
data',length(VF_FlatPlate)));
 else
  disp('no file selected')
  break
end

S_F =SD.*VF_FlatPlate+SDf;
S_S =SD.*VF_SemiCylinder+SDf;
S_C =SD.*VF_Cylinder+SDf;

PV.area=0.01;
E_load= 5;
E_storage= 5.5;
[num_hours_F,Energy_F] = sys_model2(S_F, PV.area, E_load,
E_storage, 0.15);
[num_hours_S,Energy_S] = sys_model2(S_S, PV.area, E_load,
E_storage, 0.15);
[num_hours_C,Energy_C] = sys_model2(S_C, PV.area, E_load,
E_storage, 0.15);
[y,m,d,h,mi,s]=datevec(T);        %decompose date vector
H=h;
H(find(h==0)) = 24;               %rename 24th hour from 0
to 24

%Compute start of a day
H_day = mod(h-1,24);
IND_H = H_day==0;                 %Indicies of start of the
day

%Adjust for daylight savings time (DST)
```

```
dst = f_isDST(T');                  %determine if hour is in
DST
IND_dst = find(dst);                %Indicies of hrs in DST
H_dst = H;                          %hour vector corrected
for DST
H_dst(IND_dst) = H(IND_dst)+1;      %subtract 1 hour to
correct for DST
H_dst(find(H_dst==25)) = 1;
%%
%*** Compute hourly availabilty
************************************
for k = 1:24;
  hour_F(k).ind   = find(H_dst ==k);  %indicies for each
ith hour
  disp(sprintf('Length of hour %2g record:
%g',k,length(hour_F(k).ind)));
  hour_F(k).data  = Energy_F.stored(hour_F(k).ind);
  hourlyavail_F(k)= 1 -
sum(Energy_F.badhour(hour_F(k).ind)) / 10957;
  Shourdata_F(k)  = sum(SD(hour_F(k).ind)) ;  %hourly
insolation
  Ehourdata_F(k)  = sum(Energy_F.stored(hour_F(k).ind)) /
10957 ;  %hourly insolation
end


for k = 1:24;
  hour_S(k).ind   = find(H_dst ==k);  %indicies for each
ith hour
  disp(sprintf('Length of hour %2g record:
%g',k,length(hour_S(k).ind)));
  hour_S(k).data  = Energy_S.stored(hour_S(k).ind);
  hourlyavail_S(k)= 1 -
sum(Energy_S.badhour(hour_F(k).ind)) / 10957;
  Shourdata_S(k)  = sum(SD(hour_S(k).ind)) ;  %hourly
insolation
  Ehourdata_S(k)  = sum(Energy_S.stored(hour_S(k).ind)) /
10957 ;  %hourly insolation
end


for k = 1:24;
  hour_C(k).ind   = find(H_dst ==k);  %indicies for each
ith hour
  disp(sprintf('Length of hour %2g record:
%g',k,length(hour_C(k).ind)));
```

```
  hour_C(k).data  = Energy_C.stored(hour_C(k).ind);
  hourlyavail_C(k)= 1 -
sum(Energy_C.badhour(hour_C(k).ind)) / 10957;
  Shourdata_C(k)  = sum(SD(hour_C(k).ind)) ;  %hourly
insolation
  Ehourdata_C(k)  = sum(Energy_C.stored(hour_C(k).ind)) /
10957 ;  %hourly insolation
end

%availability increments
avail_inc=[ 0.9, 0.99, 0.999, 0.9999, 0.99999, 0.999999,...
            0.9999999, 0.99999999];
logavail_inc=log10(avail_inc);
avail_label=num2str(avail_inc'*100,8);
avail_label(end,:)=char('      100');

%logarithm format
loghourlyavail1_F=log10(hourlyavail_F);
loghourlyavail_F=loghourlyavail1_F;             %because
avail is a matrix
loghourlyavail_F(find(loghourlyavail_F==0))=log10(avail_inc
(end));  %lim value

%logarithm format
loghourlyavail1_S=log10(hourlyavail_S);
loghourlyavail_S=loghourlyavail1_S;             %because
avail is a matrix
loghourlyavail_S(find(loghourlyavail_S==0))=log10(avail_inc
(end));  %lim value

%logarithm format
loghourlyavail1_C=log10(hourlyavail_C);
loghourlyavail_C=loghourlyavail1_C;             %because
avail is a matrix
loghourlyavail_C(find(loghourlyavail_C==0))=log10(avail_inc
(end));  %lim value

%%
%***
Plotting*************************************************
****
hr=1:24;                                        %hour of the
day
```

```
[hrs_F,ys_F]=stairs(hr-1,loghourlyavail_F);         %'-1'
adjusts to pre steps
loghourlyavail2_F=[loghourlyavail_F(end),loghourlyavail_F];

%%
%***
Plotting**************************************************
****
hr=1:24;                                        %hour of the
day
[hrs_S,ys_S]=stairs(hr-1,loghourlyavail_S);         %'-1'
adjusts to pre steps
loghourlyavail2_S=[loghourlyavail_S(end),loghourlyavail_S];

%%
%***
Plotting**************************************************
****
hr=1:24;                                        %hour of the
day
[hrs_C,ys_C]=stairs(hr-1,loghourlyavail_C);         %'-1'
adjusts to pre steps
loghourlyavail2_C=[loghourlyavail_C(end),loghourlyavail_C];

hr2=[0,hr];

%%
figure
semilogy(hr2,loghourlyavail2_F,'*',hrs_F,ys_F,'r',hr2,logho
urlyavail2_S,'*',hrs_S,ys_S,'b',hr2,loghourlyavail2_C,'*',h
rs_C,ys_C,'black');
legend('flatplate','flatplate','semicylinder','semicylinder
','cylinder','cylinder');
set(gca,'xlim',[0 24],'xtick',0:24,'xticklabel',[24,1:24])
set(gca,'ytick',logavail_inc,'yticklabel',avail_label)
set(gca,'ylim',[-1,-10^-9])
xlabel('Hour of the day')
ylabel('Availability [%]');
title(['15% efficient PV cells  with ',num2str(E_load),' W-
hr per day load With storage
capacity',num2str(E_storage),'W-hr and Area of the foot
print is',num2str(PV.area),'sq m'])
grid on
```

```
%legend ('Hourly Availabiltiy','Cummulative
%Availability','location','best')
%%
```

Program to calculate the availability of the flat plate and hemisphere for comparison

```
%hours
clear all;

[file,fdir]=uigetfile('insolation_*.mat');
if file ~= 0
%  diary([file(1:end-4),'.txt'])
  disp(sprintf('Time of study: %s\n',datestr(now)));
  disp(sprintf('Dataset: %s',file));
  load([fdir,file])
  disp(sprintf('\tcontains %g hours of insolation
data',length(T)));
  disp(sprintf('\tStarting on %s and ending %s.\n',...
    datestr(T(1),2),datestr(T(end),2)));
else
  disp('no file selected')
  break
end

[file,fdir]=uigetfile('viewfactors_*.mat');
if file ~= 0
  load([fdir,file])
  disp(sprintf('\tcontains %g hours of View Factor
data',length(VF_FlatPlate)));
 else
  disp('no file selected')
  break
end

VF_FlatPlate1=VF_FlatPlate*pi;
VF_HemiSphere1=VF_HemiSphere*2*pi;

S_F =SD.*VF_FlatPlate1+SDf;
S_H =SD.*VF_HemiSphere1+SDf;

 PV.area=0.01;
```

```
E_load= 5;
E_storage= 3.5;
[num_hours_F,Energy_F] = sys_model_nolosses(S_F, PV.area,
E_load, E_storage, 0.15);
[num_hours_H,Energy_H] = sys_model_nolosses(S_H, PV.area,
E_load, E_storage, 0.15);

 [y,m,d,h,mi,s]=datevec(T);        %decompose date vector
H=h;
H(find(h==0)) = 24;               %rename 24th hour from 0
to 24


%Compute start of a day
H_day = mod(h-1,24);
IND_H = H_day==0;                 %Indicies of start of the
day


%Adjust for daylight savings time (DST)
dst = f_isDST(T');                %determine if hour is in
DST
IND_dst = find(dst);              %Indicies of hrs in DST
H_dst = H;                        %hour vector corrected
for DST
H_dst(IND_dst) = H(IND_dst)+1;    %subtract 1 hour to
correct for DST
H_dst(find(H_dst==25)) = 1;
%%
%*** Compute hourly availabilty
************************************
for k = 1:24;
  hour_F(k).ind   = find(H_dst ==k);  %indicies for each
ith hour
  disp(sprintf('Length of hour %2g record:
%g',k,length(hour_F(k).ind)));
  hour_F(k).data  = Energy_F.stored(hour_F(k).ind);
  hourlyavail_F(k)= 1 -
sum(Energy_F.badhour(hour_F(k).ind)) / 10957;
  Shourdata_F(k)  = sum(SD(hour_F(k).ind)) ;  %hourly
insolation
  Ehourdata_F(k)  = sum(Energy_F.stored(hour_F(k).ind)) /
10957 ;  %hourly insolation
end
```

```
for k = 1:24;
  hour_H(k).ind   = find(H_dst ==k);  %indicies for each
ith hour
  disp(sprintf('Length of hour %2g record:
%g',k,length(hour_H(k).ind)));
  hour_H(k).data  = Energy_H.stored(hour_H(k).ind);
  hourlyavail_H(k)= 1 -
sum(Energy_H.badhour(hour_H(k).ind)) / 10957;
  Shourdata_H(k)  = sum(SD(hour_H(k).ind)) ;  %hourly
insolation
  Ehourdata_H(k)  = sum(Energy_H.stored(hour_H(k).ind)) /
10957 ;  %hourly insolation
end


  %availability increments
avail_inc=[ 0.9, 0.99, 0.999, 0.9999, 0.99999, 0.999999,...
            0.9999999, 0.99999999];
logavail_inc=log10(avail_inc);
avail_label=num2str(avail_inc'*100,8);
avail_label(end,:)=char('      100');

%logarithm format
loghourlyavail1_F=log10(hourlyavail_F);
loghourlyavail_F=loghourlyavail1_F;             %because
avail is a matrix
loghourlyavail_F(find(loghourlyavail_F==0))=log10(avail_inc
(end));  %lim value

%logarithm format
loghourlyavail1_H=log10(hourlyavail_H);
loghourlyavail_H=loghourlyavail1_H;             %because
avail is a matrix
loghourlyavail_H(find(loghourlyavail_H==0))=log10(avail_inc
(end));  %lim value

%%
%***
Plotting*************************************************
****
hr=1:24;                                        %hour of the
day
[hrs_F,ys_F]=stairs(hr-1,loghourlyavail_F);         %'-1'
adjusts to pre steps
```

```
loghourlyavail2_F=[loghourlyavail_F(end),loghourlyavail_F];

%%
%***
Plotting**************************************************
****
hr=1:24;                                        %hour of the
day
[hrs_H,ys_H]=stairs(hr-1,loghourlyavail_H);         %'-1'
adjusts to pre steps
loghourlyavail2_H=[loghourlyavail_H(end),loghourlyavail_H];



hr2=[0,hr];

 %%
figure
semilogy(hr2,loghourlyavail2_F,'*',hrs_F,ys_F,'r',hr2,logho
urlyavail2_H,'*',hrs_H,ys_H,'b');
legend('Flatplate ','Faltplate','Hemisphere','Hemisphere');
set(gca,'xlim',[0 24],'xtick',0:24,'xticklabel',[24,1:24])
set(gca,'ytick',logavail_inc,'yticklabel',avail_label)
set(gca,'ylim',[-1,-10^-9])
xlabel('Hour of the day')
ylabel('Availability [%]');
title(['15% efficient PV cells  with ',...
  num2str(E_load),'W-hr per day load'])
grid on
%legend ('Hourly Availabiltiy','Cummulative
Availability','location','best')
%%
```

VITA

Name:	Amulya Karavadi
Address:	Department of Electrical and Computer Engineering, Texas A&M University, 214 Zachry Engineering Center, TAMU 3128, College Station, Texas 77843-3128
Email Address:	amulya.karavadi@gmail.com
Education:	B.E., Electrical and Electronics Engineering, Osmania University, India M.S., Electrical Engineering, Texas A&M University, 2011